Verkennende studie van het potentieel van lithium en andere kritieke grondstoffen in de Vlaamse ondergrond

DEPARTEMENT
OMGEVING

vlaanderen.be/omgeving

VERKENNENDE STUDIE VAN HET POTENTIEEL VAN LITHIUM EN ANDERE KRITIEKE GRONDSTOFFEN IN DE VLAAMSE ONDERGROND

Dit onderzoek bespreekt de beschikbare grondwatergegevens aangaande lithium en andere kritieke grondstoffen in het Bekken van de Kempen en het Massief van Brabant. Het ondersteunt daarbij het Vlaamse beleid rond kritieke grondstoffen. In eerste instantie worden de beschikbare gegevens verzameld en op kwaliteit beoordeeld. De gegevens worden in een databank aangeleverd, die vlotte uitwisseling en hergebruik van de gegevens moet faciliteren. Op basis van de gegevens wordt het voorkomen en de spreiding van lithium en andere kritieke grondstoffen in grondwaters in Vlaanderen onderzocht, in relatie met de geologie. Eventuele anomale elementen en locaties van voorkomen worden geëvalueerd en het potentieel ervan wordt vergeleken met andere voorkomens in de Europese context. Daarnaast worden ook de risico's gerelateerd aan natuurlijk voorkomende radio-isotopen bij behandeling van gemineraliseerd grondwater besproken. Ten slotte worden aanbevelingen geformuleerd om de kennis omtrent het voorkomen van lithium en andere kritieke grondstoffen te vergroten via bijkomende gegevensvergaring enerzijds, en anderzijds mogelijke bijkomende onderzoekspistes voorgesteld die kunnen leiden tot een beter inzicht in de onderliggende processen die verantwoordelijk zijn voor eventuele aanrijkingen.

COLOFON

Verantwoordelijke uitgever
Toon Denys, secretaris-generaal
Departement Omgeving
Koning Albert-II laan 15 bus 553, 1210 Brussel (postadres)
vlaanderen.be/omgeving

Een uitgave van het Departement Omgeving, Afdeling Beleid
beleid.omgeving@vlaanderen.be

Auteurs
Ben Laenen – VITO
Thomas Hermans – UGent
Nele Horemans – SCKCEN
Roel De Koninck – VITO
Alemu Yenehun Beyene – UGent
Stijn Dewaele – UGent
Kristine Walraevens – UGent
Mirela Vasile - SCKCEN

Publicatiedatum
15 april 2026

Depotnummer
D/2026/3241/039

SAMENVATTING

Deze studie focust op het verzamelen en interpreteren van grondwateranalyses met het oog op de verkenning van het potentieel van lithium en andere kritieke grondstoffen in de Vlaamse ondergrond. Anomale concentraties van neven- en spoorelementen in het grondwater kunnen immers wijzen op het voorkomen van ertsafzettingen in de ondergrond. Daarnaast kan de geochemie van grondwater inzicht geven in de onderliggende aanrijkingsprocessen van kritieke grondstoffen in het grondwater zelf.

Als eerste stap werden bestaande grondwatergegevens verzameld en gestructureerd in het kader van een vlotte uitwisseling met andere databanken zoals bijvoorbeeld DOV (Databank Ondergrond Vlaanderen). Daarnaast werden in het kader van deze studie nieuwe grondwateranalyses uitgevoerd. Enerzijds werden in het Bekken van de Kempen, waar slechts weinig locaties met data beschikbaar zijn, nieuwe monsters genomen in samenwerking met Fluxys (4) en J&J in Beerse (1). Daarnaast is er in opdracht van DOMG (departement Omgeving) een bijkomende analysecampagne uitgevoerd op 49 putten van VMM (Vlaamse Milieumaatschappij) in het Massief van Brabant waarbij de belangrijkste ionen werden bepaald in combinatie met spoorelementen. Dit zijn ook de eerste metingen van lithium in het Massief van Brabant.

In een tweede stap werd de kwaliteit van de grondwateranalyses geëvalueerd. Vervolgens werd door middel van (geo)statistische methode gebieden met afwijkende concentraties gelokaliseerd en vergeleken met de geologie. Omwille van het verschil in datadichtheid, grondwatersamenstelling en geologie werd deze analyse opgesplitst in twee gebieden: het bekken van de Kempen en het Massief van Brabant.

<u>Bekken van de Kempen</u>
In het Bekken van de Kempen is het kalksteenreservoir van onder Carboon ouderdom het belangrijkste reservoir. Typering van water uit die lagen met behulp van Piper-diagrammen en de Stuyfzand-classificatie leert dat het een H3/H4-NaCl-type water betreft. Analyses van de hoofd- en nevenionen tonen een duidelijke link aan tussen de diepte van het reservoir en de concentraties. Uitzondering op de regel is magnesium, waarvan de concentratie niet systematisch toeneemt met de diepte van het reservoir.

De verhoudingen tussen de verschillende elementen wijzen erop dat de pekel in het reservoir een mengsel is van zeewater dat door reacties met het gesteente werd uitgedroogd en een sterk geëvolueerde secundaire pekel. Daarnaast zijn er aanwijzingen, onder andere door het relatieve tekort aan magnesium in het grondwater, voor kationenuitwisseling en interactie met de carbonaatgesteenten van het reservoir (die magnesium binden aan carbonaten of bladsilicaten) in ruil voor het vrijzetten van andere elementen zoals lithium. De mate van kationenuitwisseling/interactie lijkt toe te nemen met de diepte. De gemeten kaliumwaarden zijn indicatief voor oplossing van kalium-rijke mineralen zoals mica en veldspaten.

Verschillende geothermometers werden gebruikt om de huidige reservoirtemperaturen te vergelijken met de gerelateerde temperaturen op basis van de geochemie van het water op de verschillende locaties. Op basis van deze geothermometers kan afgeleid worden dat er aanrijking moet zijn geweest van kalium en lithium en dat er depletie is voor natrium en magnesium in vergelijking met een pekel die zuiver geëvolueerd zou zijn uit zeewater. Dit sluit aan bij de inzichten vanuit de analyse van de hoofd- en nevenelementen.

Analyse van de spoorelementen toont aan dat er aanrijking is van Al, Ba, Cd, Cr, Cu, Li, Ni, Pb, Sr en Zn in minstens 10 stalen. Barium en lithium zijn daarbij het sterkst aangerijkt.

- Lithium is aangerijkt in alle monsters van het onder Carboon, met de hoogste waarden gemeten in Mol (82-129 mg/l). Aanrijking gebeurt in hoofdzaak via kationenuitwisseling vanuit silica mineralen ten koste van kalium, natrium en magnesium. Daarnaast kan er nog een bijdrage zijn vanuit de thermische degradatie van organisch materiaal.
- Barium is het meest aangerijkt in de stalen van Peer.
- Strontium is aangerijkt in de kalksteenreservoirs, terwijl er slechts weinig van aanwezig is het boven Carboon in Peer. Dit wijst erop dat de aanwezigheid van carbonaten de bepalende factor is voor de strontiumgehaltes in de reservoirs van het Bekken van de Kempen.

Vergelijking met de literatuur voor wat betreft het voorkomen van lithium in pekels wereldwijd toont aan dat het steeds dezelfde processen zijn die verantwoordelijk zijn voor eventuele aanrijking van lithium in grondwater. Temperatuur, zoutgehalte (natrium en chloride) en aanwezigheid van mineralen die lithium bevatten zijn een noodzakelijke voorwaarde. Er is een terugkerende positieve correlatie tussen lithium en elementen zoals Na, Cl, K, B en een negatieve correlatie met onder andere Mg en U. Deze relaties wijzen op de link tussen verhoogde lithiumconcentraties en interactie van grondwater met (klei)mineralen en zijn in lijn met de bevindingen uit deze studie. Met het oog op eventuele winning van lithium uit geothermische pekels is een lage Mg/Li-verhouding gunstig. In het Bekken van de Kempen voldoet de samenstelling van de pekel in Mol aan deze voorwaarde.

<u>Massief van Brabant</u>

Typering van de waters van het Massief van Brabant via Piper-diagrammen en de Stuyfzand-classificatie toont een grote verscheidenheid aan watertypes. De spreiding is het resultaat van een complexe wisselwerking tussen fossiele mariene invloeden, zoetwaterinflux en processen zoals kationenuitwisseling. Ruimtelijk gezien er een evolutie zichtbaar van een NaCl-type water onder meer mariene invloed in het noorden en noordwesten van Vlaanderen naar een zoeter $CaHCO_3$-type water in het zuiden en zuidoosten, veroorzaakt door verdunning met zoet, meteorisch water en kationenuitwisseling.

In het Massief van Brabant zijn er geen aanwijzingen uit de metingen dat er aanrijking van lithium heeft plaatsgevonden vanuit lithium-houdende mineralen. De lithiumgehaltes zijn laag (<100 ppb, gemiddeld 43 ppb) en er worden geen anomale waarden aangetroffen. Beperkte toevoeging van lithium aan het grondwater via kationenuitwisseling lijkt evenwel van toepassing, gezien de Li/Cl-verhouding hoger ligt dan mag verwacht worden vanuit de evolutie van zeewater. Het feit dat het lithiumgehalte niettemin lager ligt dan dat van zeewater, kan worden toegeschreven aan de menging van het oorspronkelijke grondwater met jonger, zoet grondwater. Gezien de beschikbare grondwaterstalen ondiep zijn, kunnen er geen uitspraken worden gedaan over eventuele aanwezigheid van lithium-houdende mineralen op grotere diepte (inclusief in de veronderstelde graniet/pegmatiet-batholieten op basis van graviteitsanomalieën).

Er werd een ruimtelijke analyse van de verschillende parameters uitgevoerd met inachtname van de geologie gebaseerd op de overzichtskaart van Piessens et al. (2005). Hoewel de dataset van het Massief van Brabant verschillende anomale concentraties van kritieke grondstoffen aantoont, konden er geen relaties vastgesteld worden (noch statistisch, noch geografisch) tussen de spoorelementen en de hoofdionen of tussen verschillende spoorelementen onderling. Dit ligt in lijn met resultaten uit eerdere studies. Statistische analyse toont aan dat er voor de meeste elementen slechts enkele stalen hogere concentraties bevatten. Voor elk element werd een relevante drempelwaarde bepaald om

eventuele anomalieën ruimtelijk te onderzoeken. Voor de meeste elementen ligt de gemiddelde waarde beneden deze drempelwaarde behalve voor Bi, Cd en Pb.

Op basis van de ruimtelijke analyse van de verschillende elementen kunnen er twee zones in het Massief van Brabant afgebakend worden waar anomalieën meer gegroepeerd voorkomen. De belangrijkste is de zone Oostrozebeke-Waregem-Harelbeke-Deerlijk (Zone 1), de andere zone ligt meer naar het zuidoosten, ter hoogte van de regio Oudenaarde-Brakel-Geraardsbergen (Zone 2).

Het Massief van Brabant is gekend voor sulfidemineralisaties. De spoorelementen hieraan gerelateerd worden teruggevonden in de dataset van deze studie, vaak ook versterkt door oxidatie ontstaan door grondwaterextractie uit de aquifers van het Massief van Brabant. Door de sterke vereenvoudiging van de geologische complexiteit die aan de basis ligt van de overzichtskaart van Piessens et al. (2005), is een gedetailleerde vergelijking van de anomalieën niet mogelijk.

Radio-isotopen

Een laatste werkpakket in de studie betreft de bepaling en bespreking van de aanwezigheid van radio-isotopen in het Bekken van de Kempen. In kader van deze studie werden radio-isotopen bepaald op de nieuwverworven stalen van Fluxys en J&J. De uranium-isotopen liggen doorgaans beneden de – zeer lage – detectielimieten en wijzen op de afwezigheid van uranium in het grondwater. Dit is in lijn met de slechte oplosbaarheid van uranium. De gemeten concentraties van radium-226 liggen wel boven de detectielimiet, en zelfs boven de drempelwaarde voor vloeibare monsters. De stalen zijn dus gebonden aan de NORM-bepalingen (Naturally Occuring Radioactive Material). Er moet rekening gehouden worden met mogelijke accumulatie in bovengrondse installaties die gebruikt worden voor de behandeling van het grondwater. Indien het opgepompte water niet zou worden teruggepompt in het reservoir, moet het beschouwd worden als NORM-afval en als dusdanig behandeld worden. Verder onderzoek naar de natuurlijk voorkomende radioactieve elementen in het grondwater en het gedrag ervan in een bovengrondse installatie zal aan de orde zijn wanneer stappen in de richting van extractie van lithium of andere kritieke grondstoffen gezet worden.

Conclusies en aanbevelingen

Op basis van de bevindingen werden er aanbevelingen gedaan voor toekomstige exploratie in lijn met de strategische doelstellingen zoals gedefinieerd in de Critical Raw Materials Act (CRMA, EU 2024/1252).

Indien verder onderzoek naar lithium en andere kritieke grondstoffen in de toekomst gefaciliteerd wil worden, is het aangewezen om bijkomende monsters en analyses te verwerven. Om de kwaliteit van nieuwe monsters en analyses te waarborgen wordt er bij voorkeur gewerkt aan een bemonsteringsprotocol en een lijst van te analyseren parameters. Elementen zoals Br, B, I en F worden vaak niet gemeten, maar leveren wel waardevolle informatie op over de origine en evolutie van het grondwater dat aangetroffen wordt in de verschillende reservoirs.

In het Bekken van de Kempen kan er aan vergunninghouders van diepe aardwarmteprojecten gevraagd worden om wateranalyses aan te leveren. In het Massief van Brabant is bijkomende bemonstering, zowel boven de zones waar geochemische anomalieën zijn vastgesteld als in de zone met graviteitsanomalieën, aangewezen. Het plaatsen van (een) diepe boring(en) in de zone met graviteitsanomalieën zou een grote meerwaarde betekenen, bij voorkeur met verwerving van kernmateriaal en goede geofysische boorgatmetingen. Daarnaast kunnen bijkomende regionale geofysische data de kennis van de opbouw van het Massief van Brabant in relatie tot potentieel interessante grondstoffen verbeteren.

Naast nieuwe grondwateranalyses is het ook aanbevolen de reservoirgesteenten en boven- en onderliggende afzettingen die een invloed kunnen hebben op de grondwatersamenstelling in het reservoir nader te onderzoeken. Dit kan hetzij via inventarisatie van bestaande gegevens, hetzij via nieuwe analyses op bestaande of nieuw te verwerven monsters. Daarbij is, naast geochemische analyse van het gesteente, bepaling van de minerale en geochemische samenstelling van individuele mineralen (met focus op kleimineralen, mica's en sulfiden) van cruciaal belang. Dit moet toelaten de interacties tussen het grondwater en de gesteenten te modelleren om de bron van en de processen achter de aanrijking in lithium en andere elementen beter te begrijpen.

Ten slotte kan er ook ingezet worden op specifieke isotopenanalyses (lithium, boor en zuurstof) omdat deze meer inzicht verschaffen in de origine van de formatiewaters en de eventuele bijdrage van organisch materiaal aan de samenstelling van de formatiewaters in de reservoirs.

SUMMARY

This study focuses on collecting and interpreting groundwater analyses in order to explore the potential of lithium and other critical raw materials in the Flemish subsurface. Anomalous concentrations of minor and trace elements in groundwater can indicate the presence of ore deposits in the subsurface. In addition, the geochemistry of groundwater can provide insight into the enrichment processes of critical raw materials in the groundwater itself.

As a first step, existing groundwater data were collected and structured to facilitate a smooth exchange with other databases such as DOV (Databank Ondergrond Vlaanderen). In addition, new groundwater analyses were carried out as part of this study. On the one hand, new samples were taken in the Campine Basin, where only a few locations with data are available, in collaboration with Fluxys (4) and J&J in Beerse (1). In addition, an analysis campaign, commissioned by DOMG (Flemish Department of Environment), was carried out on 49 wells belonging to the VMM (Flemish Environment Agency) in the Brabant Massif, in which the most important ions were determined in combination with trace elements. These are the first measurements of lithium in the Brabant Massif.

In a second step, the quality of the groundwater analyses was evaluated. Subsequently, areas with anomalous concentrations were localized using (geo)statistical methods and compared with geology. Due to the differences in data density, groundwater composition and geology, this analysis was performed for two separate areas: the Campine Basin and the Brabant Massif.

Campine Basin

In the Campine Basin, the lower Carboniferous limestone reservoir is the most important reservoir. Characterization of water from these layers using Piper-diagrams and the Stuyfzand-classification reveals that it is an H3/H4 NaCl type water. Analyses of the major and minor ions show a clear link between the depth of the reservoir and the concentrations. An exception to the rule is magnesium, whose concentration does not systematically increase with the depth of the reservoir.

The ratios between the various elements indicate that the brine in the reservoir is a mixture of seawater that was dehydrated by water-rock interaction and a highly evolved secondary brine. In addition, there are indications—partly due to the relative magnesium deficit in the groundwater—of cation exchange and interaction with the carbonate rocks of the reservoir (which bind magnesium to carbonates or sheet silicates) in exchange for the release of other elements such as lithium. The degree of cation exchange/interaction appears to increase with depth. The measured potassium values are indicative of the dissolution of potassium-rich minerals such as mica and feldspars.

Various geothermometers were used to compare the current reservoir temperatures with the related temperatures based on the geochemistry of the water at the different locations. Based on these geothermometers, it can be deduced that there must have been enrichment of potassium and lithium and depletion of sodium and magnesium compared to a brine that would have evolved purely from seawater. This aligns with the insights from the analysis of the major and minor elements.

Analysis of the trace elements shows enrichment of Al, Ba, Cd, Cr, Cu, Li, Ni, Pb, Sr, and Zn in at least 10 samples. Barium and lithium are the most strongly enriched.

- Lithium is enriched in all samples from the lower Carboniferous, with the highest values measured in Mol (82-129 mg/l). Enrichment occurs mainly via cation exchange from silica minerals at the expense of potassium, sodium, and magnesium. Additionally, there may be a contribution from the thermal degradation of organic material.

- Barium is the most enriched in the samples from Peer.
- Strontium is enriched in the limestone reservoirs, whereas only small amounts are present in the upper Carboniferous in Peer. This indicates that the presence of carbonates is the determining factor for the strontium levels in the reservoirs of the Campine Basin.

Comparison with literature regarding the occurrence of lithium in brines worldwide demonstrates that the same processes are consistently responsible for potential lithium enrichment in groundwater. Temperature, salinity (sodium and chloride), and the presence of minerals containing lithium are necessary conditions. There is a recurring positive correlation between lithium and elements such as Na, Cl, K, and B, and a negative correlation with Mg and U, among others. These relationships point to the link between elevated lithium concentrations and the interaction of groundwater with (clay) minerals and are consistent with the findings of this study. With a view to potential lithium extraction from geothermal brines, a low Mg/Li-ratio is favorable. In the Campine Basin, the composition of the brine in Mol meets this condition.

Brabant Massif

Characterization of the waters of the Brabant Massif using Piper-diagrams and the Stuyfzand-classification reveals a wide variety of water types. The distribution is the result of a complex interplay between fossil marine influences, freshwater influx and processes such as cation exchange. Spatially, an evolution is visible from NaCl-type water under more marine influence in the north and northwest of Flanders to sweeter CaHCO3-type water in the south and southeast, caused by dilution with fresh, meteoric water and cation exchange.

In the Brabant Massif, there are no indications that enrichment with lithium has occurred from lithium-bearing minerals. Lithium levels are low (<100 ppb, average 43 ppb), and no anomalous values are found. However, limited addition of lithium to the groundwater via cation exchange is possible, given that the Li/Cl-ratio is higher than might be expected from the evolution of seawater. The fact that the lithium content is nevertheless lower than that of seawater can be attributed to the mixing of the original groundwater with younger, fresh groundwater. Given that the available groundwater samples are shallow, no conclusions can be drawn regarding the potential presence of lithium-bearing minerals at larger depths (including in the presumed granite/pegmatite batholiths based on gravitational anomalies).

A spatial analysis of the various parameters was performed, considering geology, based on the overview map by Piessens et al. (2005). Although the dataset from the Brabant Massif shows various anomalous concentrations of critical raw materials, no relationships could be established (neither statistical nor geographical) between the trace elements and the main ions, or between different trace elements themselves. This is in line with results from previous studies. Statistical analysis shows that for most elements, only a few samples contain higher concentrations. For each element, a relevant threshold value was determined to spatially investigate potential anomalies. For most elements, the average value lies below this threshold, except for Bi, Cd, and Pb.

Based on the spatial analysis of the various elements, two zones can be delineated in the Brabant Massif where anomalies are clustered together. The most important is the Oostrozebeke-Waregem-Harelbeke-Deerlijk zone (Zone 1); the other zone is located further to the southeast, around Oudenaarde-Brakel-Geraardsbergen (Zone 2).

The Brabant Massif is known for sulfide mineralizations. The trace elements related to this are present in the dataset of this study, often enhanced by oxidation resulting from groundwater extraction from

the aquifers of the Brabant Massif. Due to the significant simplification of the geological complexity in the overview map by Piessens et al. (2005), a detailed comparison of the anomalies is not possible.

Radioisotopes

A final work package in the study concerns the determination and discussion of the presence of radioisotopes in the Campine Basin. As part of this study, radioisotopes were determined on the newly acquired samples from Fluxys and J&J. The uranium isotopes are generally below the – very low – detection limits and indicate the absence of uranium in the groundwater. This is consistent with the low solubility of uranium. The measured concentrations of radium-226 are above the detection limit, and even above the threshold value for liquid samples. The samples are therefore subject to the NORM-regulations (Naturally Occurring Radioactive Material). Possible accumulation in surface installations used for groundwater treatment must be taken into account. If the pumped water is not returned to the reservoir, it must be considered NORM-waste and treated as such. Further research into naturally occurring radioactive elements in groundwater and their behavior in a surface installation needs to be considered when steps are taken towards the extraction of lithium or other critical raw materials.

Conclusions and recommendations

Based on the findings in this study, recommendations were made for future exploration in line with the strategic objectives as defined in the Critical Raw Materials Act (CRMA, EU 2024/1252).

If further research into lithium and other critical raw materials wants to be facilitated in the future, it is advised to acquire additional samples and analyses. To ensure the quality of new samples and analyses, a sampling protocol and a list of parameters to be analyzed is recommended. Elements such as Br, B, I, and F are often not measured, but do provide valuable information regarding the origin and evolution of the groundwater found in the various reservoirs.

In the Campine Basin, permit holders of deep geothermal projects may be asked to provide water analyses. In the Brabant Massif, additional sampling is recommended, both above the zones where geochemical anomalies have been detected and in the zone with gravity anomalies. Installing (a) deep borehole(s) in the zone with gravitational anomalies would represent significant added value, especially in combination with the acquisition of cores and good geophysical borehole measurements. Additionally, newly acquired regional geophysical data can improve knowledge of the structure of the Brabant Massif in relation to potentially interesting raw materials.

In addition to new groundwater analyses, it is also recommended to investigate the reservoir rocks and overlying and underlying deposits that may have an influence on the groundwater composition in the reservoir in more detail. This can be done either through an inventory of existing data or through new analyses on existing or newly acquired samples. In this regard, in addition to geochemical analysis of the rock, the determination of the mineral and geochemical composition of individual minerals (with a focus on clay minerals, micas, and sulfides) is of crucial importance. This allows the modeling of the interactions between groundwater and (reservoir) rocks in order to better understand the source of and the processes behind the enrichment of lithium and other elements. Finally, specific isotope analyses (lithium, boron and oxygen) can also be utilized, as these provide greater insight into the origin of the formation waters and the potential contribution of organic material to the composition of the formation waters in the reservoirs.

TABLE OF CONTENTS

1 DEFINITION

1.1 OBJECTIVE AND RESEARCH QUESTIONS

In October 2024, the Flemish Department of Environment (DOMG) launched a tender for an exploratory study of the geological potential for lithium and other critical raw materials (CRMs) in the Flemish subsurface, focusing on the Brabant Massif and the Campine Basin. This study is carried out in the framework of the Flemish Exploration Program, which is part of the National Exploration Program of Belgium. Such exploration plan for all European Member States is imposed by article 19 of the Critical Raw Materials Act (CRMA, EU 2024/1252). This Act sets strategic goals to ensure a safe and sustainable supply of critical raw materials such as lithium, nickel and copper, which are essential for the EU's economic and environmental objectives.

Since the study is relevant in a European context and the project team is staffed with international researchers, this report is written in English. This contributes to making the results accessible to European and international experts and to a smoother exchange within the framework of the EU.

The study has two main objectives:

- performing an evaluation of existing and new geochemical data of deep formation waters to map locations and rock formations enriched in lithium and other CRMs. The study is based on groundwater analyses, as abnormal element concentrations in groundwater can serve as indicators of ore deposits in the subsurface. Moreover, the ionic concentrations and ratios can provide insight into the processes and minerals underlying enrichments of CRMs in formation waters.
- drafting recommendations for future exploration, based on the insights of this evaluation, and aligned with the strategic objectives of the CRMA.

These objectives were translated into the following research questions:

- At what concentration does enrichment of Li and other CRMs occur?
- Are there indications for enrichment of Li and/or other CRMs in the Flemish subsurface?
- How do possible enrichments correlate with geology (e.g., mineralogy, specific formations, hydrogeology)?
- Are there specific safety and legal standards regarding radioactivity that need to be considered account in further exploration of the potential?

1.2 GENERAL RESEARCH APPROACH

The study comprises two main parts:

The first part focuses on the geochemistry of formation waters in Flanders. It includes an evaluation of the quality of the chemical analyses, typing of the formation waters encountered in the deep subsurface of Flanders and geostatistical analyses. Statistical approaches and comparison with international literature provide a substantiated explanation for any anomalous concentrations identified. First, a data structure has been defined that allows efficient management and analysis of the geochemical data, and ready integration with DOV, the database on the subsurface of Flanders. The findings are visualized using standard groundwater plots and GIS software.

The analysis of the geochemistry of the formation water has been carried out separately for two key geological areas:

- The Campine Basin: focus on the analysis of deep geothermal water to evaluate lithium and other CRM concentrations;
- The Brabant Massif: analysis of relatively shallow groundwater to interpret and assess lithium and other CRM concentrations based on existing and new data.

The second part deals with the evaluation of the subsurface potential for CRMs in Flanders and recommendation for further exploration. This part of the work includes an evaluation of the impact of naturally occurring radioactive elements (NORs) for the exploration and potential extraction of CRMs from deep formation water. Available water samples from the Merksplas geothermal well (Vandenberghe et al., 2000) and the VITO geothermal site in Mol (Vasile et al., 2017) exhibit elevated concentrations of NORs. Other mineralized formation waters may also contain high concentrations of radioactive isotopes. This poses a risk to the treatment of these samples and the processing of tailings. Furthermore, the isotope ratio is partly determined by interactions between the formation water and the host rock and could potentially be used as a proxy for the presence of mineralization in the deep subsurface.

1.3 OUTLINE OF THE REPORT

The first substantive chapter (Chapter 2) discusses the data management structure that has been developed for the study.

Chapters 3 and 4 deal with the geochemistry of formation waters from the Campine basin and the Brabant Massif respectively. Both chapters have a similar outline:

- An overview of the available geochemical data collected in the context of the study and a discussion of the data quality;
- Visualisation of the geochemical data in relation to the regional and/or local geology. For this purpose, the subcrop map of the Brabant Massif by Piessens et al. (2005) is used. This allows visualisation of the relationship between the examined groundwater sample and the surrounding rock type and the proximity of faults. In the Campine Basin, the number of sampling locations is limited. Therefore, known reservoir geology (stratigraphy and depth) are the main factors considered during interpretation;
- Interpretation of the geochemical signature of the water samples. Quality of the samples is assessed by calculating the chemical balance error (CBE). General geochemical characteristics are evaluated with Piper-plots and the Stuyfzand-classification. Since the geochemistry of the brines from the Campine Basin differ from those of the Brabant Massif, more relevant details about the classification of the formation waters are provided in the dedicated chapters;
- Comparison of the groundwater geochemistry with literature and conclusions with respect to possible enrichment processes.

The next chapter discusses the results of the radiological analyses of deep formation waters from the Campine Basin and NORM.

In the final chapter, recommendations for further expansion of the dataset and research possibilities on the presence of lithium and other CRMs are given.

2 DATA MANAGEMENT STRUCTURE

2.1 CONTEXT

The first step in this study is to make an inventory of relevant geochemical groundwater data in the Campine Basin (see Chapter 3) and the Brabant Massif (see Chapter 4).

When setting up the data structure, several aspects need to be considered.

- Data sources are variable in nature and complexity;
- Data should be stored as it is originally reported. Preprocessing of the data (for instance conversion of units of measurement) should be avoided in the first stage of data collection;
- Metadata should be included where possible;
- Location of the groundwater measurement should be clear and traceable;
- Extraction of the data should be easy and straightforward (e.g. for reporting purposes in other projects);
- The data structure needs to be flexible and yet robust.

In the region of Flanders, subsurface and groundwater data is stored in DOV (https://dov.vlaanderen.be/). The data collected in this study is often linked to objects present in DOV, so communication between this geochemical dataset and the data in DOV should be guaranteed as far as possible. However, since a considerable amount of datapoints is quite old, linking it directly to DOV-objects is not always possible. This is especially true for the data in the Brabant Massif. Historically, research was more focused on the Brabant Massif, which means that there is a larger proportion of older data, for which establishing a link to DOV-objects is a complex operation. In the Campine Basin, the main reservoirs of interest for this study are located at much greater depths. Therefore, only a limited amount of datapoints is available. The data are generally younger in age, which makes establishing a link to the correct DOV-object quite straightforward.

To guarantee easy incorporation in DOV, we try to find a balance between what is suitable for this study and how similar data is stored in DOV. To ensure this, we aim for compliance with the DOV OSLO standards on 'Observaties' (=observations) (https://data.vlaanderen.be/doc/applicatieprofiel/bodem-en-ondergrond/observaties/) and (https://data.vlaanderen.be/doc/applicatieprofiel/observaties-en-metingen/) which are implemented for, among other types of observations, groundwater data. One of the reasons for the development of these standards is allowing easy exchange of data in the European context.

The standard is not yet fully operational, but is already being implemented in DOV, where the principles of these standards are being used to store different types of data on the composition of the subsurface (including groundwater analyses). It is beyond the scope of this project to give an elaborate overview of the standard itself, but we intend to provide functional interoperability of the dataset of this study and DOV by incorporating the key elements of this standard in our data structure.

All measurable aspects are treated as *parameters*, each accompanied by a measured value and an associated measurement unit. In addition, supplementary metadata describing the time of sampling or analysis, measurement procedure and related context can be linked to each parameter. Within the scope of this study, parameters are associated with an *object*, namely a groundwater sample. Each

sample is collected from a specific well or filter, creating a clear linkage from well or filter (also defined as *object* in DOV), through the groundwater sample, to the individual analysed parameters.

Within DOV, these objects are assigned permanent identifiers (PID), enabling measurements to be reliably linked to a specific location while ensuring data integrity. The relevant identifier is marked in the dataset of the study under '*parent_permkey'*. In principle, this identifier allows all groundwater data generated in this study to be consistently linked to the corresponding DOV objects and facilitates the transfer of individual measurements into DOV.

In most cases, only a link to a higher-level DOV-object like a well is available for the geochemical data of this study. The intermediate level (the groundwater sample itself) is usually not present in DOV, except for the Brabant Massif, where the groundwater samples of the new sampling campaign from VMM-DOMG (see 4.1) are objects in DOV. However, these data were not yet (publicly) available at the start of this study (see 4.1), so the geochemical results used here are likewise linked to the level of the well in the project database.

As stated above, it is not always possible to find a permanent identifier from DOV. Reasons can be for instance:

- Historical data (especially in the Brabant Massif) is not always present (in the same way) as in the original dataset or might have become obsolete in DOV;
- Some data may come from (partially) confidential sources, which means that there is no DOV object publicly available.

Nonetheless, efforts have been made to provide a *parent_permkey* where possible within the timeframe of this study. This was mainly done by comparing the historical data with DOV-objects in the vicinity of the datapoint and comparing parameters like depth etc. If this comparison leads to a valid candidate DOV-object, the link was established. In the end, a *parent_permkey* was assigned to over 40% of the historical wells in the Brabant Massif (excluding the ones from the VMM-DOMG dataset, which all have a *parent_permkey)*.

2.2 DATA STRUCTURE

The new structure based on OSLO '*Observaties*' is reflecting data storage in a database, in its basic form representing a '*long table*' format. In this format, each parameter that is measured on a groundwater sample is stored as a single record (line). This has several advantages:

- A long table format is more robust, as including a new parameter (that was not measured on any sample before) does not imply a change in the table structure as opposed to in a column-based table;
- There is no space required to document parameters that are not measured in one sample: there is no empty record in the table for a specific parameter that is not measured on a specific sample. Only measurements that are performed are included;
- It is possible to incorporate metadata on the individual measurement level, for instance on measurement unit, error, methodology, detection status and so on. This allows for more detail than what can be stored in a column-based table.
- The data can be stored raw ('as is'), without already converting data to fit in a rigid structure or to a specific measurement unit. Conversions can be efficiently done on the data in a postprocessing step by the individual users according to their needs.

– Long Tables have overall better performance and associated faster querying times and are more machine readable. This also allows for easier exchange of data.

Postprocessing on the dataset is performed for the interpretation of the data in this study to standardize measurement units etc., but for documentation purposes it was decided to use the initial reporting values for traceability.

Table 1. Data structure used to store relevant groundwater data in this study.

Attribute	Description
sample_id	ID of the sample in the data tables of this study. Starting from 1 in the Campine Basin and from 1001 in the Brabant Massif.
wellname	name of the well as used in this study
observatie_id	ID of the groundwater sample in DOV. Not given in this study, but possible to add for the VMM-DOMG data and when samples are added in DOV (backward compatibility)
datum_monstername	date of sampling
tijdstip_monstername	time of sampling
datum_analyse	date of analysis
tijdstip_analyse	time of analysis
parameter	element or parameter that is analysed
meetwaarde	measurement result (value)
meeteenheid	measurement unit of the reported parameter
meetfout	measurement error
meetfout_type	type of measurement error
analysemethode	analytical method of measurement
detectieconditie	detection condition. LT is used for values below the lower level of detection; GT is used for values above the upper level of detection.
uitvoerder	executor of the analysis
betrouwbaarheid	reliability
opmerking	remark
diepte	depth of groundwater sampling
naam	name of groundwater sample
parent_permkey	unique identifier in DOV
parent_type	type of identifier in DOV (‘boring’, ‘put’, ‘filter’, ‘monster’)
bron	data source, only used for the Brabant Massif dataset (‘LTGH’, ‘Sterpin’, ‘VMM_DOMG’), see also Table 12

Measurement units are included in the database, using a specific code for each measurement unit. Numerous measurement units in the dataset are already in use in observation reports in DOV through a specific code. When applicable, the corresponding code is included in Table 2, which provides an overview of all the different measurement units used in the dataset of this study.

Table 2. Measurement units used in the dataset.

Measurement Unit	Name	DOV_code
bq_l	Becquerel per liter	
deg_c	°C	3
fh	French degrees	118
g_l	gram per liter	
kg_l	kilogram per liter	
meq_l	milliequivalent per liter	114
mg_l	milligram per liter	9
ms	millisiemens	
ms_cm	millisiemens per centimeter	104/105
nano_ci_l	nanocurie per liter	
ppb	parts per billion	121
ppm	parts per million	120
s_cm	siemens per centimeter	
ug_l	microgram per liter	18
us_cm	microsiemens per centimeter	4

Metadata that is only indirectly related to the water sampling results is preferably not stored together with the directly related metadata, specifically for the indirect metadata on coordinates (location) of the water sample and stratigraphy. Coordinates are associated with the well from which the groundwater sample is taken and are stored at that level. Should changes be applied to a coordinate at some point, it is inherited by link rather than having to change it in the data table itself, which is a more robust process and less likely to lead to discrepancies in the future. Preferably, a similar approach is used for the stratigraphy, which can also change over time considering new or alternative interpretations. An overview of additional indirect metadata used in this study is given in the following table.

Table 3. Indirect metadata table structure.

Attribute	Description
wellname	name of the well as used in this study
X_L72	X coordinate in Lambert72
Y_L72	Y coordinate in Lambert72
Z_L72	Z coordinate in Lambert72
parent_permkey	unique identifier in DOV
parent_type	type of identifier in DOV ('boring', 'put', 'filter', 'monster')
X_RD	X coordinate in Rijksdriehoeksstelsel - RD (Dutch wells in Campine Basin only)
Y_RD	Y coordinate in RD (Dutch wells in Campine Basin only)
Z_RD	Z coordinate in RD (Dutch wells in Campine Basin only)
diepte	Depth of the well (Dutch wells only), since this data cannot be inherited from DOV for these wells.
bron	data source, only used for the Brabant Massif dataset ('LTGH', 'Sterpin', 'VMM_DOMG'), see also Table 12
GW-ID	DOV-name for parent_type 'put' (Brabant Massif only)
formatie	DOV code for stratigraphy (Brabant Massif only)

Given the different nature and origin between the data from the Campine Basin and the data from the Brabant Massif, a slightly different approach is used.

In the Campine Basin an indirect table containing location information is used for this study. Should all the well data become available in DOV, this indirect table can become obsolete and the location information in DOV should be used. The stratigraphy of the reservoir linked to the groundwater samples as used in the context of this study is given in Table 9.

In the Brabant Massif dataset, several identifiers are used to provide information on the different well locations included. Since this dataset consists of 3 different datasets (see 4.1), the consistency of the identifiers for the merged dataset is an issue that needs to be addressed. Following approach is used for the different subsets.

- VMM-DOMG: the data from this subset is the most straightforward to incorporate, because of the pre-existing unique link with a DOV-object. In this case: *wellname* = existing DOV-name.

- Sterpin: in this dataset, datapoints have a specific name, which is often based on the company where the well is located, combined with the community it is in. For traceability, this specific name is used as *wellname* in the overall long table. In some cases, multiple wells are located at the same company and/or community. For these wells, X and Y coordinates of the individual wells act as additional information to make a distinction between the wells. Therefore, these X and Y values are added as suffixes to the original name if the initial name is not unique:

Table 4. Example of *wellname* creation for non-unique specific names in the Brabant Massif dataset.

Name	X	Y	Resulting *wellname*
Beaulieu-Wielsbeke	79450	179120	Beaulieu-Wielsbeke_79450_179120
Beaulieu-Wielsbeke	79657	178930	Beaulieu-Wielsbeke_79657_178930

- The most diverse dataset on *wellname* level is the LTGH subset. Names are a variety of community names, be it in combination with the name of the company where the well is located or not; specific LTGH codes and (non-standardized) GSB-numbers (from the Geological Survey of Belgium well code system). Following system is applied:

1. If a (non-standard) GSB number is given, this is used;
2. If not, the community's name (including company name if given) is used;
3. If this leads to duplicate names that belong to different locations, X and Y are included as suffix

If a DOV-identifier exists for any of these wells in the Sterpin and LTGH subsets, the DOV *parent_permkey* and *parent_type* ('put') are included.

For the dataset of the Brabant Massif, lithostratigraphy on Formation level is stored together with the location information for the different wells as the stratigraphic interpretation is used in this study for evaluation purposes and can be considered as a study specific stratigraphy.

3 CAMPINE BASIN

3.1 OVERVIEW OF THE AVAILABLE DATA

3.1.1 Pre-existing data

Focus of the present evaluation is the formation waters of the Lower Carboniferous Limestone Group. The number of wells reaching the Dinantian limestone reservoir in the Campin Basin is limited. There are data available from past research projects or exploration wells in Merksplas-Beerse and Turnhout, the VITO Geothermal project in Mol and there is one analysis publicly available in the Loenhout region (DZH4 well).

Additional data are available for some reservoirs above the Dinantian limestones, which are included in the dataset. In the northwest the Merksplas-Beerse system has provided information on the Cretaceous and in the eastern part of the Campine Basin there is a set of measurements in Peer from the Westphalian. In addition, data are available from the Namurian in the Turnhout well.

The majority of the samples is attributed to three locations (see Table 7): the geothermal plant of VITO in Mol (labelled in this study as 'VITO Geothermal'), the Peer well and the two wells from the Merksplas-Beerse system.

The most extensive documentation of formation water reservoir properties in the lower Carboniferous limestones is available for the VITO Geothermal plant in Mol. For this location, there are samples of produced water taken at the surface during testing of well MOL-GT-01, downhole samples taken in MOL-GT-01 and a series of periodic measurements taken in the surface installation during normal operation of the geothermal plant. A general description of the brine is given in Bos & Laenen (2017). Its radiological characteristics are discussed by Vasile et al (2017).

The data from the Peer well are the result of the coalbed methane exploration well which was drilled in 1992. In 1993-1994 an extensive pump test project was undertaken, during which a series of water samples were taken and analysed for several interesting elements, including metals like Li and Sr, and B. All samples were taken at the surface. More information on the project is available in Wenselaers (1996).

The Merksplas-Beerse project (see Vandenberghe et al, 2000) was developed to study in detail the geothermal potential of the Lower Carboniferous Limestone Group in the Campine Basin for the first time. Two wells were developed for this project. A deep well (Merksplas-Beerse I) reaching the Lower Carboniferous Limestone Group and destined to be the production well and a shallower well (Merksplas-Beerse II) reaching the chalk of the Cretaceous. The idea was to produce hot water from the Lower Carboniferous Limestone Group and store the cooled water after heat exchange in the shallower Cretaceous reservoir. Several analyses of the formation water from both wells are available. The data from Merksplas-Beerse I include downhole samples and surface samples taken during well testing at the outlet of the gas separator and in a closed corrosion loop (Vandenberghe et al, 2000). Additional samples are available from before and after a heat exchanger. Only the high temperature sample is included in the database. The samples from Merksplas-Beerse II were taken at the surface during cleaning of the well by air lift and during the subsequent pump test. Most information is restricted to more general geochemical parameters, but other parameters are measured on occasion.

Next to that, a few other sampling locations provide information on the composition of the brine in the lower Carboniferous limestones in the Campine Basin in Belgium. A complete overview is provided in Table 7.

Additional data from the Californië geothermal project in Venlo in the Netherlands is collected from publicly available sources on NLOG (see Table 8).

3.1.2 New sampling and measurements

Since the number of pre-existing samples and sampling locations is limited, collecting and analysing additional samples in the deep subsurface of the Campine Basin is part of this study. Existing and operational wells are scarce but are present in the Loenhout region and in Beerse.

In the Loenhout region, multiple wells reaching the Lower Carboniferous Limestone Group are operated by Fluxys for seasonal gas storage. Fluxys agreed to provide samples for four selected wells (DZH14, DZH15, DZH23, DZH24, see Table 5 for details), which are taken simultaneously with their normal operational maintenance on the wells. Samples are collected downhole using pressure valve equipped sample containers which allow sampling of water on the desired reservoir depth, and they are stabilized directly upon return to surface by means of HNO_3 (until a pH < 2 is obtained). Two samples were taken near the top of the Lower Carboniferous Limestone Group reservoir, the other two are taken deeper in the reservoir (Table 5).

Table 5. Overview of the sampled Fluxys wells with sampling depth and approximate depth of the top of the Lower Carboniferous Limestone Group reservoir according to G3Dv3.

Well	Sampling depth (m)	Top reservoir (m)
DZH14	1315	1320
DZH15	1325	1330
DZH23	1485	1355
DZH24	1395	1276

One additional sampling point is located at the geothermal plant of J&J in Beerse (see Table 7, Beerse-GT-01a), at the time of a scheduled water and gas sampling operation in their system, performed by PanTerra. The sample is collected at the surface installation sampling point which is located between the degasser and the heat exchanger. Temperature of the brine at the sampling point was 82.5°C at the time of sampling. Two samples were taken. One sample was immediately stabilised by HNO_3 (until pH < 2) for the analysis of the radionuclides, for the other one no conservation was applied (general geochemistry + metals). Analysis of the new samples was performed by VITO for the general geochemistry and metals and by SCKCEN for the radioisotopes.

The full dataset (historic and new data) is available in digital appendices 1 (longtable) & 2 (GIS-file).

3.1.3 Quality control

The dataset from the Campine Basin consists of water samples taken under various conditions. Both the timing (e.g., immediately after drilling, during a pumping test, during production) and the location of sampling (e.g., downhole, at the wellhead, before or after the degasser) influence the analysis results. The way the samples were preserved and the analysis techniques used also differ. All these aspects lead to a heterogeneous dataset for the Campine Basin. This complicates the interpretation

of results and the (statistical) recognition of trends. Information about the sampling and the analysis techniques used, if available in the literature, reports or archives, was included in the database.

To have an idea of the overall quality of the data, the Chemical Balance Error (CBE) is calculated for all samples in the dataset that contain the necessary information required. Samples with an absolute error of >10% in the CBE were discarded for the interpretation. Out of the 118 samples, only 64 samples contain the full set of necessary parameters to calculate the CBE. 59 of these samples have a CBE error below the 10% threshold and are used for geochemical interpretation.

Figure 1. Charge Balance Error statistics report for the dataset of the Campine Basin.

```
============================================================
CHARGE BALANCE ERROR (CBE) STATISTICS REPORT
============================================================

Total samples with CBE: 64
CBE range: -22.13% to 9.79%
CBE mean: -1.26%
CBE standard deviation: 5.07%
CBE median: -0.08%

Samples with |CBE| ≤ 10%: 59 (92.2%)
Samples with |CBE| > 10%: 5 (7.8%)


Samples with |CBE| > 10% (n=5):
------------------------------------------------------------
  Sample 117 (Beerse-GT-01a): CBE = -10.03%
  Sample 72 (VITO Geothermal): CBE = -10.37%
  Sample 77 (VITO Geothermal): CBE = -10.55%
  Sample 70 (VITO Geothermal): CBE = -12.73%
  Sample 63 (VITO Geothermal): CBE = -22.13%
```

54 samples (46% of the dataset) lack some information to perform standard CBE assessment. In some cases, the reason for missing information is clear. For the samples of the Peer well, not all cations are reported for most of the samples. Samples used for the quantification of radioisotopes require specific measurements, where no standard geochemical parametrisation is performed. Discarding these samples would strongly limit the data available for interpretation. Therefore, it was decided to retain the samples without CBE values in the discussion. Apparent outliers, that can or cannot be explained, are excluded on the level of individual parameters. Individual analytical results that are changed or discarded for interpretation are documented, rather than changed in the original dataset. An overview of corrected and discarded analytical results is provided in Table 6.

Table 6 Overview of corrected and discarded analytical results of individual parameters in the Campine Basin dataset.

Well	Sample_id	Parameter	Original value (mg/l)	Corrected value (mg/l)	Correction factor	Reason
Peer	1	Rb	0.02366			Inexplicable outlier – excluded from interpretation
Peer	1	Mg	22.85			Inexplicable outlier – excluded from interpretation
VITO Geothermal	80	Sr	3860	386	0.1	Reporting error – divided by 10
VITO Geothermal	80	B	276	27.6	0.1	Reporting error – divided by 10
VITO Geothermal	68	Li	42.5			Inexplicable outlier – excluded from interpretation
VITO Geothermal	70	Li	13.1			Inexplicable outlier – excluded from interpretation
VITO Geothermal	71	SO4--	988			Inexplicable outlier – excluded from interpretation
VITO Geothermal	109	Sr	602			Inexplicable outlier – excluded from interpretation
Merksplas-Beerse I	52	Br	320			Uncertainty about reported parameter - excluded from interpretation
Merksplas-Beerse I	53	Mg	1700			Inexplicable outlier – excluded from interpretation
Beerse-GT-01a	104	Br	266			Inexplicable outlier – excluded from interpretation
Beerse-GT-01a	117	Cl	93000			Measurement error – excluded from interpretation

A specific feature of the dataset for the Campine Basin is the number of repetitive samplings on specific locations. This often results in a range of parameter values. The range is a representation of different factors. It can reflect changes over time in the water extracted from the subsurface. This can either reflect different stages in the development of a project or changes within the reservoir. However, it also reflects the difficulty of sampling deep formation waters (e.g., location of sampling, changes in temperature and pressure, degassing) as well as of parameter measurement. Measuring minor and trace elements in brines with a high NaCl content is complex. It requires dilution of the samples which results in lower precision. It is, in the scope of this study, not possible to make a distinction between the reasons for different measurement results in a single well over time.

3.2 SPATIAL DISTRIBUTION

In the Campine Basin, groundwater data providing information on the composition of the brine in the lower Carboniferous limestones is available for 9 wells (Table 7). The full dataset is available in digital appendices 1 (longtable) & 2 (GIS-file). There are 5 wells from Fluxys in the northern part of the Antwerp Campine (Loenhout region), labelled as DZH-wells. A bit further to the southeast, there is a

cluster of three wells: Merksplas-Beerse I (KB165), the old deep well in Turnhout (KB120) and the new Beerse-GT-01a well of the geothermal plant at J&J in Beerse. The last well with information on the lower Carboniferous Limestone reservoir is located more to the southeast, in Mol, at the geothermal plant from VITO (MOL-GT-01).

Table 7. Overview of the different wells in the Campine Basin with information on the geochemistry of the deep formation waters, including the number of samples available per well.

Name	DOV	X	Y	Z	Total depth	Top reser-voir	#
VITO-Geothermal	https://www.dov.vlaanderen.be/data/boring/2016-148767	201783	212961	25	3610	3175	36
DZH4	https://www.dov.vlaanderen.be/data/boring/1980-044203	174629.1	228593.6	26	1356	1240	1
DZH14	https://www.dov.vlaanderen.be/data/boring/1989-083067	175587.4	227348.6	26.9	1407.5	1320	1
DZH15	https://www.dov.vlaanderen.be/data/boring/1990-042943	172063.5	228538.7	22.8	1390	1330	1
DZH23	https://www.dov.vlaanderen.be/data/boring/2022-189177	172101	229919	23.05	1572	1355	1
DZH24	https://www.dov.vlaanderen.be/data/boring/1995-042928	175059.8	230351.7	24.5	1551	1276	1
Merksplas-Beerse I	https://www.dov.vlaanderen.be/data/boring/1983-038292	181968	225865.4	29.5	1761	1630	8
Merksplas-Beerse II	https://www.dov.vlaanderen.be/data/boring/2016-124262	182015.3	225737.9	29	800	690	11
Turnhout	https://www.dov.vlaanderen.be/data/boring/1952-083175	190620	223850	29.63	2705	2174	2
Beerse-GT-01a	/	184850	222107	24	2835	1730	6
Peer	https://www.dov.vlaanderen.be/data/boring/1992-031722	224826	196069	75.36	1348	900	43

The second well in Merksplas-Beerse (Merksplas-Beerse II), which provides information on the Cretaceous reservoir in the region, is also included in the dataset. In the Eastern part of the Campine Basin, the Dinantian limestones are situated much deeper and no direct groundwater information from this reservoir is available. However, the Peer well (KB206) provides information on the composition in the Westphalian sandstone reservoir.

To extend the dataset on the Lower Carboniferous Limestone Group, data from the Netherlands is included (see 3.1.1). Although the Dutch wells were drilled in the context of geothermal projects targeting the lower Carboniferous limestone reservoir, production data indicate that part of the geothermal fluid comes from mixed carbonate and siliciclastic deposits that mark the transition to the underlying Devonian sandstones. For display purposes, the position data of the Dutch wells was converted from the Dutch RD (Rijksdriehoeksstelsel) coordinate system to the Belgian Lambert72 system. This was done making use of *gdaltransform* from the *gdal* geospatial library (in OSGeo4W Shell). Recalculation of ground level from Dutch NAP system to Belgian TAW system is also applied.

Table 8. Overview of the Californië wells in the Venlo region, including original RD coordinates and converted L72 coordinates.

Name	X_L72	Y_L72	Z_L72	Depth AH	TVD	Top Reser -voir	X_RD	Y_RD	#
CAL-GT-01	269737.92	236023.69	35.33	2730	2510.17	1486	203895	381599	1
CAL-GT-04	269163.82	237224.53	33.53	3037.2	2591.02	1576	203337.28	382807.38	5
CAL-GT-05	269167.01	237233.88	33.53	2433	2011.12	1357	203340.6	382816.69	1

Figure 2 shows the location of the different wells. Since the number of wells is limited and a single well often has multiple measurements, analysing and displaying the geochemistry based on location (i.e. on a map) is not the most informative option. Instead, representation of the geochemistry will be done based on diagrams. To ensure a good correlation with the geographic position of the wells, the same colour coding as used in Figure 2 will be maintained throughout the figures in this chapter as far as possible.

Figure 2. Location of the wells in the Campine Basin used in this study.

In terms of spatial distribution, other than the type of reservoir (lower Carboniferous limestones, Cretaceous chalk or Westphalian siliciclastic rocks), depth of the reservoir is the most obvious discriminating variable throughout the different wells. We explicitly use 'reservoir depth' instead of depth, because the exact sampling depth often is unknown. Some of the samples are actual downhole samples, but most of the samples were taken on or near surface during pumping tests or in surface installations like the geothermal plants in Mol or Beerse.

3.2.1 Relation between reservoir depth and major ions + minor ions Li and Sr

The main components Na^+ and Cl^- show an overall increase in salinity related with depth of the reservoir, as to be expected. The water from the Cretaceous reservoir in Merksplas-Beerse II is significantly less saline than the water of the Westphalian reservoir in Peer. Age of the reservoir plays a role in the salinity as well. The salinity in the CAL-GT wells is significantly lower than in the lower Carboniferous reservoir in the Belgian part of the Campine Basin, when compared with the Loenhout and Merksplas region, where the depth of the reservoir is comparable. In the Belgian part of the lower Carboniferous limestone reservoir, there is an overall increase in salinity from north to south, correlating with an increase in depth of the reservoir. However, Na^+ and Cl^- values in the central part, i.e. in the Merksplas-Beerse I, Beerse-GT-01a and Turnhout wells are comparable, although reservoir depth is different, especially for Turnhout. The highest salinity values are recorded in the VITO Geothermal well. Remarkable is the extensive overall range for Na^+ and Cl^-. This is probably a cumulated effect of the number of measurements and of the pumping regime applied during operation of the geothermal plant in relation to the moment of sampling. We see a similar effect in other wells with multiple measurements.

a)

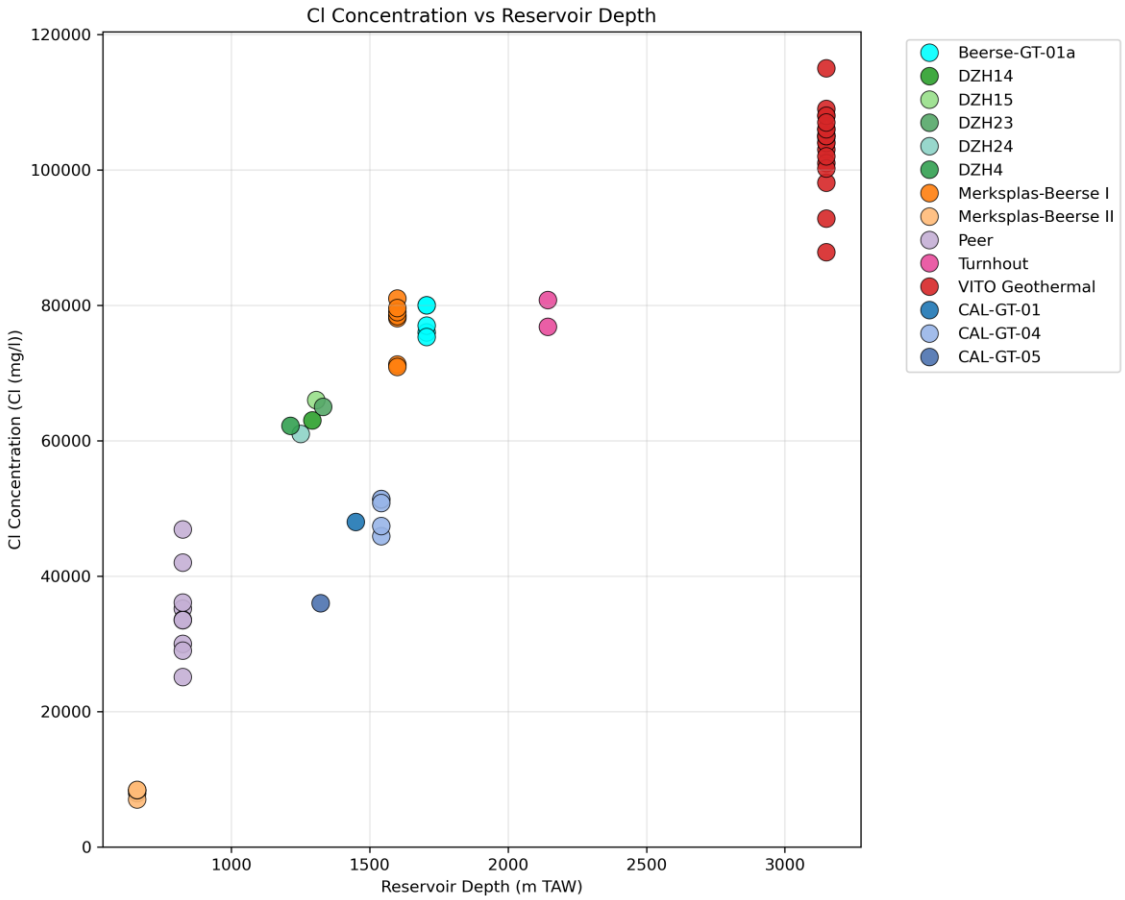

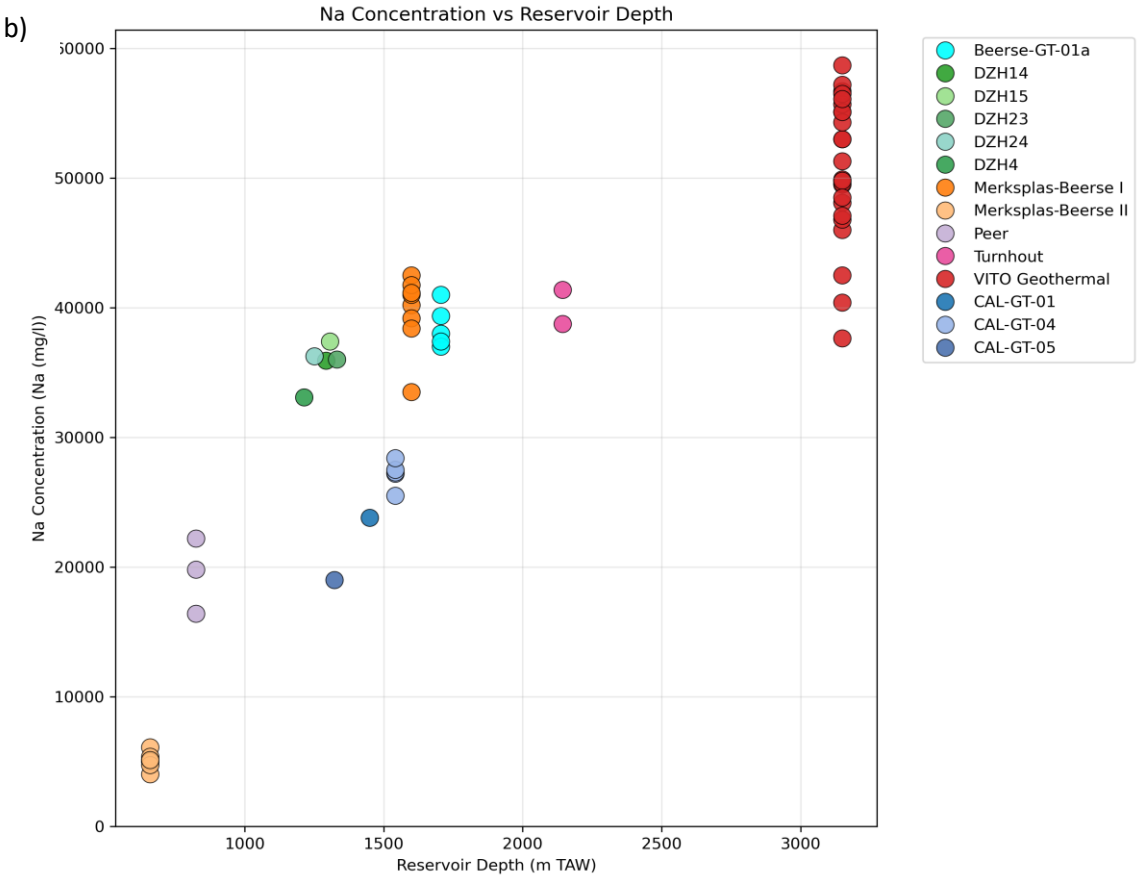

Figure 3. Concentrations of the main components versus reservoir depth: a) Cl^- and b) Na^+.

The concentrations of Ca^{2+} and Mg^{2+} are very low in Peer and Merksplas-Beerse I compared to the wells in the lower Carboniferous.

In the lower Carboniferous, Ca^{2+} shows a similar pattern as Na^+ and Cl^-: the CAL-GT wells display an overall lower trend, whereas in the Belgian part of the Campine Basin there is an overall increase from the north towards the south, with again comparable values for Merksplas-Beerse I, Beerse-GT-01a and Turnhout. In the Merksplas-Beerse I well, two samples plot significantly higher. Upon investigation, other parameters reported for these two samples also show deviated values. It is not clear what the exact reason for these differences is. Not much information is available on the sampling circumstances, but Vandenberghe (2000) reports that these samples are downhole samples retrieved after nitrogen lifting of the reservoir fluids for gas testing. This procedure might have had an effect on the sample composition.

Looking at the data for Mg^{2+}, the pattern is different. The CAL-GT wells have consistently lower values, but in the Belgian part of the lower Carboniferous reservoir, striking differences are visible. There is no overall increase in the Mg^{2+}concentration from the shallower part in the north to the deeper part of the reservoir more to the south. Values in the northern part are comparable overall, with no distinction between the Loenhout region (DZH wells) and the Merksplas-Beerse-Turnhout region. In the south, at the VITO Geothermal well, the Mg^{2+} values are lower than expected, based on the other main components and even lower than in the northern part of the reservoir.

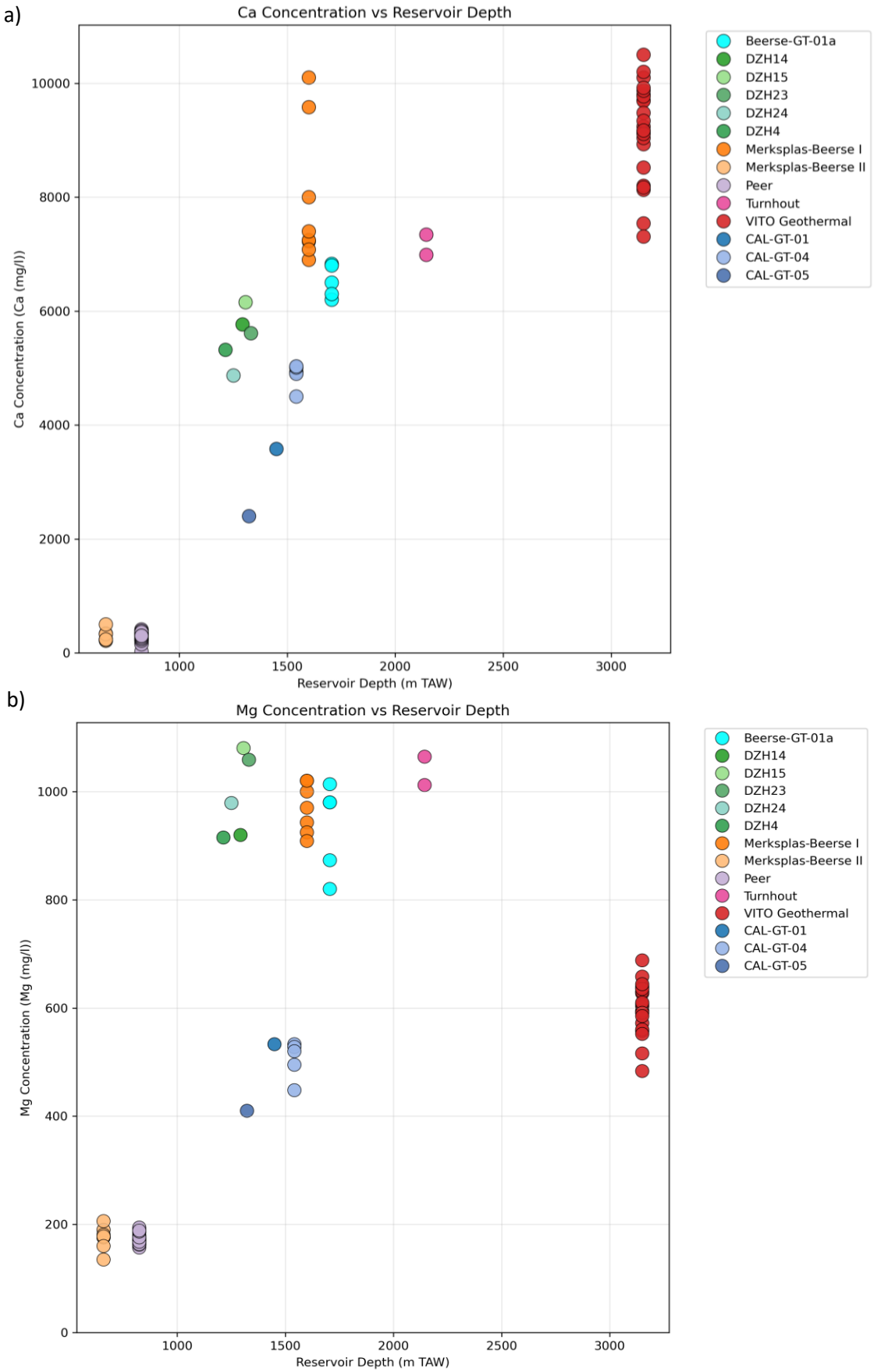

Figure 4. a) Ca^{2+} concentration versus reservoir depth, b) Mg^{2+} concentration versus reservoir depth.

Interesting minor elements with a good correlation with reservoir depth, which are present in quite substantial amounts are Li^+ and Sr^{2+}. Samples from the Cretaceous (information on Sr^{2+} only) and Westphalian reservoir tend to hold low values. In the lower Carboniferous limestones, information on Li^+ is limited to the DZH wells in the Loenhout region, Beerse-GT-01a and VITO Geothermal and a single measurement in the Venlo region. However, the overall trend seen in the main elements, i.e. an increase in concentrations with increasing reservoir depth also is present for Li^+. The range in the VITO Geothermal well is also significant. For Sr^{2+}, information in more wells is available. Again, the overall trend seems to fit that of the main elements: CAL-GT shows lower values than the Belgian part of the Campine Basin, the Loenhout region shows lower values than the Merksplas-Beerse region and the highest values are again found in the Mol region. Again, the range in any single well with multiple measurements is striking.

In the DZH wells, for Li^+ and Sr^{2+} the historical sample of DZH4 systematically has (much) lower values than the 4 samples of the sampling campaign performed for this project. It is possible that these differences are (partially) related to sampling depth. Whereas the new samples were taken at or very near to the reservoir (Figure 5), the DZH4 sample was taken at a shallower depth of 200m below surface, but the well is only open at the level of the Dinantian reservoir. The effect is noticeable in some of the other (main) components, but not in all of them. Some elements might be more prone to (co-)precipitate at shallower depths (pressures).

a)

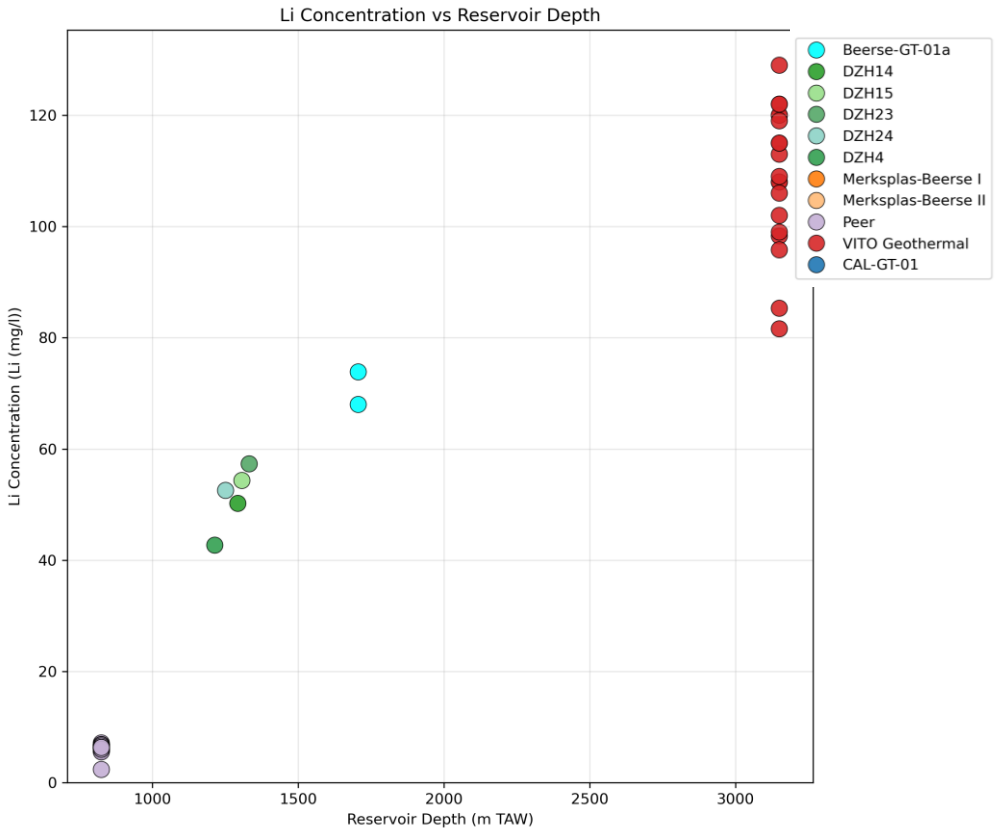

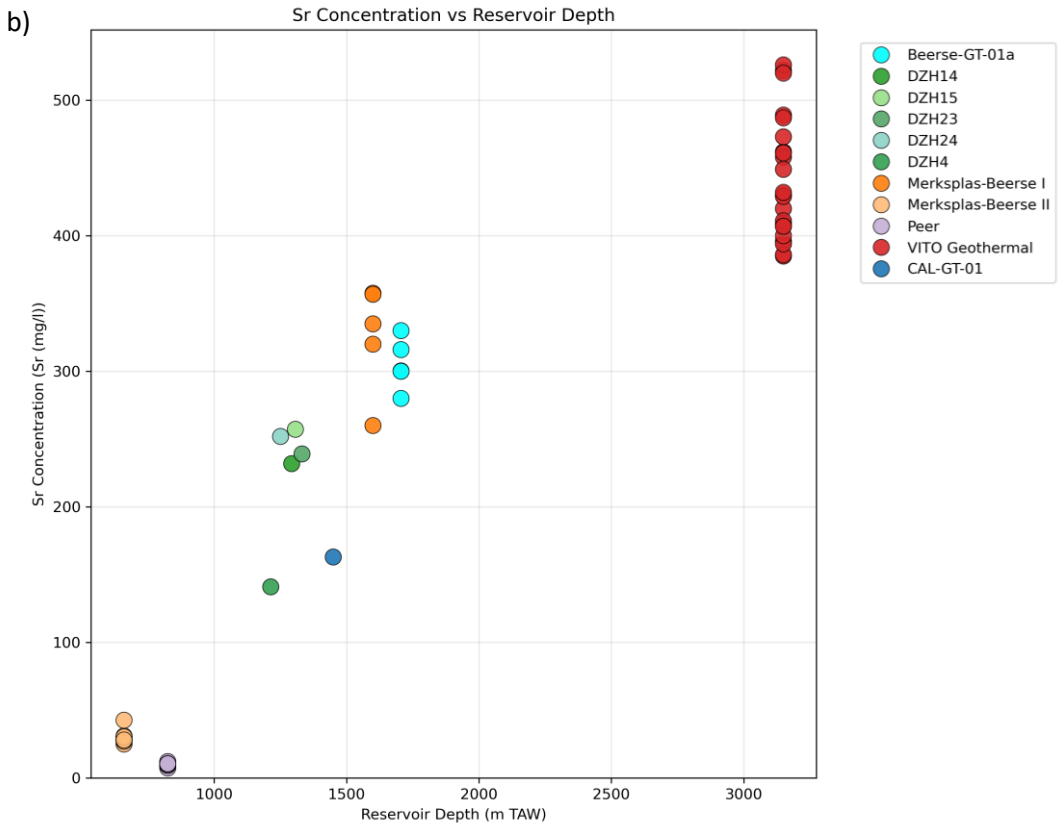

Figure 5. a) Li^{+} concentration versus reservoir depth, b) Sr^{2+} concentration versus reservoir depth

3.3 INTERPRETATION OF THE FORMATION WATER CHEMISTRY

3.3.1 Geochemical characteristics

Data on the major anions and cations is required to evaluate the general geochemical characteristics and to plot the samples on a Piper-diagram. In the dataset of the Campine Basin 29 samples out of 118 meet all the requirements to be plotted on a Piper-diagram. 49 samples have recorded values for Ca^{2+}, Mg^{2+}, Na^{+}, K^{+}, Cl^{-} and SO_4^{2-}. However, many of these samples lack information on HCO_3^{-} and/or CO_3^{2-}. Based on the HCO_3^{-}/Cl^{-}-ratio of the samples for which this data is available, the amount of data points can be increased since Cl^{-} is by far the dominant anion in all the samples. This ratio is usually below 0.01. This is the case for the samples in the Cretaceous reservoir, as well as for the wells in the lower Carboniferous reservoir that do have full information on all parameters. The only exception is found in Peer, where the ratio is around 0.08. This indicates a different origin of the groundwater extracted from the Westphalian in Peer than the one encountered in the Cretaceous and the lower Carboniferous reservoir. Therefore, assuming a HCO_3^{-}-value of zero for the samples without reported values on HCO_3^{-} does not significantly alter the anion composition and the resulting position on the Piper-plot. Applying this modification leads to a total amount of 57 samples plotted instead of the original 29. As a result, at least one sample of all the wells in the dataset is represented on the Piper-diagram.

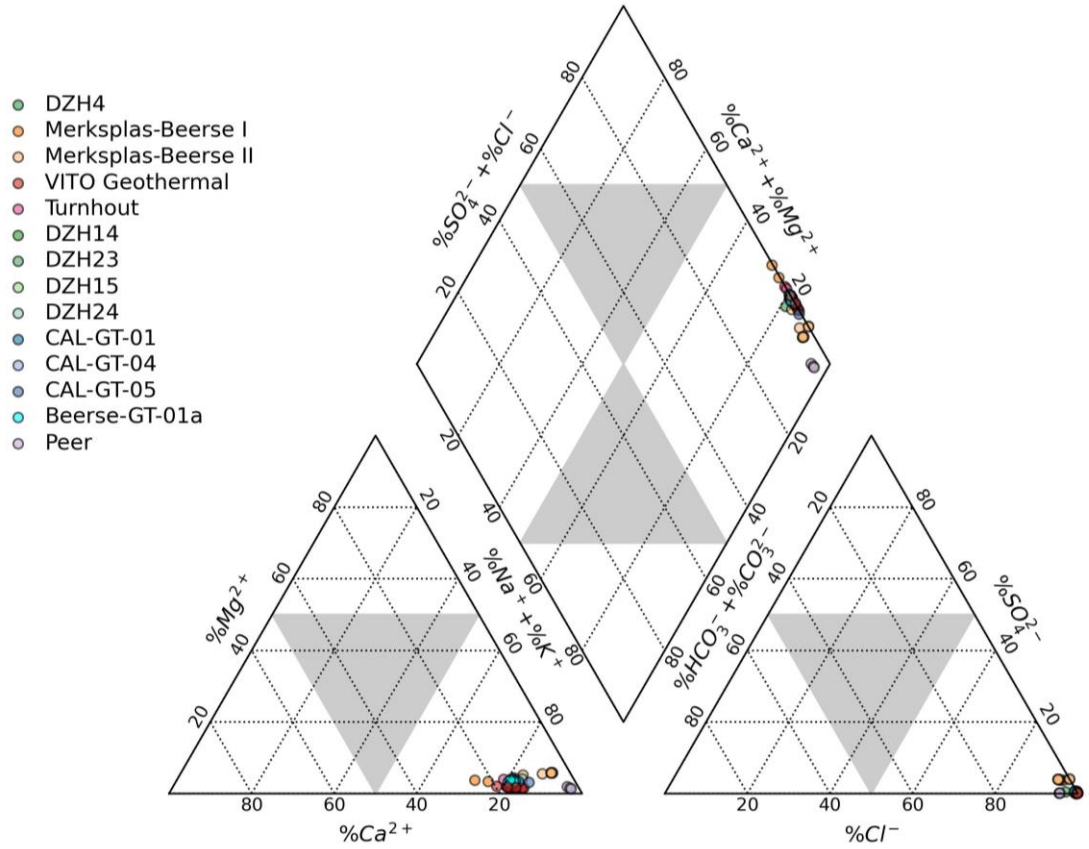

Figure 6. Piper-diagram of the groundwater data with a CBE error < 10%, modified for HCO3- in the Campine Basin (see text). All datapoints plot in the hypersaline NaCl-type zone. Piper-diagram courtesy of Yang et al., 2022.

The resulting Piper-diagram shows that the water in the deep reservoirs of the Campine Basin is of the sodium chloride type with Na^++ K^+ as dominant cations and Cl^- as dominant anion. The absolute values of these elements indicate that Na^+ and Cl^- are the main contributors. This is typical of (hyper)saline deep and old aquifers. In the Peer well, there is very little contribution of Ca^{2+} and Mg^{2+}, which is consistent with a siliciclastic reservoir. In the Cretaceous and lower Carboniferous reservoirs, there is significant contribution of Ca^{2+} and Mg^{2+}, and (in line with section 3.2.1) Mg^{2+} is slightly less important in the VITO Geothermal well compared to the rest of the wells.

In the Stuyfzand-classification a water type is determined based on 4 components: the Cl-content, alkalinity, the most important cation and anion and the [Na + K + Mg]-value corrected for the contribution by sea salt (Stuyfzand, 1989). Although the classification was initially developed for coastal aquifers with cation exchange, it can be applied to other aquifer systems as well. The 4 components of the code provide a direct picture of salinity, alkalinity and the extent to which the water composition is determined by cation exchange and/or water-rock interactions. For the deep formation waters discussed here, alkalinity and the [Na + K + Mg] excess term are diagnostic for possible water-rock interactions.

The classification for the analysed formation waters is given in Table 9. For the formation water from Turnhout and Loenhout (DZH wells) the Stuyfzand-code could not be established due to the lack of HCO_3^- and CO_3^{2-} data and the lack of reliable pH values.

Table 9. Stuyfzand-classification and calcite saturation index for the studied formation waters from the Campine Basin.

Well name	Reservoir	Stuyfzand-code	Alkalinity subcode	Na+K+Mg excess	SI calcite
Merksplas-Beerse II	Cretaceous chalk	b3-NaCl. to b2-NaCl-	2 – 3	-2 – -24	0.2 – 0.9
Peer	Westphalian siliciclastic rock	H6-NaCl-	6	-27 – -28	-0.35 – 0.1
Merksplas-Beerse I	lower Carboniferous limestone	H4-NaCl-	3 – 4	-444 – -560	-0.3 – 0.6
Beerse-GT-01a	lower Carboniferous limestone	H3-NaCl-	3 – 4	-379 – -690	-0.1 – 0.2
MOL-GT-01	lower Carboniferous limestone	H3-NaCl-	2 – 5	-520 – -972	-0.2 – 0.3
CAL-GT-01	lower Carboniferous limestone	H3-NaCl-	3	-331	0.1
CAL-GT-04	lower Carboniferous limestone to Devonian sandstone	H3-NaCl-	3	-236 – -266	-0.03 – 0.01
CAL-GT-05	lower Carboniferous limestone to Devonian sandstone	H3-NaCl-	3	-151	-0.4

Alkalinity reflects the sum of bases that can neutralize acids. In most natural waters, carbonate species are the major contributors, and alkalinity is given by:

$$TA \approx [HCO_3^-] + 2 \times [CO_3^{2-}] + [OH^-] - [H^+]$$

For most natural waters with a pH in the range of 4.5 to 9.5, alkalinity hence is approximately equal to the sum of HCO_3^- and CO_3^{2-} (eq/l). For samples from the deep reservoirs, degassing during or after sampling affects the pH, HCO_3^- and CO_3^{2-} measurements. Reliable data is only obtained from pressurized (downhole) samples. However, a large shift in alkalinity is only to be expected in case degassing also results in the precipitation of carbonate minerals. Given the pH range of the deep brines (5.4 to 6.8), HCO_3^- is not expected to change much due to degassing in case no precipitation takes place. Except for Merksplas-Beerse II, SI values are below or near 0. Calite precipitation therefore cannot be ruled out but often a certain degree of supersaturation (SI ≥ 1) is necessary to initiate precipitation.

Stuyfzand (1989) presents the [Na + K + Mg] excess term as a proxy for cation exchange due to the in- or extrusion of salt groundwater. In case of salt groundwater ingress, Ca^{2+} is released by cation exchange resulting in a [Na + K + Mg] deficit relative to mean ocean water (Stuyfzand, 1989). However, other processes also affect the [Na + K + Mg] excess term. Dissolution of minerals containing Na, K, Mg or calcite precipitation will result in a surplus, whereas dolomitization or the precipitation of silicates can lead to a deficit of [Na + K + Mg].

3.3.2 Major and minor cations

To get an idea about the origin of the formation water and the processes that affected its composition, both the concentrations of conservative ions like Cl^- and Br^- and the excess or deficit of major cations with respect to reference brine are informative (Stuyfzand, 1989; Fontes & Matray, 1993a & b). In the following discussion seawater is used as the reference brine. During the early stages of seawater evaporation, Na^+, Cl^- and Br^- behave conservatively, meaning that their molar contents increase

proportionally as the seawater becomes more concentrated. Chemical data from different stages of seawater evaporation is given by Fontes & Matray (1993a). They used the concentrations of conservative elements and element ratios and mixing models to derive the origin and formation of brines from the Paris Basin.

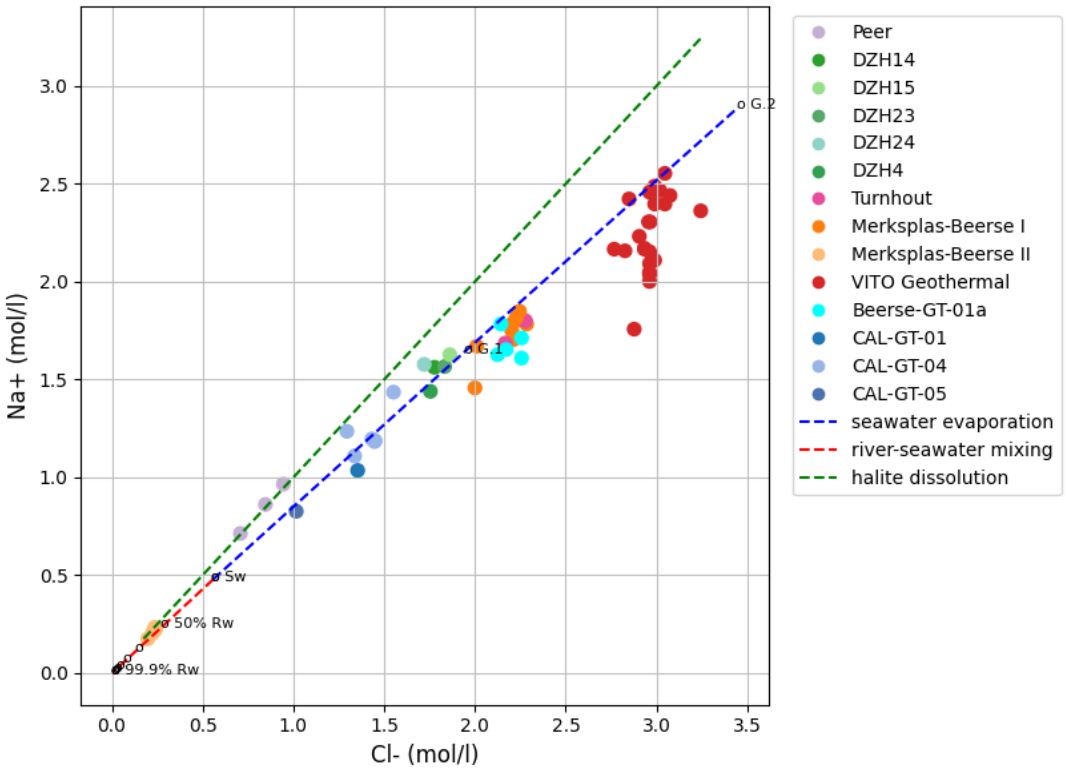

Figure 7. Na^+ versus Cl^- plot for deep water samples of the Campine basin. The labelled dots on the seawater evaporation line correspond to the stages discussed in Fontes & Matray (1993a).

The approach of Fontes and Matray is complementary to the use of the seawater corrected Na+K+Mg factor of the Stuyfzand-classification. Other seawater corrected excess/deficit factors can be defined to get an understanding of the process that affected the composition of the formation waters. The seawater-corrected Ca^{2+} concentration can be used to evaluate the effect of interaction with carbonates. Dolomitization will result in a correlated increase in Ca^{2+} and decrease in Mg^{2+}. The seawater-corrected K^+ concentration will be determined by processes like illitisation (K^+_{corr} deficit), the alteration of K-rich minerals like K-feldspar or muscovite (K^+_{corr} excess) or cation exchange. Deviation of the Na^+ concentration from the evaporation trend may indicate cation exchange, the formation of Na-containing clay minerals, zeolites and albite (Na^+_{corr} deficit) or the alteration of feldspars (Na^+_{corr} excess). As summary of the processes that may affect the cation balance is given in Table 10.

Table 10: Processes that may result in a deficit of excess of major cations in deep groundwater with respect to seawater.

Process	Minerals formed	Deficit/Excess
Dolomitisation	dolomite	Mg^+_{corr} deficit
Illitisation	illite, quartz	K^+_{corr} deficit
Alteration of plagioclase	kaolinite (, calcite)	Ca^{2+}_{corr} deficit
Alteration of Na,K-feldspars	clay minerals, quartz	K^+_{corr} excess, Na^+_{corr} excess
Alteration of muscovite	clay minerals, quartz	K^+_{corr} excess
Alteration of volcanic glass	zeolites, smectite, albite	Na^+_{corr} deficit (K^+_{corr} deficit)
Albitisation	albite	Na^+_{corr} deficit
Cation exchange		deficit/excess of specific cations

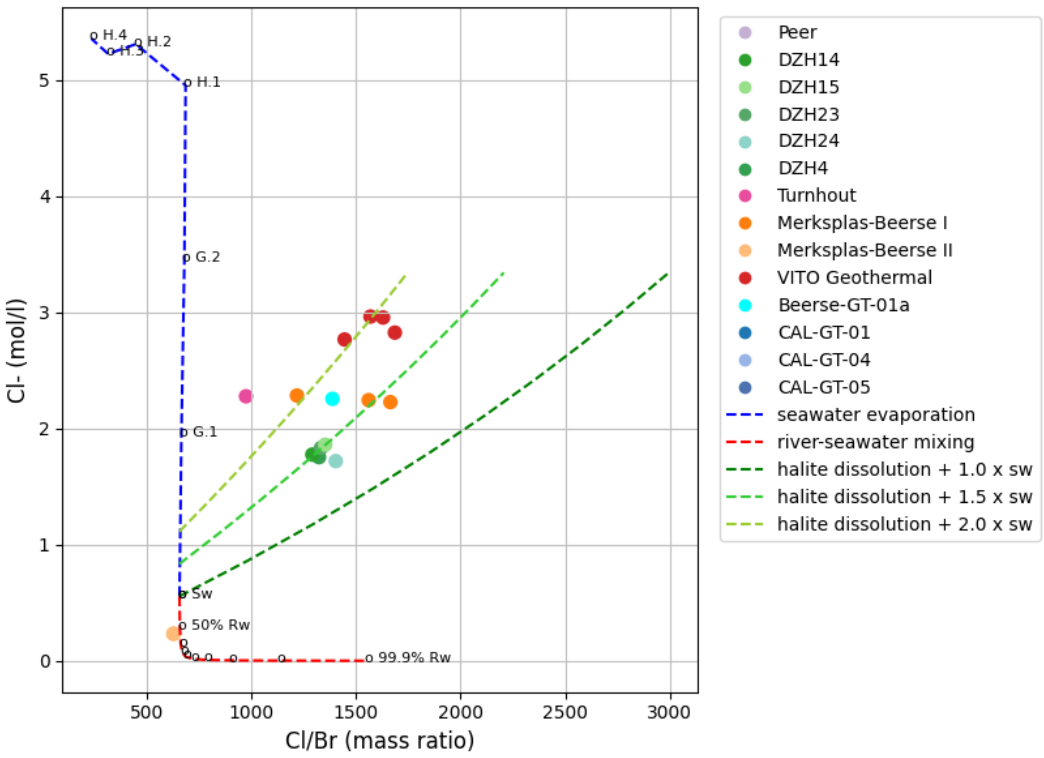

Figure 8. Plot of Cl^- versus Cl/Br for deep water samples from the Campine Basin. The labelled dots on the seawater evaporation line correspond to the stages discussed in Fontes & Matray (1993a). A Br^- content of 130 ppm of secondary halite was used to draw the halite – seawater mixing lines. 1.0 x sw, 1.5x sw and 2.0 x sw respectively stands for a fluid with a Cl^- and Br^- concentration that is 1, 1.5 and 2 times the concentration in seawater.

The concentrations of Na^+ and Cl^- in the samples from Campine Basin vary between 0.35 and 5.5 times the average concentration in seawater. The samples of the Lower Carboniferous Limestone Group plot along the seawater evaporation trend (Figure 7). The samples from Beerse, Turnhout and Mol have a Cl^- concentration that is above the concentration at which gypsum precipitates (point G.1 on Figure 7). Primary gypsum deposits have not been reported from the Campine Basin. Therefore, the high concentrations most likely do not reflect a hypersaline primary brine. It is more likely that the lower Carboniferous formation water is a diagenetically dehydrated seawater brine. Processes that lead to dehydration include water-mineral hydration reactions (e.g., the alteration of feldspar, illitisation, chloritization), osmotic water transfer, steam loss and radiolysis. The last process involves the splitting of H_2O into H_2 and oxygen radicals by radiogenic elements such as U and Th.

Alternatively, the brine composition can be the result of mixing of a seawater derived primary brine with a highly evolved basement brine. The ratio of the conservative elements Cl^- and Br^- can be used to distinguish between primary and secondary brines (Fontes & Matray, 1993a). The molar Cl/Br-ratio of seawater is about 650 and is considered not to have changed significantly over time (Kaufmann, 1999). The precipitation of halite causes fractionation of Cl^- and Br^-, which results in a decrease of the ratio within the residual brine (see points H.1 to H.4 in Figure 8 the labelled dots correspond to the seawater evaporation stages given in Fontes & Matry, 1993a). Consequently, Br^- concentrations in halite tend to be low (Br^-: 20 – 300 ppm, $\{Cl/Br\}_{mol}$: 4550 – 68000; Fontes & Matry, 1993a, Sun et al., 2019). Brines that originate from the dissolution of halite, so called secondary brines, therefore have Cl/Br-ratios higher than 650.
The Cl/Br-ratio of the samples from the Lower Carboniferous Limestone Group range from 974 to 1685. These values point to a contribution of a secondary brine. It is likely that the brine is a mixture of (slightly dehydrated) primary seawater and a secondary brine that has been enriched in Cl^- due to dissolution of halite and/or other Br-depleted salts like sylvite (KCl) and sylvinite ($NaKCl_2$) (Figure 8).

The Cretaceous samples from Merksplas-Beerse II plot on the mixing line between seawater and river- or rainwater at a fresh-over-seawater ratio of about 1.4 (Figure 7). The Cl/Br-ratio is line with such mixing (Figure 8).
The samples from Peer plot along the halite dissolution line (Figure 7). This suggests that this brine primarily has a secondary origin. As no Br^- data is available, this hypothesis cannot be verified.

Figure 9a shows the balance of the sum of the major cations over the concentration of Cl^- with respect to seawater. All samples are depleted in Na+K+Mg with respect to seawater. For the Cretaceous samples, the sum of Na^+, K^+, Mg^{2+} and Ca^{2+} is close to the trend for the mixing of seawater and river water. The slight depletion of Na+K+Mg can point to cation exchange. As it is a chalk reservoir, the formation water is expected to be Ca-dominated and Na-depleted relative to non-carbonate systems. The samples of the Lower Carboniferous Limestone Group are depleted in Na+K+Mg with respect to seawater. The Na+K+Mg unbalance is partly compensated by an excess of Ca^{2+} (Figure 9b and Figure 10a). The unbalance increases with the Cl-content. Mixing of a seawater derived brine with a chlorine-rich secondary brine indeed would result in an increase of the Na+K+Mg(+Ca) depletion with increasing Cl-content (green dashed lines in Figure 9). However, the observed trend is stronger than expected. When the cations are plotted separately against Cl^-, the Na+K+Mg deficit appears to be a consequence of groundwater depletion in Na^+ and Mg^{2+} (Figure 7, Figure 10). Given the paragenesis of the Lower Carboniferous Limestone Group, dolomitization is likely responsible for (a large part of) the Mg^{2+}_{corr} deficit. Possible causes for the Na^+_{corr} deficit include the formation of Na-bearing minerals through the weathering of volcanic glass, albitization, the formation of authigenic albite (Cuadros et al., 2013; Hofmann & Sherry, 2025; Wu et al., 2022), or a relative undersaturation of the deep brine due to cation exchange. The increasing unbalance with depth can point to an intensification of these processes with depth (Figure 3).

Mg^{2+} is depleted in all samples (Figure 10b). The depletion increases with Cl-concentration. This can indicate progressive removal of Mg^{2+} from the brine, e.g., due to cation exchange, the incorporation of Mg^{2+} in carbonates (Mg-calcite, dolomite) or phyllosilicate (chloritization) and/or mixing of a seawater derived brine with a Mg-depleted secondary bine.

The trend in K^+ suggests that dissolution of K-rich minerals (mica, feldspars) also contributes to the chemistry of the lower Carboniferous brine (Figure 10c). In the Cretaceous samples, as well as in the samples from the upper Carboniferous (Peer and one of the samples from Turnhout), K^+ is depleted with respect to seawater, which can indicate suppression by cation exchange and/or halite dissolution. The Na^+ concentrations measured on samples from the VITO geothermal site span a large range (Figure 7). The samples were collected over a period of over nine years. Most samples were taken at a sample point at surface before the heat exchangers when the geothermal plant was in operation. The dataset also includes analyses of downhole samples. There is no systematic difference in Na^+ concentration between the downhole and surface samples, nor is there any difference between analyses from different laboratories. Therefore, the variation cannot be attributed to differences in sampling or the analytical method used. Although the dataset does show no clear trend over time nor with flow rate or production time, the spread in Na^+ concentration can therefore indicate differences in composition of the pumped water.
Na^+ depletion of the samples of the VITO geothermal site on average is larger than for the other sampling locations of the lower Carboniferous reservoir. This points to differences in water-rock interactions. A possible cause of this difference is co-precipitation of authigenic albite and dolomite in the carbonate reservoir. Two models have been defined to explain the co-precipitation of albite and dolomite in carbonates. The first relates to metasomatic processes involving the migration of deep NaCl-rich basement fluids in open systems (Hofmann & Sherry, 2025; Spötl et al., 1999). The second

links the co-precipitation to iso-chemical processes with ions supplied by trapped formation waters or through mineral transformation during burial diagenesis in closed systems.
Both models are plausible for the lower Carboniferous in the Campine Basin. On the one hand, a hydrothermal influence in the deeper reservoirs cannot be ruled out given the indication of mixing of evolved seawater with a basement brine. On the other hand, the reservoir at the VITO geothermal site consists of finely bedded limestones and thin clay-rich layers and is in direct contact with fine-bedded, clay-rich carbonates of the Goeree Formation (Van Der Voet et al., 2020). Hofmann & Sherry (2025) identified thin clay mineral rich interbeds as a first-order control on the formation of authigenic albite and dolomite in a fine-grained, low-permeability carbonate system. These assumptions can be verified by a comparative diagenetic study of the lower Carboniferous at the different locations.

a)

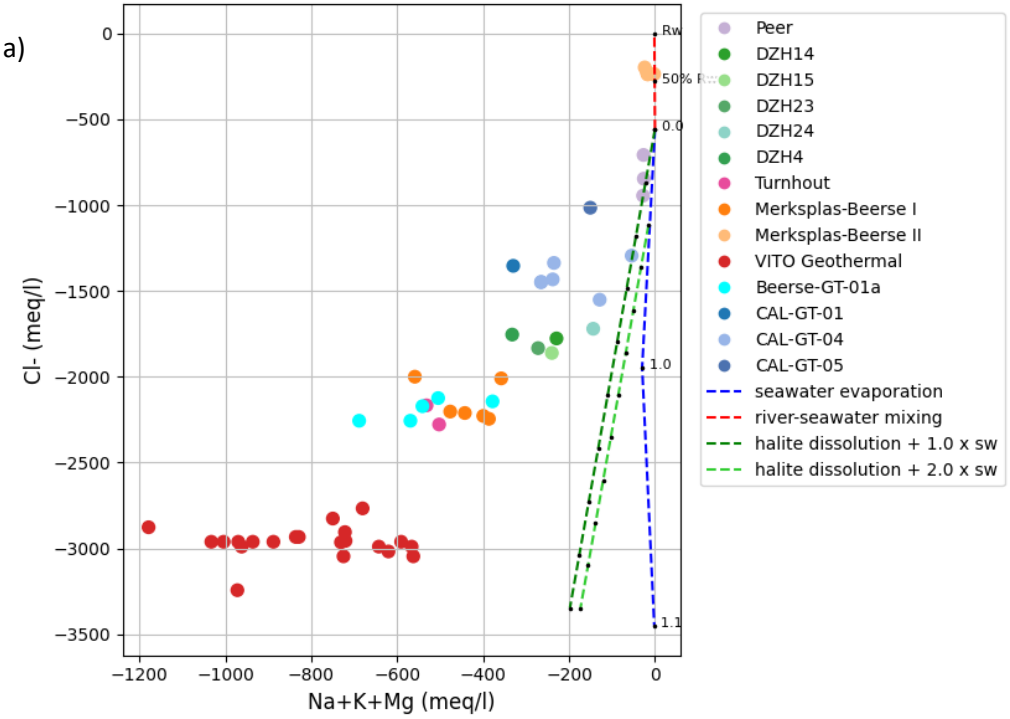

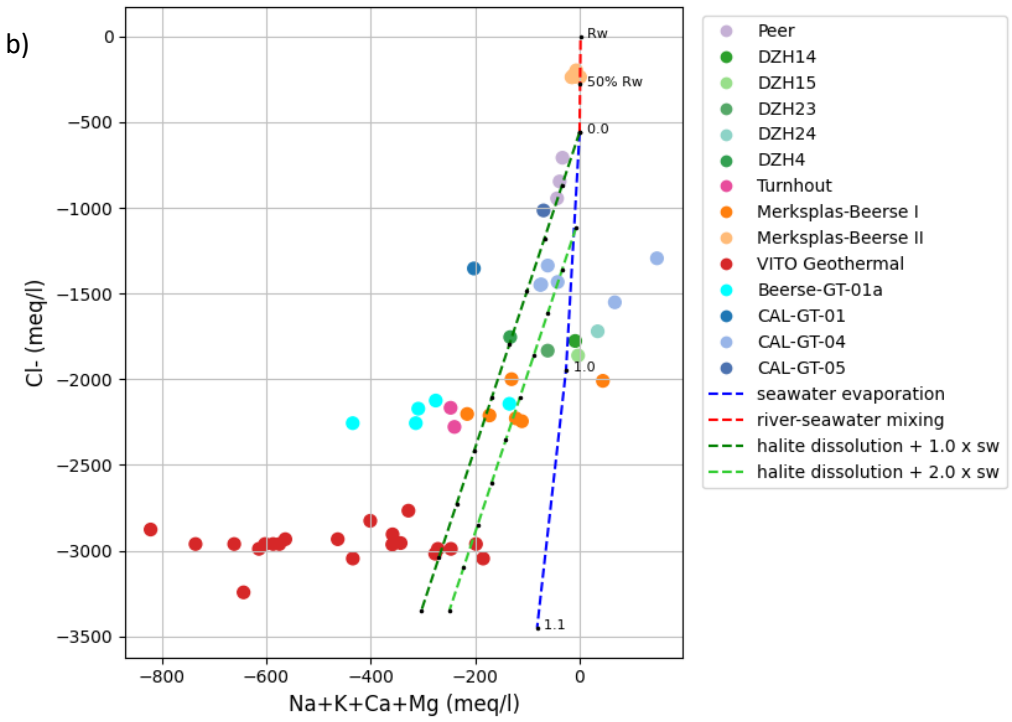

Figure 9. Plot of the seawater corrected a.) Na+K+Mg concentration and b.) Na+K+Mg+Ca concentration for deep water samples from the Campine Basin.

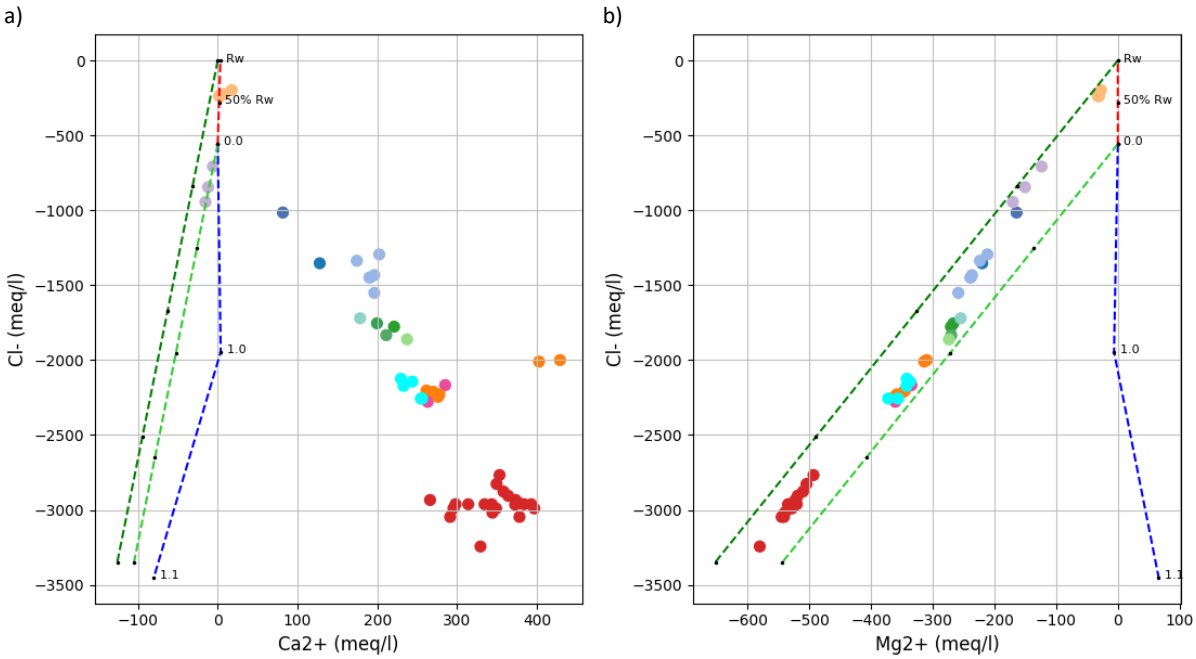

c)

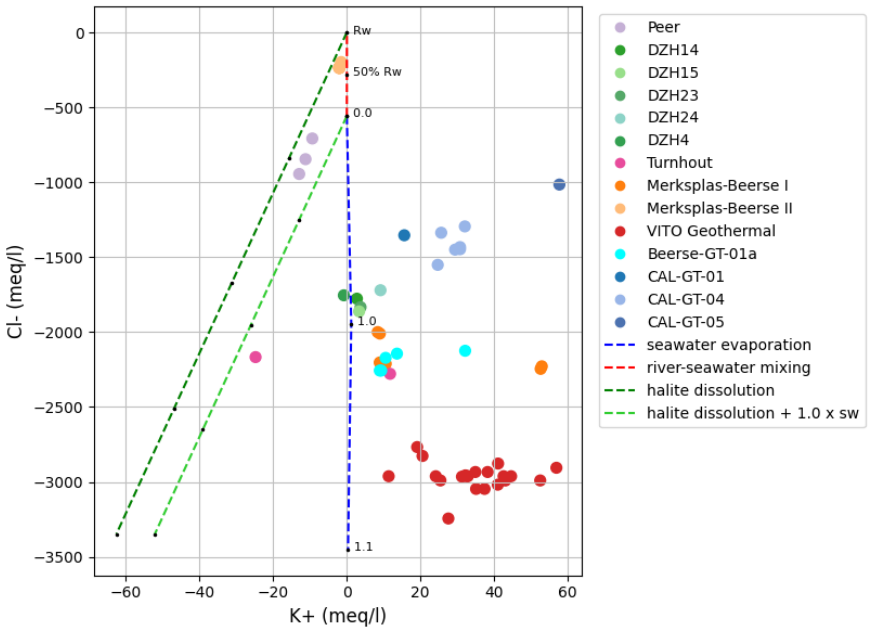

Figure 10. Plot of seawater corrected a) Ca concentration b) Mg concentration and c) K concentration for deep water samples from the Campine Basin.

3.3.3 Geothermometers

Reservoir temperatures were calculated using different chemical geothermometers:

- The Na/K-geothermometers published by Truesdell (1976) and Fournier (1979, 1981).
- The improved Na/K-geothermometer derived by Verna (1997).
- The Mg-corrected Na+K/Ca-geothermometers (Giggenbach, 1988; Kharaka and Mariner, 1989).
- The SiO_2-geothermometers for quartz and chalcedony (Fournier, 1981).
- The Na/Li- and Mg/Li-geothermometers (Verna and Santoyo, 1997)

The SiO_2- and Na+K/Ca-geothermometers were corrected for the high salinity of the water samples and reservoir pressures and temperature using the procedure given in Kharaka and Mariner (1989).

In the figures below, the calculated temperatures are compared with the maximal bottom hole temperature (BHT) and maximal production temperature reported for the sampled wells. As no correction for temperature loss in the wellbore is applied, the production temperatures should be regarded as minimal reservoir temperatures. Maximal burial temperature for the Westphalian and lower Carboniferous has been substantially higher than the actual reservoir temperature (Van Keer et al., 1998; Helsen and Langenaeker, 1999; Ferket, 2007).

The Mg-corrected Na+K/Ca-geothermometer (Figure 11) as well as the SiO_2-geothermometers (Figure 12) give rock-water interaction temperatures that are in line with the observed BHT and production temperatures. The correlations suggest that the brine composition is largely consistent with water-mineral interaction within the reservoir of which the water sample was extracted.
The Na+K/Ca-geothermometer is sensitive to variations in the CO_2 and Ca^{2+} content of the brine. It assumes equilibrium of the brine with a mineral assemblage containing feldspar, illite, calcite and SiO_2 (Giggenbach, 1988). It is affected by degassing in case calcite precipitation occurred. The SiO_2 geother-mometers are derived from the solubility of quartz and chalcedony at the vapor pressure of the

solution in the temperature range from 0°C to 250°C. At temperatures below about 110°C, chalcedony tends to control the dissolved silica concentrations, whereas the solubility of quartz is the controlling factor at temperatures above 180°C. In the intermediate temperature range, the silica content is controlled by the dissolution of the present SiO_2-mineral(s). In case of the Lower Carboniferous Limestone Group, chert (microcrystalline quartz) and quartz are the dominant SiO_2-polymorphs.

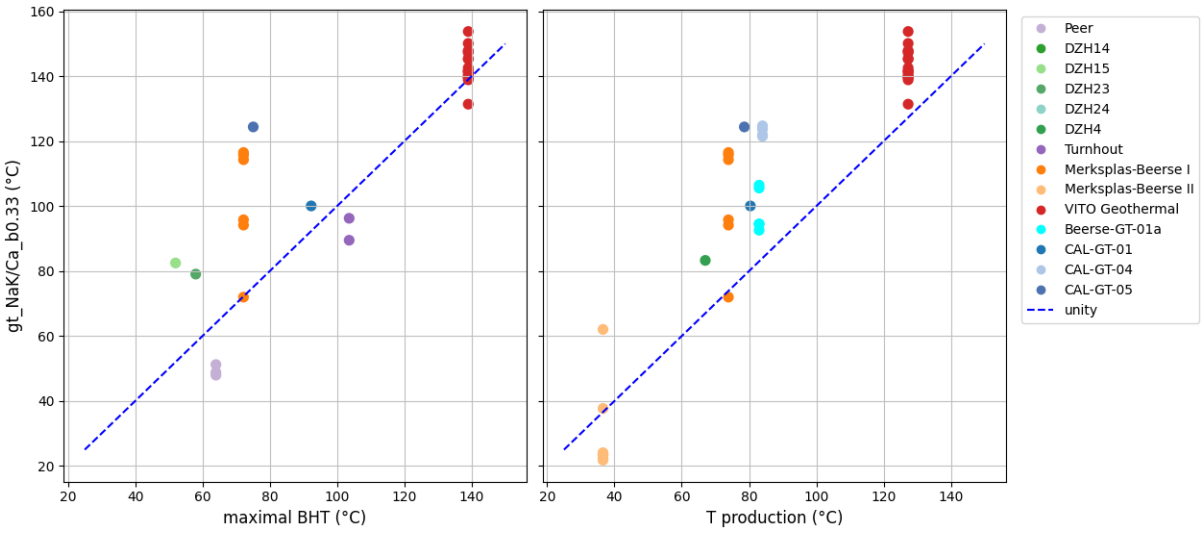

Figure 11. Mg-corrected Na+K/Ca-geothermometer versus recorded maximal BHT and production temperature.

a)

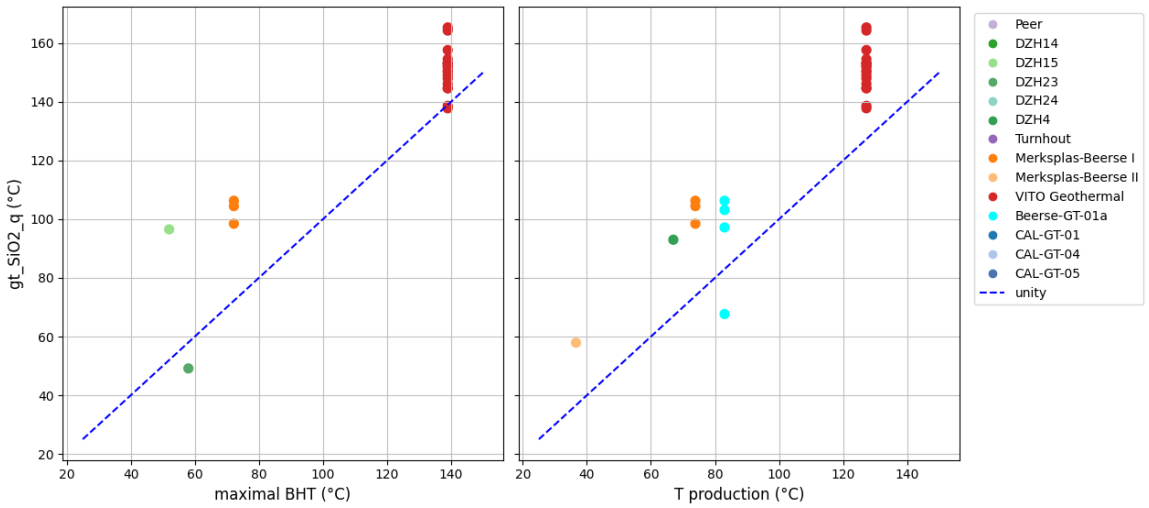

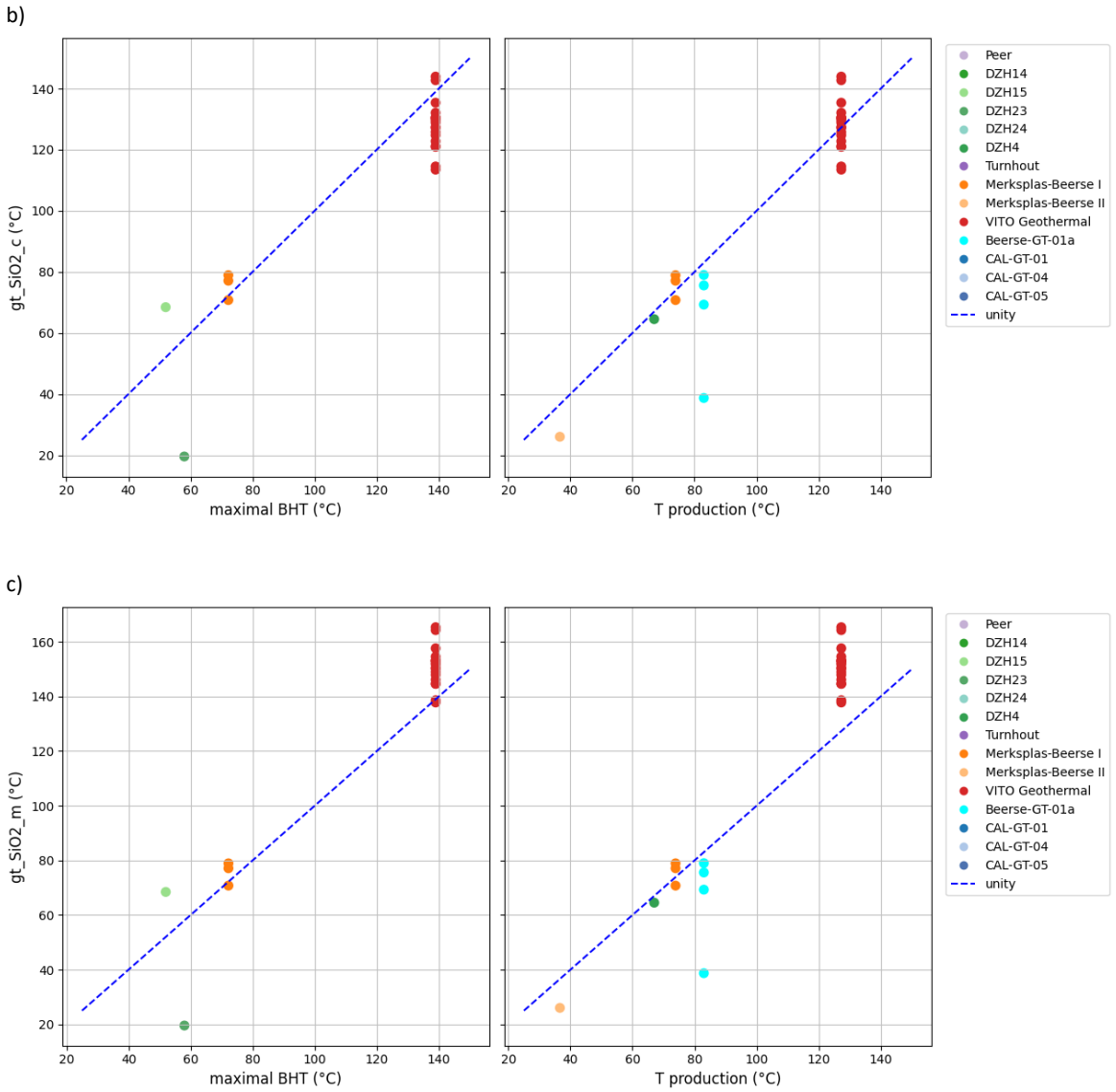

Figure 12. SiO_2-geothermometer versus recorded maximal BHT and production temperature based on a) quartz dissolution, b) chalcedony dissolution, and c) mixed chalcedony - quartz dissolution.

The other geothermometers give equilibrium temperatures that are above the reported BHT and production temperatures. The temperatures for the samples of the Lower Carboniferous Limestone Group calculated using the Ca/Mg-geothermometer are 10 to 30°C higher than the maximal BHT (Figure 13). This points to a Ca/Mg-ratio that is higher than expected for the present reservoir temperature. This deviation is in line with the seawater corrected trends in Mg^{2+} and Ca^{2+} discussed above.

The Na/K- and Mg/Li-geothermometers point to an equilibrium temperature of 150 – 200°C for the lower Carboniferous, the Na/Li-geothermometer of 250 – 300°C (Figure 14, Figure 15). The difference between the sample locations is limited. The high estimates are due to lower Na/K-, Mg/Li- and Na/Li-ratios than expected for the present reservoir temperature. The absence of a clear trend with the reported BHT and production temperatures indicates that these ratios are not or only to a limited extent determined by the current reservoir temperature.
At temperature above 150°C, the ratio of Na^+ over K^+ in geothermal waters is due to ion exchange with co-existing alkali feldspars and interaction with clay minerals. The rate of re-equilibration of the Na-K

exchange is slower than the silica dissolution-precipitation and K-Mg exchange equilibrium (Nicholson, 2012). In that sense the maximal equilibration temperature is better preserved by the Na-K-geothermometer than by the SiO_2- and Na+K/Ca-geothermometers. The reactions underlying the Li-geothermometers are less well understood. They likely involve interaction of groundwater with clay minerals, mica, pyroxenes and amphiboles (Kharaka & Mariner, 1989; Verma & Santoyo, 1997). The main process leading to re-equilibration at lower temperatures is cation exchange. Moreover, the Mg/Li-geothermometer will be affected by the precipitation or dissolution of dolomite or Mg-calcite. Given the high Na^+ concentration of the groundwater and the low cation exchange selectivity of Li^+, Li-geothermometers are expected to be less affected by re-equilibration at lower temperatures than the SiO_2-and Na+K/Ca-geothermometers.

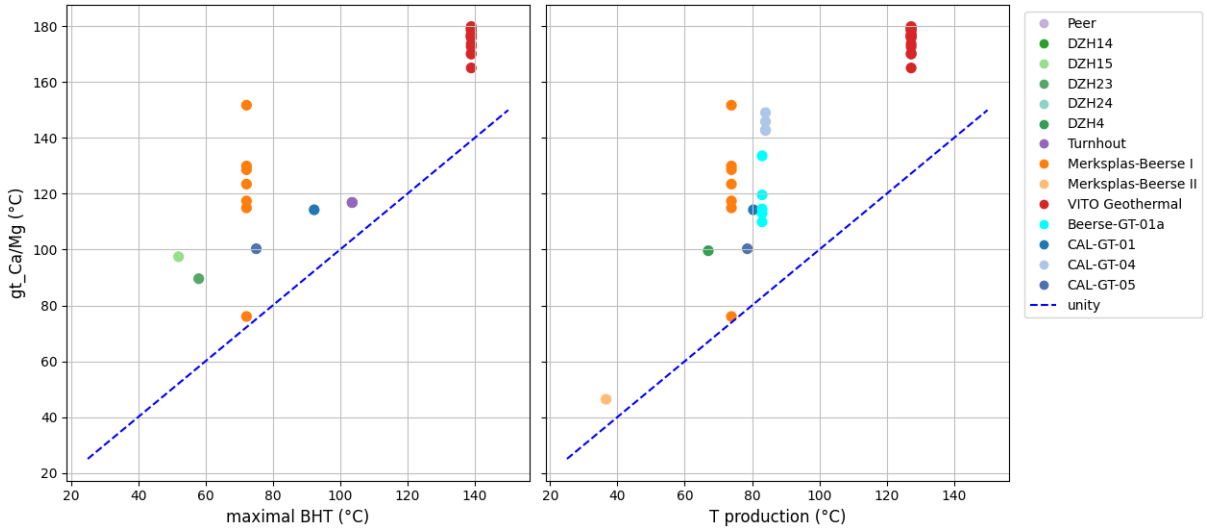

Figure 13. Ca/Mg-geothermometer versus recorded maximal BHT and production temperature.

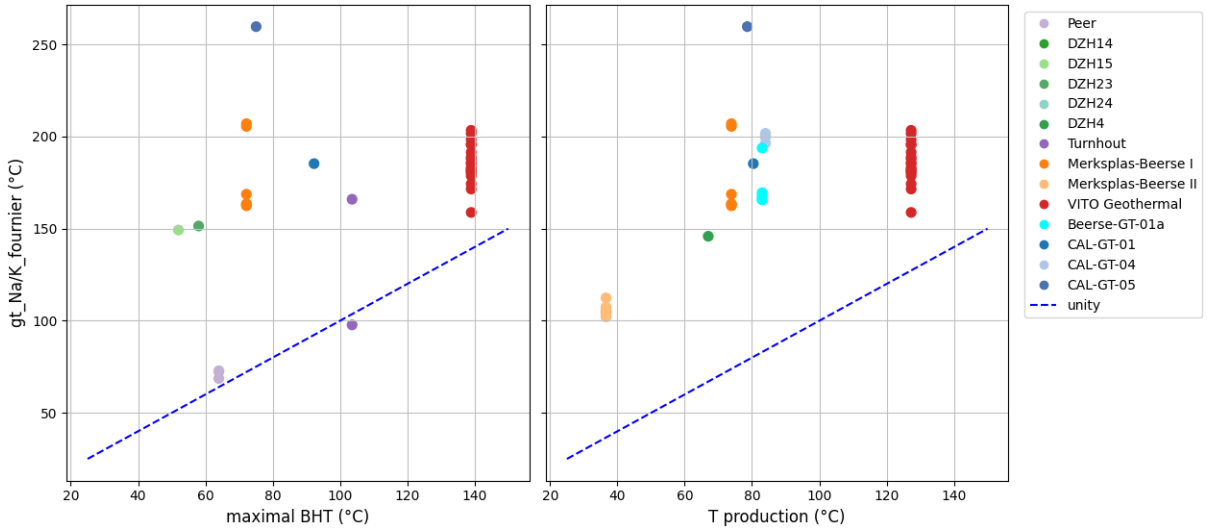

Figure 14. Na/K-geothermometer versus recorded maximal BHT and production temperature.

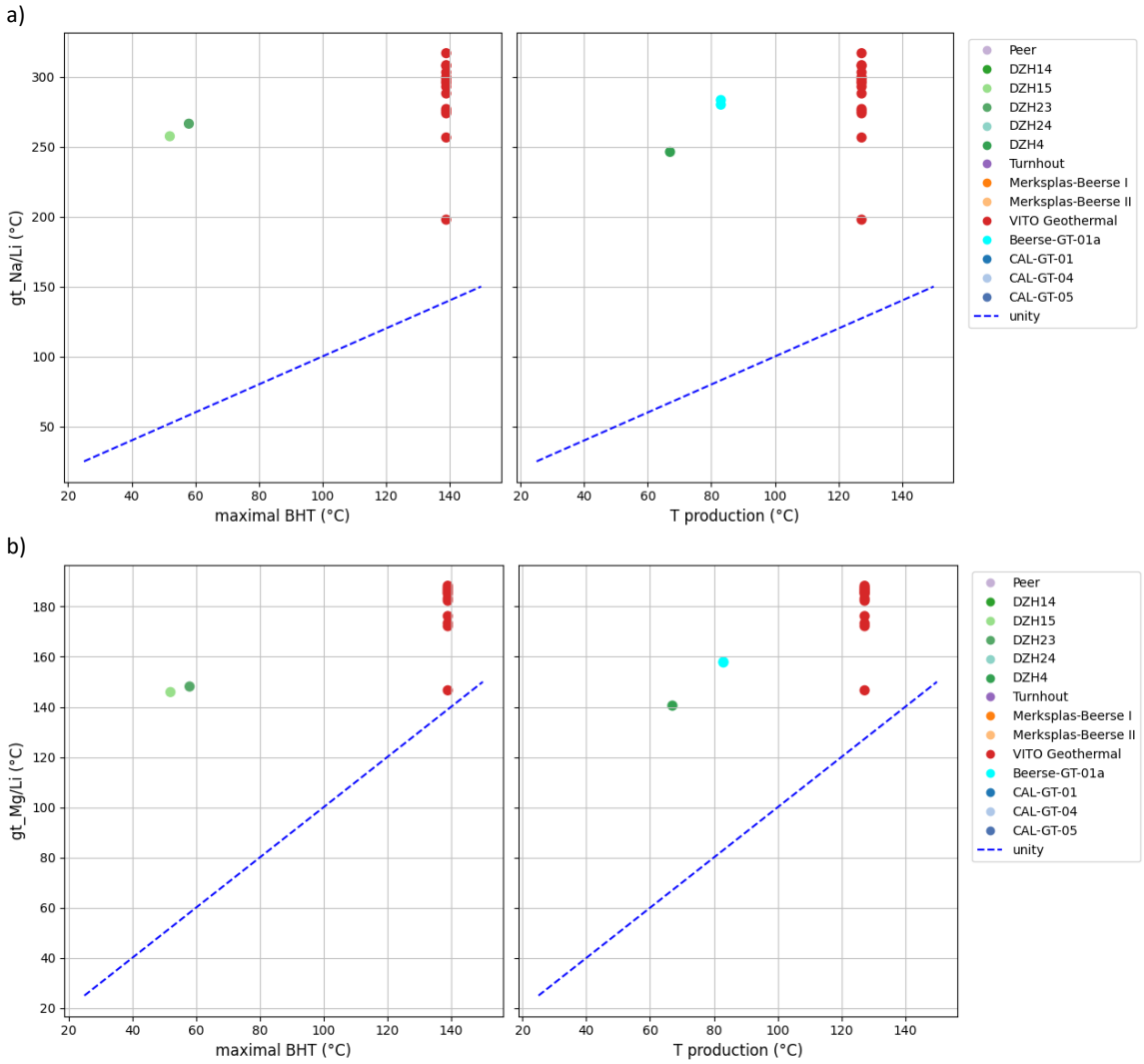

Figure 15. a) Na/Li- and b) Mg/Li-geothermometer versus recorded maximal BHT and production temperature.

Ferket (2007) modelled the thermal history of 74 boreholes from the Campine Basin using the basin analysis software PetroMod-1D®. Modelling was based on a thermomechanical approach, the regional context, criteria for the timing of coalification and a conceptual model incorporating new insights into the basin's structure and paleogeography. The maximal burial temperature at the top of the Lower Carboniferous Limestone Group was estimated at 225°C in the Turnhout well and at 220°C in the Merksplas-Beerse well. Correlation of the Namurian succession of the Meer well with MOL-GT-01-S1 yields an extrapolated maximal burial temperature at the top of the Lower Carboniferous Limestone Group of 240°C. Finally, the maximal burial temperature at the top of the Lower Carboniferous Limestone Group in MOL-GT-01 is estimated at 250°C based on vitrinite reflectivity data and correlation with the modelled thermal history of the Meer and Turnhout wells. The maximal burial temperature at the base of Loenhout in MOL-GT-01 is estimated at 270 - 275°C. These temperatures are in line with the estimates derived from the Na/Li-geothermometer. The lower equilibration temperatures calculated using the Mg/Li- and Na/K-geothermometers may be due to cation exchange or diagenetic reactions that took place after the maximal burial temperature was reached.

The calculated Na/K-, Mg/Li- and Na/Li-temperatures are in line with enrichment of the water samples from the Lower Carboniferous Limestone Group in potassium and depletion in sodium and magnesium with respect to seawater.

3.3.4 Trace elements

In the following overview, enrichment is defined as a concentration that is at least 10 times higher than the concentration of the element in seawater corrected for the Cl-concentration:

$$\left\{\frac{[c]_m \times [Cl]_{sw}}{[c]_{sw} \times [Cl]_m}\right\} \geq 10$$

Where $[c]_m$ and $[Cl]_m$ are respectively the measured concentration of the element c and of Cl, and $[c]_{sw}$ and $[Cl]_{sw}$ are respectively the concentration of the element c and of Cl in seawater. The seawater concentrations used are given in Appendix 3.

From the ions present in the dataset, Ba, Br, Cr, F, Hg, Li, M, Ni, Rb, Sc, Si, Sn, Sr, V and Zn are above the detection limit in more than 50% of the samples (Table 11). Sc was only measured on samples from Peer. For Sn, all values above the detection limit are from Peer.

Elements that are enriched with respect to seawater in at least 10 water samples are Al, Ba, Cd, Cr, Cu, Li, Ni, Pb, Sr and Zn. The highest level of enrichment is observed for Ba and Li, with enrichment factors in the range of 100 – 1000.

Enrichment of Al is highly variable. Except for 4 samples, the Al^{3+} concentration is lower than 1 mg/l and close to the reported detected limit. These low concentrations are in line with the low solubility of Al. The high values found in 4 samples most likely are caused by contamination of the samples by clay minerals. For these reasons, aluminium is not further discussed. The other trace elements are discussed in the paragraphs below.

Table 11. Number of analyses per trace element in the data set of the Campine Basin. The column '> DL' gives the percentage of samples with a concentration above the detection limit. The column 'enriched' gives the percentage of samples having a concentration above the enrichment level. '-': not determined by lack of clear range of the concentration in sea water

Trace element	Total	Cretaceous	Westphalian – Namurian	lower Carboniferous	> DL (%)	Enriched (%)
Al	51	3	4	44	41	41
As	35			35	20	3
B	69	3	37	29	100	0
Ba	52	5	3	44	100	96
Be	28			28	25	-
Br	19	3		16	100	0
Cd	38	2	3	33	47	47
Co	33		3	30	0	0
Cr	43	2	3	38	65	42
Cs	3			3	33	-
Cu	45	2	5	38	38	29
F	26	2	10	14	88	0
Hg	4		2	2	75	0
I	12		7	5	92	25
Li	65		34	31	100	45
Mo	70	2	37	31	66	4
Ni	47		10	37	64	21
Pb	45	2	5	38	73	53
Rb	60		34	26	95	0
Sb	31		3	28	29	13
Sc	34		34		100	-
Se	32			32	0	0
Si	44	1		43	98	-
Sn	69		37	32	49	0
Sr	91	11	35	45	100	19
Ti	34		3	31	0	0
U	3			3	33	-
V	32			32	53	28
Zn	47	2	10	35	91	79
Zr	32			32	0	0

3.3.4.1 Lithium

Lithium concentrations range from < 2.4 to 129 mg/l (Figure 16). Li^+ is enriched in all samples from the lower Carboniferous limestones with respect to seawater. On average, the Li^+ concentration is about 100 times higher than what would be expected based on the chlorine content. The highest concentration is found in the brine from the VITO geothermal plant (82 – 129 mg/l). At Beerse, the concentration is about 75 mg/l, in the DZH wells 50 – 55 mg/l.

The concentration measured in the Westphalian Peer samples varies between 2.4 and 7.1 mg/l. These levels are similar to those expected in case of conservative behaviour of a seawater derived brine.

The Li^+ concentration increases with the concentration of K^+ and Ca^{2+} and declines with the concentration of Mg^{2+}. Li^+ also increases with the depletion of the brine in Na+K+Mg relative to seawater (Figure 17).

Lithium is occurring predominantly in silicate minerals, and to a lesser extent in K-feldspar. In these minerals, Li is substituting K^+, Na^+ and Mg^{2+} (Salminen et al., 2005). In smectites, illite-smectite mixed layers and muscovite, concentrations of up to 6000 ppm have been measured (Dugamin et al., 2023). Concentrations in illite and kaolinite are lower (10 – 340 ppm). The cation exchange selectivity sequence for monovalent cations is $Cs^+ > Rb^+ > K^+ > Na^+ > Li^+$ (Caroll, 1959). The fact that Li^+ is most easily released by cation exchange can explain the observed trend with the seawater corrected Na+K+Mg content. Moreover, processes like the recrystallisation of smectite to illite or the alteration of K-feldspar are expected to be accompanied by an increase in the Li^+ concentration of the formation water. Li also absorbs on organic matter.

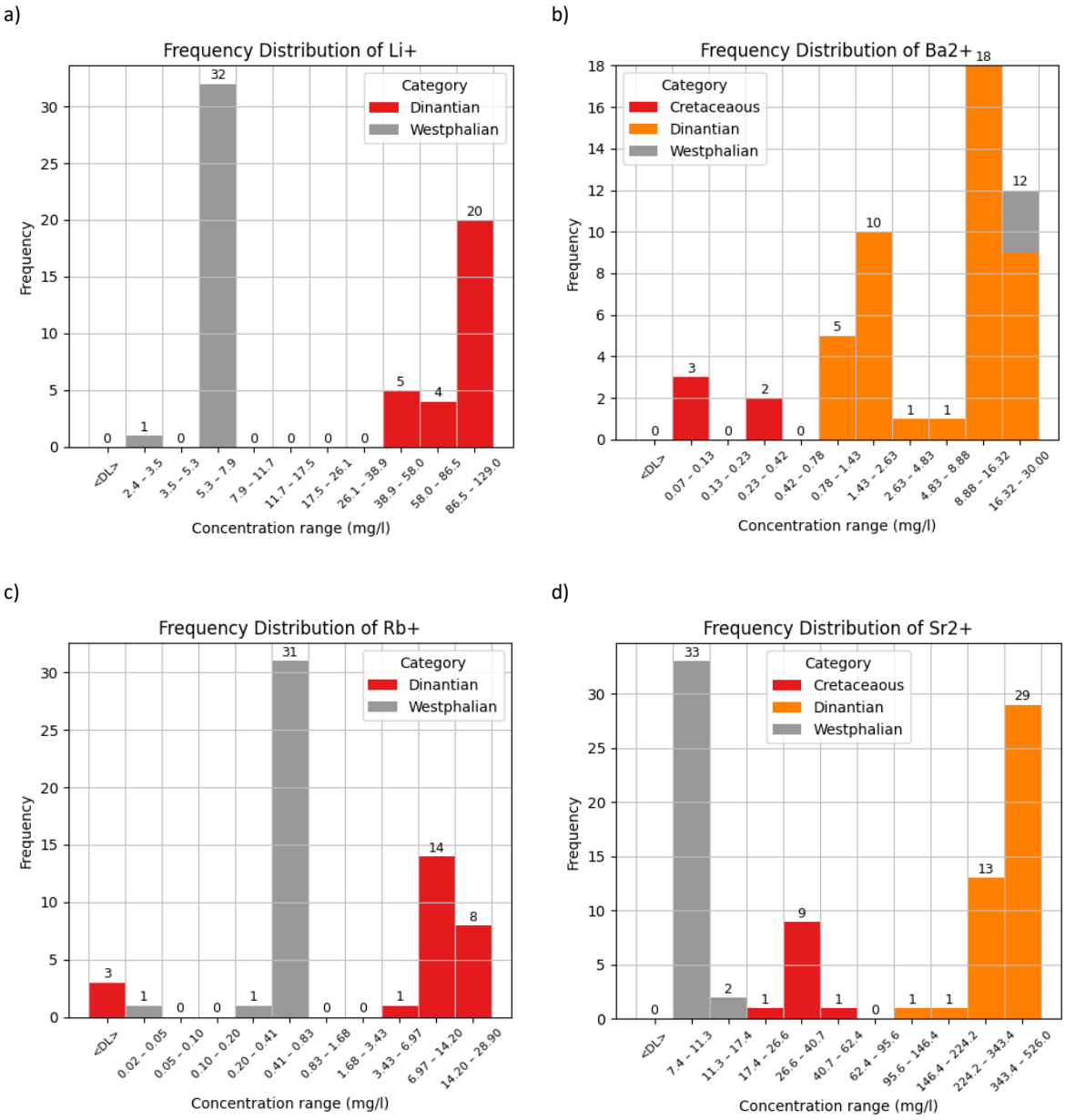

Figure 16. Histograms of the concentration of Li^+, Ba^{2+}, Rb^{2+} and Sr^{2+} in samples from the Campine Basin.

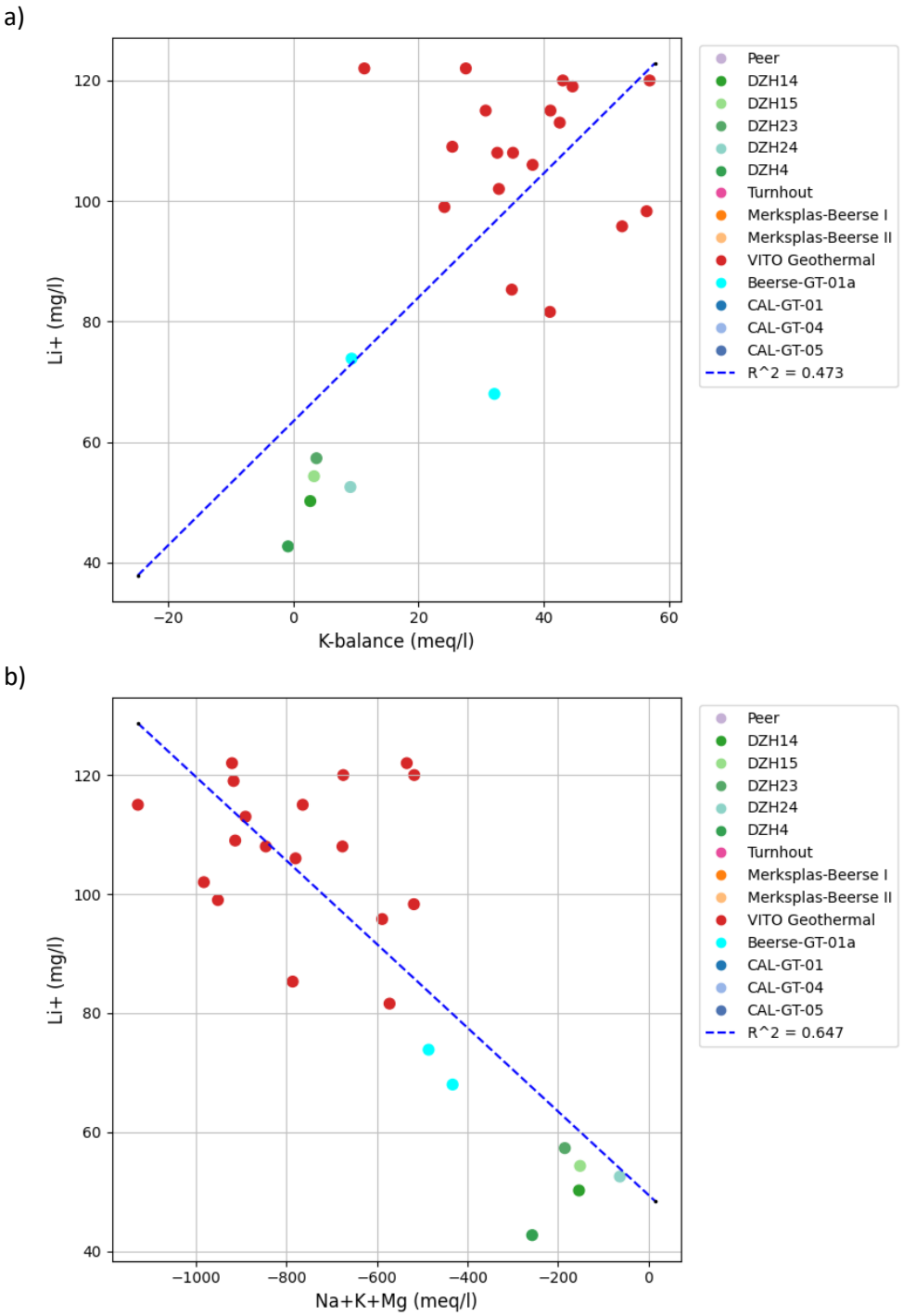

Figure 17. Plot of the concentration of Li^+ versus a.) the K-balance and b.) the Na+K+Mg balance relative to seawater.

Cation exchange can explain the high Li^+ concentrations of the water samples from the lower Carboniferous. Diagenetic dehydration of a seawater derived primary brine, mixing with a NaCl-rich secondary brine and equilibration with the carbonate rock matrix result in the observed progressive enrichment of the brine in Na^+ and Ca^{2+}. As Li^+ is most easily expelled from clays by cation exchange, it will be replaced by Na^+ and Ca^{2+}. This will increase the concentration in the brine. In the same way, K^+ may be released.

A mass balance calculation assuming a Li-content of the clay fraction before cation exchange of 2000 ppm and a final Li-content of 30 ppm, and an average porosity of 5% shows that interaction with 0.12%

of the rock matrix is sufficient to obtain the Li-enrichment that is observed in the VITO geothermal brine. The impact on the major cations Na^+ and Ca^{2+} is limited and within the precision of the chemical analysis. A similar result is obtained for illitisation. Starting from the mean Li-content of smectite-illite mixed layer of 3750 ppm given in Castor et al. (2020) and assuming a Li-content of 120 ppm in illite (Tardy et al., 1972) an interaction with 0.06% of the rock matrix is required to reach the observed Li^+ concentrations. The mass balance calculation shows that interaction with a small portion of the rock matrix is sufficient for the observed Li^+ enrichment. This seems realistic considering the clay content of the Lower Carboniferous Limestone Group (between 0 and 9% for samples of the VITO geothermal site (Pauwels, 2021) and the fact that the exchange will primarily occur along veins/fractures. The associated decrease of the K^+ concentration of the brine would be 80 mg/l. This impact is much smaller than standard deviation on the samples of the VITO geothermal plant. The figures are realistic given the mineralogy of the limestones.
Similar results are obtained when alteration of muscovite is assumed to be the source of Li^+. With an average Li^+ content of 1500 ppm for muscovite (Dugamin et al., 2023) and 150 ppm in the resulting kaolinite (Tardy et al., 1972) would require interaction with 0.19% of the rock matrix and increase the K^+ concentration of the brine with about 80 mg/l.

The thermal degradation of organic matter also can contribute to the observed trend. Lithium is weakly bound to net negative charge organic groups (e.g. carboxyl groups, phenolic groups, alcohols). Thermal degradation will result in the breakdown of these functional groups, which releases Li^+ into pore fluids.

3.3.4.2 The lithophyllic elements Ba, Rb and Sr

Barium concentrations range from 0.07 to 30 mg/l (Figure 16b). Except for the Cretaceous samples (Merkplas-Beerse II), all samples are enriched with respect to seawater. The samples from Peer have the highest concentrations and are most enriched. The samples from the lower Carboniferous show a weak trend towards stronger enrichment with depth.
When the samples from Peer are ignored, Ba^{2+} tends to increase with K^+ and depth (Figure 18a). In case of the Peer samples, Ba^{2+} increases with sulphate and bicarbonate concentration (Figure 18b).

The barium concentration in formation water strongly correlates with the abundance of Ba in the rock matrix (Salminen et al., 2005). The correlation with sulphate and bicarbonate observed in the Peer samples may point to the presence of barite and barium-rich carbonates. Ba^{2+} is known to substitute for K^+ in feldspars and mica, and for Ca^{2+} in plagioclase and carbonate minerals. Ba^{2+} is also easily displaced by other bivalent cations from clay minerals. In that respect, the correlation with K^+ observed in the samples from the lower Carboniferous can indicate the expulsion of Ba^{2+} from clay minerals or the alteration of feldspars or mica.

a)

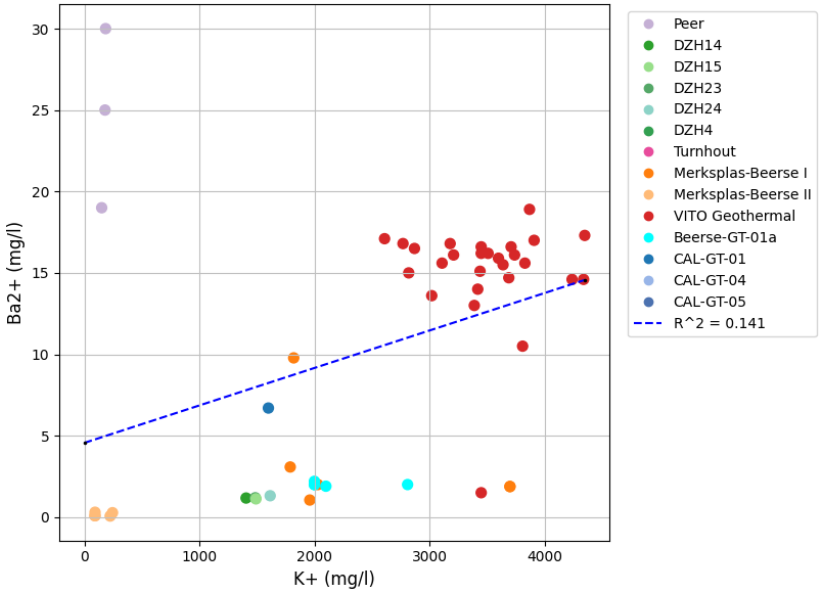

b)

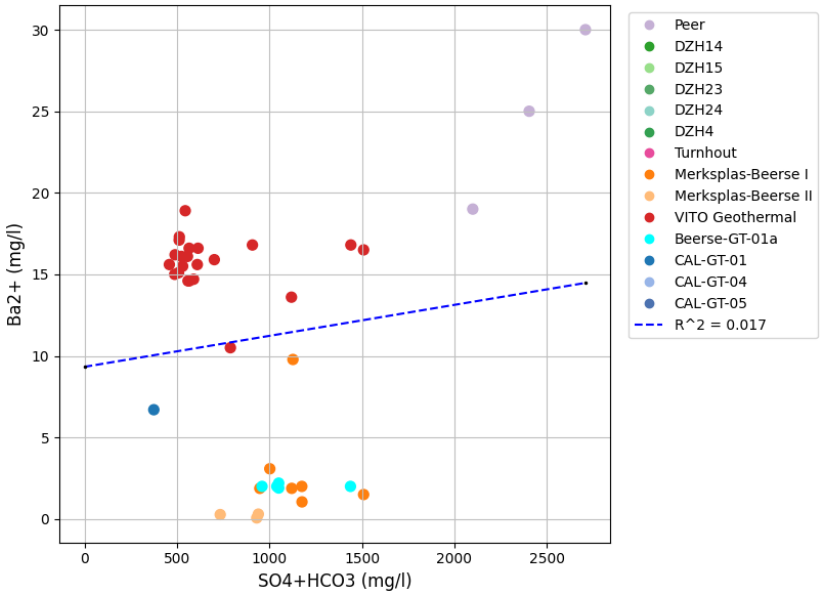

Figure 18. Plot of the concentration of a) Ba^{2+} versus K^{+} and b) Ba^{2+} versus the sum of SO_4^{2-} and HCO_3^{-}.

Rubidium concentrations range from < 0.02 to 28.9 mg/l (Figure 16c). None of the samples is enriched in Rb^{+} with respect to seawater. Rb^{+} increases with the concentration of the major monovalent cations and manganese (Figure 19).

Rubidium is found in several common minerals in which it substitutes for potassium (Salminen et al., 2005). High concentrations are found in mica, and to lesser extent in K-feldspar. The Rb^{+} content found in formation waters is largely controlled by the stability of K-bearing phyllosilicates, coupled with the adsorption on clays and organic matter. The correlation with K^{+} and Mn^{2+} observed in the samples from the Campine Basin may point to alteration of mica. The fact that none of the samples is enriched with respect to seawater can be explained by the fact that Rb^{+} tends to be more strongly bound to clay minerals than K^{+} (Kabata-Pendias 2001).

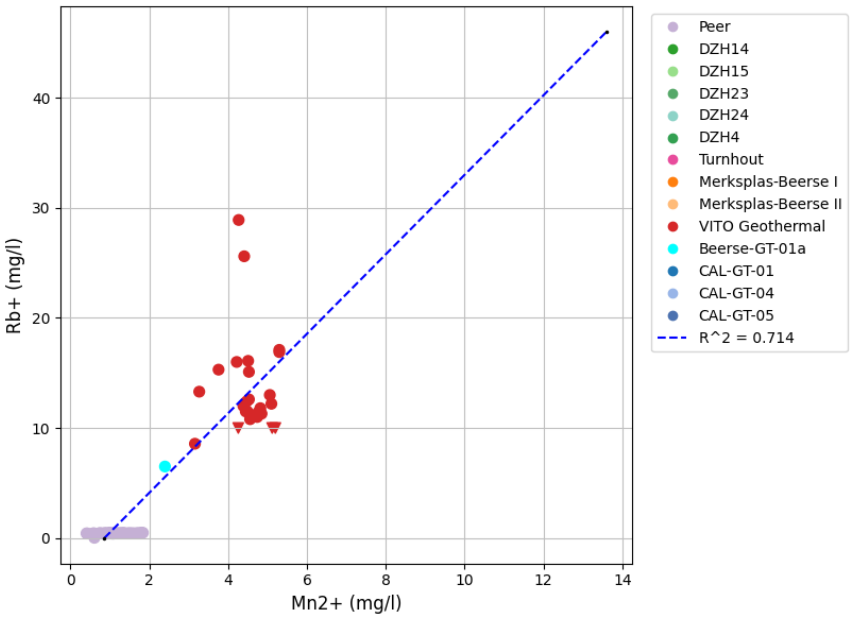

Figure 19. Plot of the concentration of Rb^{+} versus Mn^{2+}.

Strontium concentrations range from 7.4 to 602 mg/l (Figure 16d). Many samples from the carbonate reservoirs are enriched in Sr^{2+} with respect to seawater, although the level of enrichment is low. The samples of the upper Carboniferous are depleted with respect to seawater. The Sr^{2+} concentration is highly correlated with the calcium concentration (Figure 20).

The distribution of strontium in sedimentary rock is controlled by strong adsorption on clay minerals, and extensive substitution of Sr^{2+} for Ca^{2+} in carbonates and sulphates, and to a lesser extent in feldspars (Salminen et al., 2005). The high correlation between Ca^{2+} and Sr^{2+} content in the brines of the Campine Basin is largely controlled by interaction with carbonates.

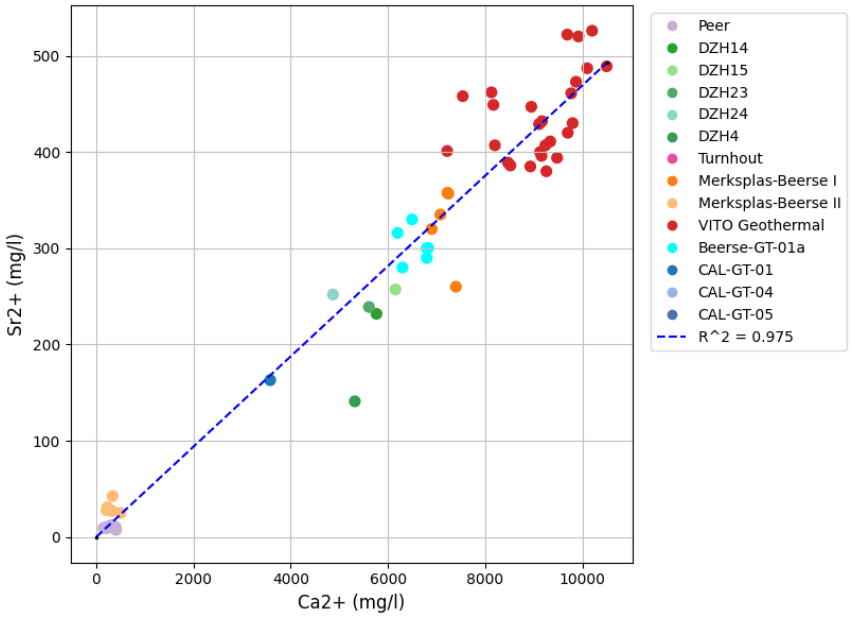

Figure 20. Plot of the concentration of Sr^{2+} versus Ca^{2+}.

3.3.4.3 The chalcophile elements Cu, Pb, Zn, Mo, Ni and Cr

The concentrations of the chalcophile elements Cu^{2+}, Pb^{2+}, Zn^{2+}, Mo^{4+}, Ni^{2+} and Cr^{3+} are highly variable. They span several orders of magnitude (Figure 21). As for the lower Carboniferous, the highest degree of enrichment in Cu^{2+}, Zn^{2+}, Mo^{4+}, Ni^{2+} and Cr^{3+} compared to seawater is found in the DZH and Beerse samples. The distribution of Pb^{2+}-concentrations is distorted by some very high concentrations in the samples from the VITO geothermal plant. These may be due to contamination by lead precipitation in the wellbore and geothermal system (Pauwels, 2021; Pauwels et al., 2021).

Significant pairwise correlations (90% and 95% confidence level) are found between the chalcophile elements (Figure 22). This suggests that the concentrations of these elements in deep formation waters of the Campine Basin are determined by similar processes. Their chalcophile nature and weak association with sulphate (Figure 23) may point to sulphide minerals as a source for these elements. The relative enrichment of these elements in the DZH and Beerse samples compared to the samples from MOL-GT-01 can then be explained by recent karst-related oxidation of sulphides and/or leaching of these minerals by active fluid flow. The difference in reservoir characteristics implies that these processes are less pronounced in the reservoir of the VITO geothermal plant.

There is no clear correlation with the major ions, nor with the stratigraphic position of the reservoir or reservoir depth. When the Westphalian Peer samples are excluded, a weak association with sulphate can be identified for the elements Cu, Zn, Ni, Mo and Cr (Figure 23).

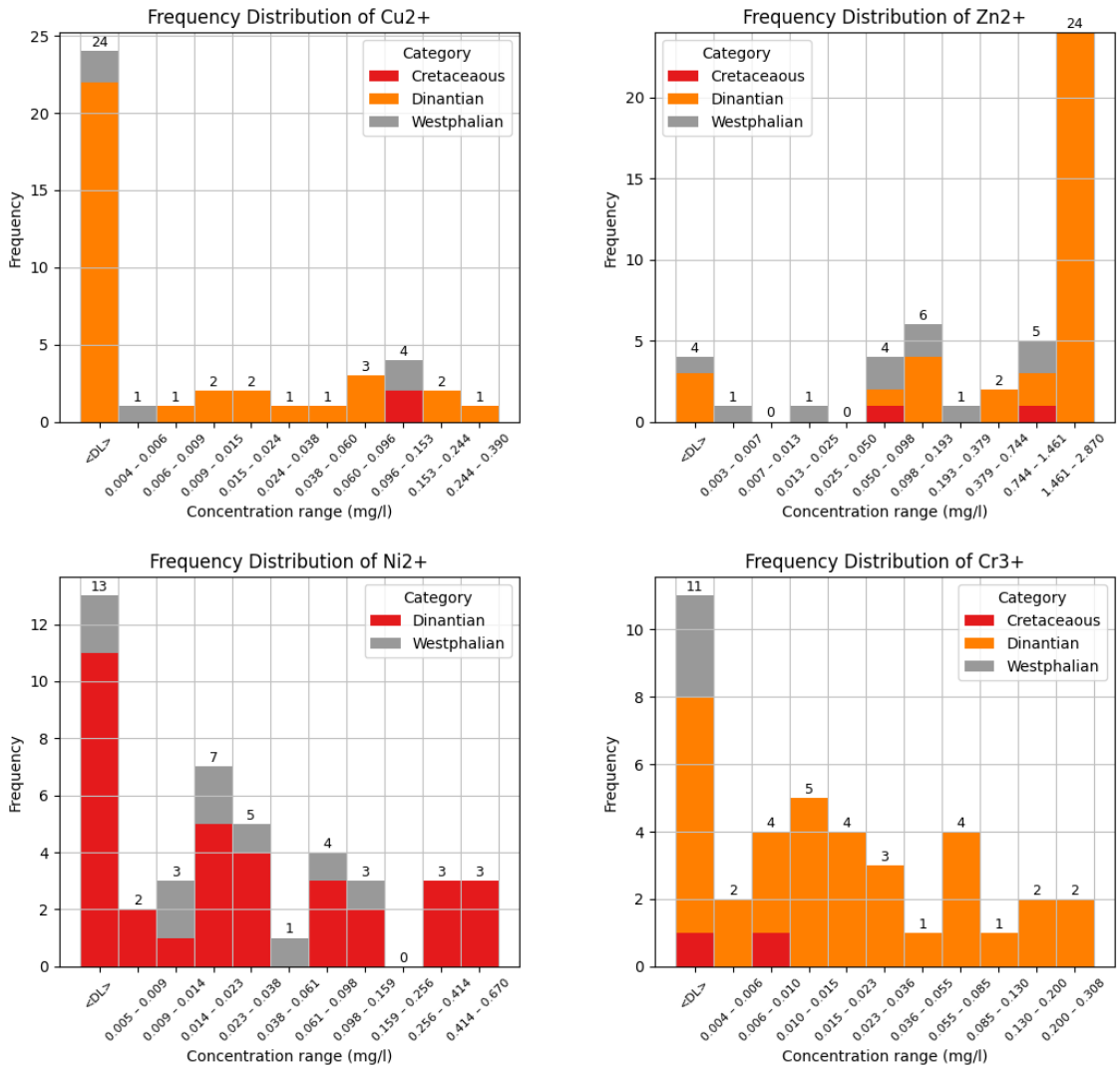

Figure 21. Histograms of the concentration of Cu^{2+}, Zn^{2+}, Ni^{2+} and Cr^{3+} in samples from the Campine Basin.

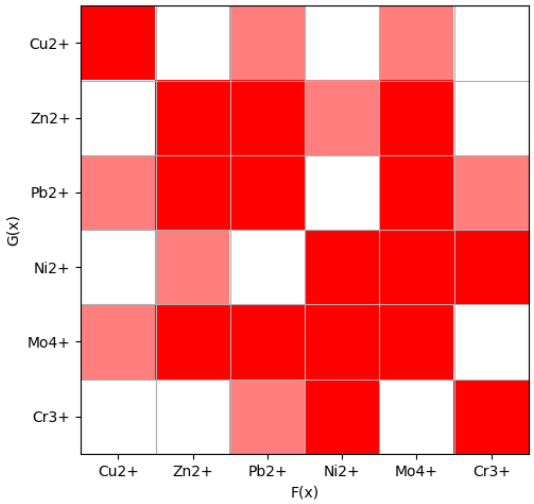

Figure 22. Pairwise Spearman's rank correlation for the chalcophile elements. Bright red squares point 95% significance, light red squares to 90% significance.

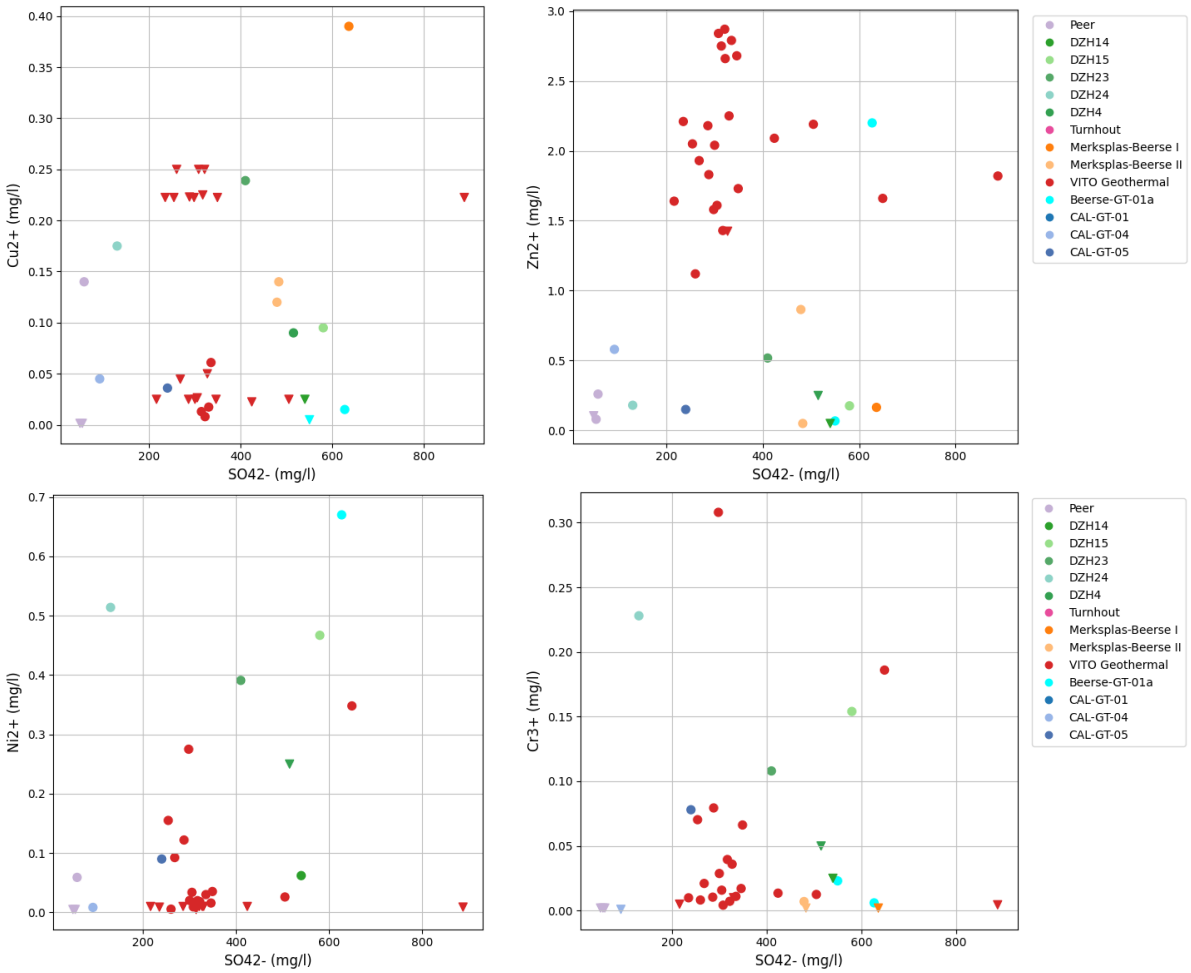

Figure 23. Plots of Cu^{2+}, Zn^{2+}, Ni^{2+} and Cr^{3+} versus SO_4^{2-} Downward pointing markers refer to values below the detection limit (plotted as LoD/2).

3.4 COMPARISON WITH LITERATURE AND POSSIBLE ENRICHMENT PROCESSES

Since the rising importance of and subsequent interest in lithium, numerous studies have made an overview of Li in brines throughout the world. Near Belgium, an important and well-studied Li-bearing reservoir is the Upper Rhine Graben between the Vosges and the Black Forest on the border of France and Germany and stretching to the north in Germany in the direction of Mannheim. Elevated Li-values (115-169 mg/l) were first discovered in the Soultz-sous-Forêts geothermal wells (Sanjuan et al, 2006). Since then, several other geothermal plants have been developed in the region (Landau, Bruchsal), which also contain elevated Li-values (159-210 mg/l) (Sanjuan, 2022). German company Vulcan currently operates a number of these geothermal plants (i.e. at Insheim) and started extracting Li from the reservoir brine. They currently operate two pilot plants to process the lithium. In the first one, lithium is harvested from the brine through the adsorption of LiCl. In a second pilot plant, this LiCl is converted into battery-grade lithium hydroxide monohydrate.

Values on what is considered to be the threshold for defining a lithium-enrich brine differ somewhat throughout different studies, but lower boundaries are mostly in the range of 90-125 mg/l, while other studies include reservoirs with concentrations as low as 15 mg/l. A concentration of 150 mg/l or higher is considered recommended to make Li extraction effectively possible (Sanjuan et al., 2020). Although, this threshold might lower in the future depending on, among other, more (cost-)effective extraction techniques and increased market demand.

Gourcerol et al. (2024) compiled an 'Atlas of lithium geothermal fluids in Europe' in which over 180 occurrences of Li-bearing brines (lower threshold 15 mg/l) are considered and geostatistically analysed. No geothermal fluids from the Campine Basin are included in this overview. Correlation of the dataset by compiled by Gourcerol and co-authors shows a positive correlation Li with B, Rb, K, SO_4, Na, Cl and F. Furthermore, there is a negative correlation between Li on the one hand and Mg, Mn, U and NH_4 on the other hand. These elements can be used as proxy for lithium enrichment in geothermal fluids. Other studies (Dugamin et al., 2021, Dugamin et al., 2023) come to similar conclusions, stating that the highest Li concentrations are strongly linked to high TDS values.

The Li concentration in formation water tends to correlate with reservoir temperature, with higher Li concentrations found in hotter reservoirs (Dugamin et al., 2021, Dugamin et al., 2023, Sanjuan et al., 2022, Coffey et al., 2021). Higher temperatures lead to more intense water-rock interactions (Sanjuan et al., 2022, Gourcerol et al., 2024).

The correlation between Li on the one hand and B, Rb, K and F on the other hand is considered to reflect the dissolution of clay minerals at higher temperatures. The correlation with high Na and Cl concentrations shows that high Li concentrations are found in reservoirs with high salinity. The negative correlation between Li and Mg is also an effect of hydrothermal alteration of clay minerals, which is more prominent at higher temperatures and in reservoirs with high Na and Cl concentrations (Yuan et al., 2021). Lab experiments indicate that Mg^{2+} substitutes for Li^{+} in clay minerals and that this substitution is more outspoken at higher temperatures (Decarreau et al., 2012, Coffey et al., 2021, Gourcerol et al., 2024, Yuan et al., 2021).

Multiple studies on different types of reservoirs worldwide thus come to similar conclusions on the driving factors for Li-enrichment in deep groundwater reservoirs. Key factors are:

- High salinity (Na and especially Cl concentrations);

- High temperature;
- The presence of Li-bearing minerals in the reservoir or in the surrounding rocks, because evaporation of the initial groundwater alone is not sufficient to explain the high Li-concentrations.

The data of the brines of the Lower Carboniferous Limestone Group in the Campine Basin are in line with the conclusions and observations reported in literature. Based on the above analysis, cation exchange appears to be the primary cause of the elevated Li concentrations observed in the formation water of the lower Carboniferous limestone. The increasing diagenetic dehydration of a primary seawater derived brine and its interaction with the carbonate matrix with rising temperatures lead to an increase in cation concentration (mainly Ca^{2+} and Na^{+}) and a shift in the cation exchange equilibrium toward higher Li concentrations in the formation water. The Cl/Br ratios suggest that this effect is further enhanced by the addition of a NaCl-rich secondary brine. This conceptual model seems plausible based on published lithium concentrations for clay minerals. Verification of the model is possible through thorough mineralogical analysis of the lower Carboniferous reservoir and analysis of the Li content of the clay fraction.

From an economic perspective, a Mg/Li-ratio <10 is favourable as Mg^{2+} prevents the formation of lithium chloride, which is the first composition required to produce lithium carbonate as product for the industry (Dugamin et al., 2021 & 2023, Yuan et al., 2021). In the Lower Carboniferous Limestone Group in the Campine Basin, this condition is met in the VITO Geothermal well, but not in the shallower wells in the northern part. Taking into consideration all the factors contributing to Li enrichment, it can be expected that the lithium concentration in the eastern part of the Campine Basin, where the top of the lower Carboniferous limestone reservoir is situated much deeper, will be higher than in VITO Geothermal, and that the Mg/Li-ratio might be lower. Since there are at present no wells reaching the reservoir in that part of the basin, it is not possible to verify that yet.

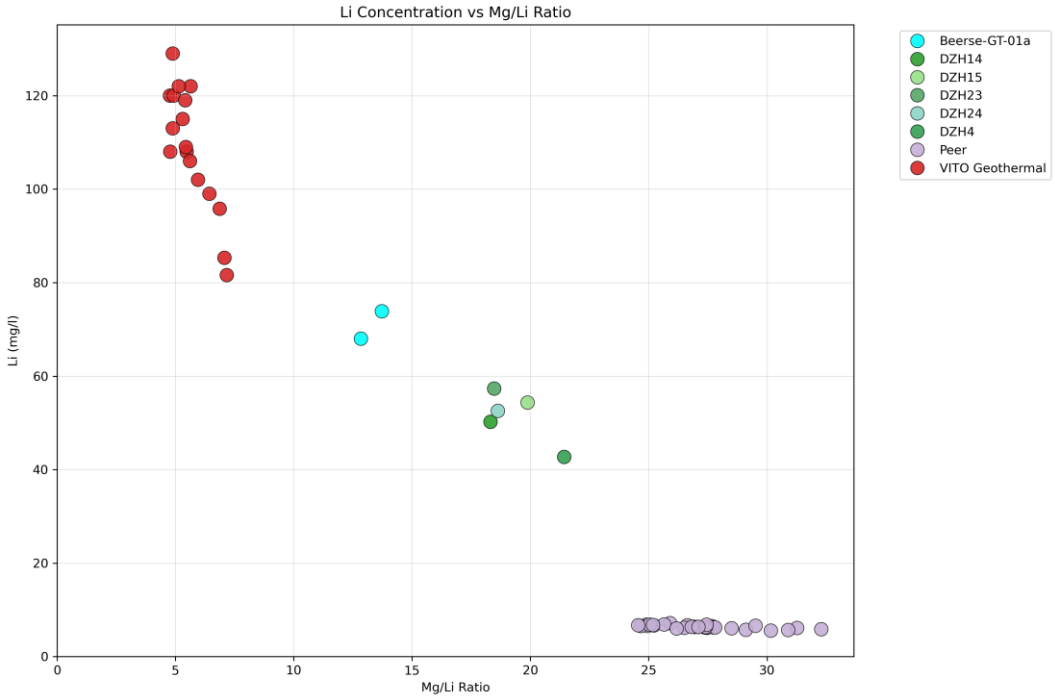

Figure 24. Li^{+} versus Mg/Li-ratio plot, where a value <10 for the Mg/Li-ratio is considered favourable for exploitation of lithium.

3.5 GENERAL CONCLUSIONS FOR THE CAMPINE BASIN

The deep groundwaters found in the Campine Basin are of the Na-Cl type. Na and Cl are the dominant ions. Their concentration increases almost linearly with depth. The concentrations of most other major and minor elements also increase with depth. The trends indicate the mixing of two types of water: seawater that was dehydrated through interaction with the rock and other diagenetic processes (e.g., osmotic water transfer, radiogenic splitting of H_2O into H_2 and oxygen radicals) and a saline basement brine. Except for the samples from Peer, there are no indications of halite dissolution. The signature is consistent with an 'old' brine that has been circulating in a closed reservoir for a very long time.

Mg is an exception to the general trend. The highest concentrations of Mg are measured in the samples from Beerse and Turnhout. The concentrations in the samples from the VITO geothermal project are approximately half compared to those measured in Beerse and Turnhout. When plotted against Cl, Mg initially shows a linear increase to approximately 1,100 mg/l at a Cl concentration of 70,000 mg/l and subsequently decreases almost linearly to values around 600 mg/l at a Cl concentration of 105,000 mg/l. The trend can be explained by a difference in diagenesis between the locations where the samples were taken. The relatively higher concentrations in the northern part of the basin (Beerse - Turnhout region) indicate a greater contribution from interaction with dolomite than the samples from the Mol region.

Enrichment of trace elements in the groundwater samples was calculated based on the concentration in seawater. Concentrations 10 times or more higher than the Cl-corrected concentration in seawater were labelled as 'enriched'. Ba is enriched in all samples. The enrichment can be explained by interaction with sulphates (barite, gypsum) and silicates (feldspar, phyllosilicates). Sr, Li, and I are enriched in all boreholes where lower Carboniferous groundwater was sampled. The enrichment of Sr is a result of interaction with carbonates in the reservoir rock. The Li enrichment can be attributed to interaction with Li-rich phyllosilicates and cation exchange. For I, the enrichment is limited. No correlation with other elements was found due to the limited number of analyses in which I was measured. Cu, Pb, Zn, and Ni are enriched in samples from the Loenhout - Beerse region and in a few samples from the Peer borehole. No clear correlations were found with other elements, but the weak correlation with SO_4 may indicate oxidation of sulphides.

4 BRABANT MASSIF

4.1 COLLECTING GROUNDWATER HYDROGEOCHEMICAL DATA

As a result of different previous projects, the Laboratory for Applied Geology and Hydrogeology (LTGH) of UGent has analysed groundwater samples taken from the Basement Aquifer of the Brabant Massif of Flanders for many decades. The data of these previous studies conducted at the LTGH, available both in paper and digital form, have been collected and form the base of this study.

The MSc study by Bogaerts (1998) forms an important document since she had compiled most of the data from the LTGH archives in a database in the framework of her MSc thesis. She had collected and analysed groundwater sample data from different sources: 75 from TGO Report 84/15, 74 from TGO 87/33, 70 from TGO 92/011, 45 from TGO 93/02 and 10 from TGO 93/041. An additional 70 samples taken from the LTGH archives originating from different smaller projects, and 44 samples obtained from the National Institute for Ornamental Plant Cultivation, were added to the database. However, no coordinates are available for the latter data sets. Therefore, she deduced the coordinates of the wells from NGI topographic maps at 1/50,000 and 1/25,000 scales, by considering that the wells were located in the center of the respective municipalities. Finally, analytical results from 25 wells from the TGO Report 96/39, and an additional 41 water samples analysed in 1998, were included in her database. It should be mentioned that for this database, trace elements were only measured in about 221 samples. However, the values of these analyses are mostly below the detection limit. Therefore, we have not included these trace metal analyses in our statistical data analysis and interpretation. The analyses are included in the database, accompanied with their respective detection limit (specific for each analysis).

The other main base of information of our study is the Sterpin (1966) data. This study contains 136 samples analysed in the framework of project VLA/94-3.5 (Sterpin, 1996). Water samples from these 136 wells were analysed for 44 elements and physicochemical parameters. This data source contains many analyses of trace elements. The following trace elements, namely, Mn, Cu, Zn, Cr, Co, Ni, As, Se, Nb, Mo, Cd, Sn, Sb, Ba, W, Pt, Au, Pb, Bi, Ag, Ta, Hg and Ti, were analysed with ICP-MS which allowed a very low detection limit (up to the order of 10 ppt). These analyses were performed in 1992, 1993, and 1994 by the Laboratory of Analytical Chemistry of the Free University of Brussels on the ICP-MS apparatus set up in the Royal Museum for Central Africa at Tervuren. Some elements, including B, Mn, Fe, Sr, Cu, and Zn, were analysed on the same samples with a DCP apparatus in the Pedology Department of the Université Catholique at Louvain-la-Neuve. The conductivity, hardness (permanent, transient, and total), pH, oxygen, Eh, and major (with some trace) ions, such as Na^+, K^+, Ca^{2+}, Mg^{2+}, NH_4^+, Cl^-, F^-, SO_4^{2+}, NO_3^-, NO_2^-, HCO_3^{2-}, CO_3^{2-}, PO_4^{3-}, of these samples were analysed at LTGH, mostly by Atomic Absorption Spectroscopy.

In addition to these data, Melger (2018) sampled 21 groundwater samples in 2017 at wells distributed in both the western and eastern parts of the Brabant Massif aquifer (basement aquifer). The electrical conductivity, redox potential, pH, and water temperature, and the main anions, (such as Cl^-, SO_4^{2-}, HCO_3^-, CO_3^{2-}, NO_3^-, NO_2^-, PO_4^{3-}) and cations (Na^+, K^+, Ca^{2+}, Mg^{2+}, Fe^{2+}, Fe^{3+}, Mn^{2+}, NH_4^+, Al^{3+}) were measured at the laboratory of LTGH.

Finally, the 49 new samples analysed by Eurofins Analytico, ordered by the Vlaamse Milieumaatschappij (VMM) and the Department of Environment of the Flemish Government (DOMG),

have been added to the database of this study. The following trace elements were analysed: Mn, As, Ni, Zn, Cd, Hg, Cr, Pb, Cu, Fe, Co, Sb, V, W, Hf, Nb, Li, and Be. However, for the main anion and cation concentrations of these samples, existing data from the DOV portal corresponding to previous analyses made in 2021 have been used, as the results of the new samples were not available in time to be included in the in-depth analysis. However, the recent major ions concentrations were later compared with the previous ones, and no significant variation that could change water types and correlation results with trace elements has been found. Therefore, for the main or major ions, GIS plots and statistical analyses included in this report use the 2021 data for the VMM-DOMG samples. It should again be mentioned that for most of the trace elements in the VMM-DOMG samples, especially for Sb, W, Hf, Nb, and Be, the concentrations are below the detection limit. The specific detection limits are included in the database.

Table 12. Summary of hydrogeochemical data collected, including data source. Number of samples per source, and type of analysed elements.

Data source	Number of samples	Analysed elements
LTGH (TGO 84/15, TGO 87/33, TGO 92/011, TGO 93/02, and TGO 93/041, TGO 96/39)	446	204 only on major ions; 221 are with some trace elements, but are mostly below the detection limit
Melger (2018)	21	Only major cations
Sterpin (1996)	136	Major ions plus most of the trace elements
New VMM-DOMG	49	Major ions plus some trace elements, but only Li and V are above the detection limit

The summary of all the collected data is presented in Table 12. In total, about 652 samples have been collected and used in the analysis. However, repeated sampling and analyses are present for some locations, especially for major ions. The 652 samples correspond to 366 individual wells. The 446 analyses from the LTGH archives (Table 12) contain mostly major ions, but some have also trace element data. 204 of these samples contain only major ions, while 221 have some trace elements (mostly below the detection limit). The 136 water samples from the study of Sterpin (1996) include the analyses of most of the trace elements. The full dataset is available in digital appendices 4 (longtable) & 5 (GIS-file).

In general, there is a fair representation of water samples in the central and northwest part, but there is less representation in the southeastern part of the Brabant Massif (Figure 25). In addition, there are also less trace element data available for the eastern part of the Brabant Massif.

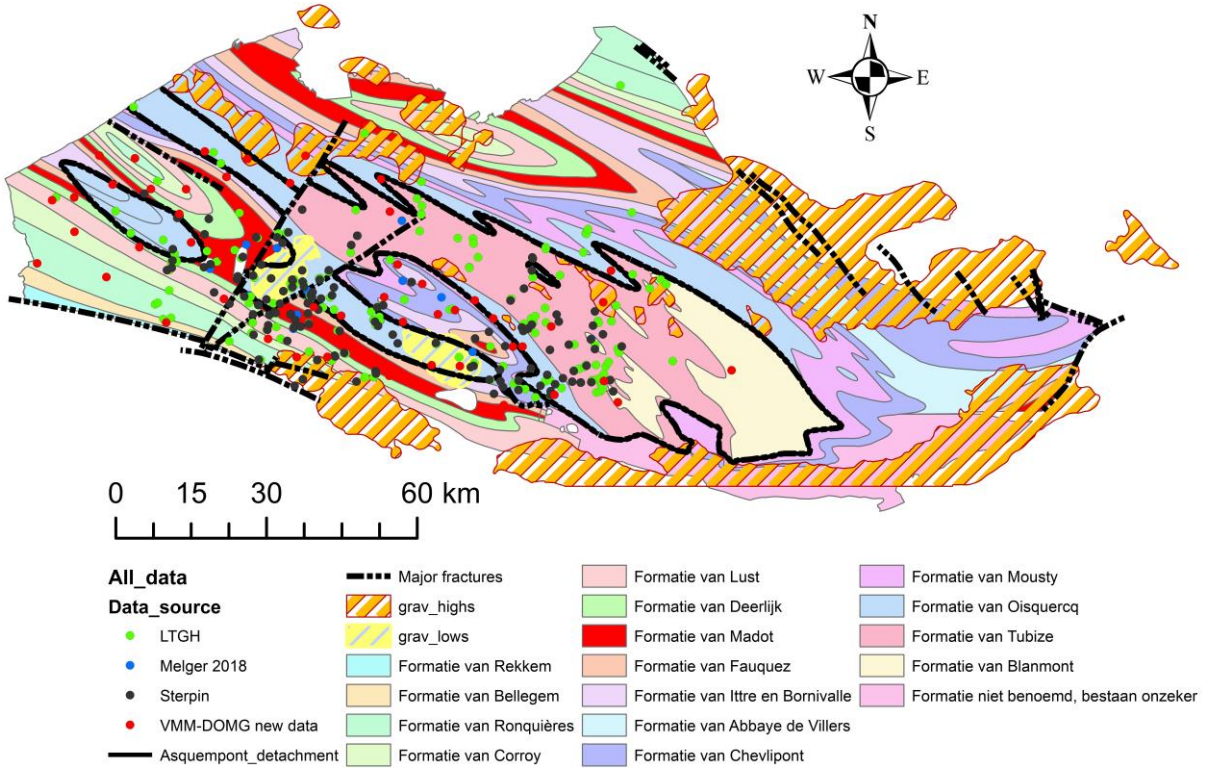

Figure 25. Location of sampling wells overlaid on the geological map of Piessens et al. (2005), gravity anomalies of Everaerts and De Vos (2012). The samples are classified based on the data source.

Table 13 presents the number of available measurements for 24 trace elements across three different data sources: LTGH (collected for various projects), data from the Sterpin (1996) study and newly analysed data by VMM-DOMG. The study by Melger (2018) included only major ion analyses and is used in this study solely for the purpose of water type classification and characterization. The Sterpin (1996) dataset stands out as the most important, with nearly a complete dataset (except for Li, V, and Hf) for 21 trace elements. The data from the LTGH also provides substantial coverage for several elements, particularly Zn (108 samples), Pb (84), Cu (78), and Cd (78). However, data for other elements, such as Pt, Ag, and Au are completely missing. The new VMM-DOMG data set is the only one that has Li data. Therefore, our Li analysis and interpretation rely on those analyses at 49 wells. It should, however, be mentioned that these 49 wells seem relatively fairly spatially distributed.

Table 13. Number of measured samples for each trace metal per data source. Only values above the detection limit are included in the table.

Element	LTGH studies	Sterpin (1996)	VMM-DOMG new data	Melger (2018)	Total analyses
Bi	62	130	0	0	192
Pt	0	130	0	0	130
Ag	0	128	0	0	128
Nb	0	130	3	0	133
Cd	78	130	8	0	208
Au	0	130	0	0	130
Sn	27	130	0	0	157
Co	66	128	8	0	202
Sb	65	130	3	0	198
Pb	84	130	8	0	222
W	0	130	11	0	141
Ni	70	129	8	0	207
As	71	128	8	0	207
Mo	48	130	0	0	178
Cu	78	130	8	0	216
Cr	53	130	8	0	191
Se	65	129	0	0	194
Ba	0	130	0	0	130
Li	0	0	49	0	49
Zn	108	130	8	0	246
Sr	66	129	1	0	196
Hg	27	52	8	0	87
V	0	0	19	0	19
Hf	0	0	3	0	3

The number of wells that have been sampled from each geological formation as well as the total number of analyses, are shown in Table 14. The geological formation represented reflects the formation at the top of the Brabant Massif, which is evidently not outcropping in the sampled areas. It does, however, not necessarily mean that the sampled aquifer is only drilled in that formation. Numbers in Table 14 are both analyses that include trace metals and those with only major ions. About 9 wells, of which 39 analyses have been done, could not be grouped into one formation type. On the other hand, the most well-represented geological formation with analysis of the trace elements is the Formation of Oisquercq (Cambrian age) (on 60 wells), and the second is the Formation of Madot (Ordovician age) (44 wells). However, the total number of wells corresponding to these geological formations, considering both wells with only major-ion analyses and those with trace-element analyses, exceeds these figures (Table 14). In the Oisquercq Formation, repeated analysis of trace elements, such as Bi, Pt, Ag, Cd, Nb, Sb, Pb, Ni, As, Mo, Cu, Se, Zn, and Sr, and in the latter, Bi, Nb, Co, Sb, Pb, Cu, and Cr are well studied.

Table 14. Distribution of 325 sampled wells and analyses per geological formation.

Geological formation	Number of wells	Number of analyses
Formatie van Bellegem	2	4
Formatie van Ronquières	10	13
Formatie van Corroy	9	15
Formatie van Lust	28	51
Formatie van Deerlijk	20	51
Formatie van Madot	39	91
Formatie van Fauquez	9	16
Formatie van Ittre en Bornivalle	12	22
Formatie van Chevlipont	27	38
Formatie van Mousty	6	12
Formatie van Oisquercq	102	179
Formatie van Blanmont	12	14
Formatie van Tubize	90	127

Before dealing with the visualization and interpretation of spatial and statistical correlation results of Li and other CRMs, understanding the hydrogeochemical system and governing processes might help to explain the trace metal mineralization processes.

4.2 GROUNDWATER CLASSIFICATION AND HYDROGEOCHEMICAL PROCESSES

4.2.1 Quality control and ionic balance check

Prior to the analysis and classification of the hydrochemical data, the quality of the hydrochemical analyses has been assessed. In hydrochemical studies, data errors may occur during sampling, storage, analysis, or during reporting. Quality checking is therefore of crucial importance. All data of the 652 analysed water samples from the 366 sampled wells underwent a quality assessment. This includes verification of the major ionic balance to ensure the chemical validity of the analyses. Incomplete analyses and analyses with high ionic balance errors (more than 10%) were discarded. 576 samples, of which the ionic balance error is between 0.01% and 10%, are considered for visualization purposes and for further classification of water types and major cation and anion interpretation.

4.2.2 Stuyfzand (1986)-classification

The core of most groundwater classification systems lies in identifying the dominant cations and anions present in the water. In some cases, these systems also incorporate indicators of total mineralization or salinity. The Stuyfzand (1986)-classification method integrates both chemical composition and salinity, while also including a water hardness indicator and a cation exchange code. This comprehensive approach makes the system especially valuable for assessing groundwater salinization and freshening processes.

Stuyfzand (1986) established a groundwater classification in which each water type is classified by four symbols. Each of these refers to a classification element. The first symbol, which is the major type, is based on the Cl^- content in mg/l. The water types based on Cl^- are classified into six classes, such as Fresh (F) (Cl^- < 150 mg/l), fresh-brackish (Fb) (Cl^- ranges from 150–300 mg/l), brackish (B) (Cl^-

ranges from 300–1,000 mg/l), brackish-salt (Bs) (Cl^- ranges from 1,000–10,000 mg/l), salt (S) (Cl^- ranges from 10,000–20,000mg/l), hyperhaline (H) ($Cl^- > 20{,}000$ mg/l). The second symbol is based on the total hardness (TH), which can be expressed in French hardness degrees:

$$TH\ (°F) = 5 \times (Ca^{2+} + Mg^{2+})\ \text{in meq/l}$$

Based on total hardness, groundwater can be grouped into 10 classes, from very soft (code: *) to extremely hard (with symbols given 1 to 9 with increasing TH values) (Stuyfzand, 1986). The third symbol consists of the water type, which is based on the names of the main cation and anion (in meq/l). The last symbol in the classification name indicates if cation exchange has taken place and the nature of this exchange. Symbols -, ø, + are given for (Na + K + Mg)-deficit, (Na + K + Mg)-equilibrium, and (Na + K + Mg)-surplus, respectively. The sum of Na^+, K^+, and Mg^{2+} (meq/l) is corrected for the seawater contribution, determined from the Cl^- content. The details about the Cl^- correction and the criteria to classify into Na^+, K^+ and Mg^{2+} deficit, equilibrium, and surplus are given by Stuyfzand (1986). All the water samples that are qualified for analysis are classified accordingly and displayed in Figure 26. The map depicts groundwater samples classified according to the four hydrochemical parameters (salinity, total hardness, dominant cation–anion pairs, and cation exchange status) discussed above. Each coloured dot on the map represents a unique water type code derived from these parameters.

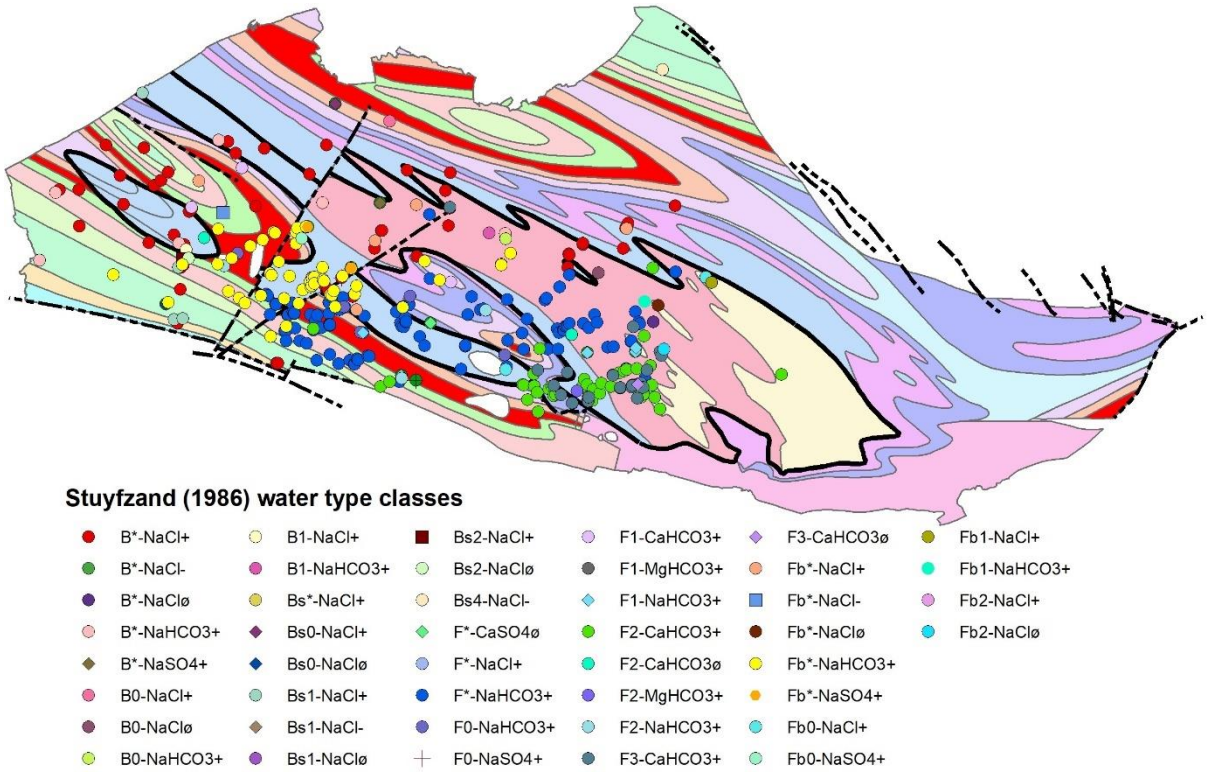

Figure 26. Classification of water type using the Stuyfzand (1986)-classification system.

The groundwater quality across the region is shaped by a long-term interaction between fossil marine influences, meteoric water recharge and hydrochemical processes such as cation exchange. In the northern part of the Brabant Massif, the dominant water types are brackish to brackish-salt, characterized by NaCl chemistry. These are typically coded as B*-NaCl+, Bs0-NaClø, or Bs1-NaCl+, indicating moderate to high chloride concentrations, dominance of Na^+, and evidence of cation exchange (surplus). The "+" code signifies that Na^+ is being released into the water through cation exchange processes, likely because Ca^{2+} from infiltrating freshwater is replacing Na^+ adsorbed on the surfaces of clay minerals. These chemical signatures are indicative of aquifers that retain a significant

marine imprint, due to past seawater intrusion and to limited flushing of the aquifer (Bogaerts, 1998; Walraevens, 1987).

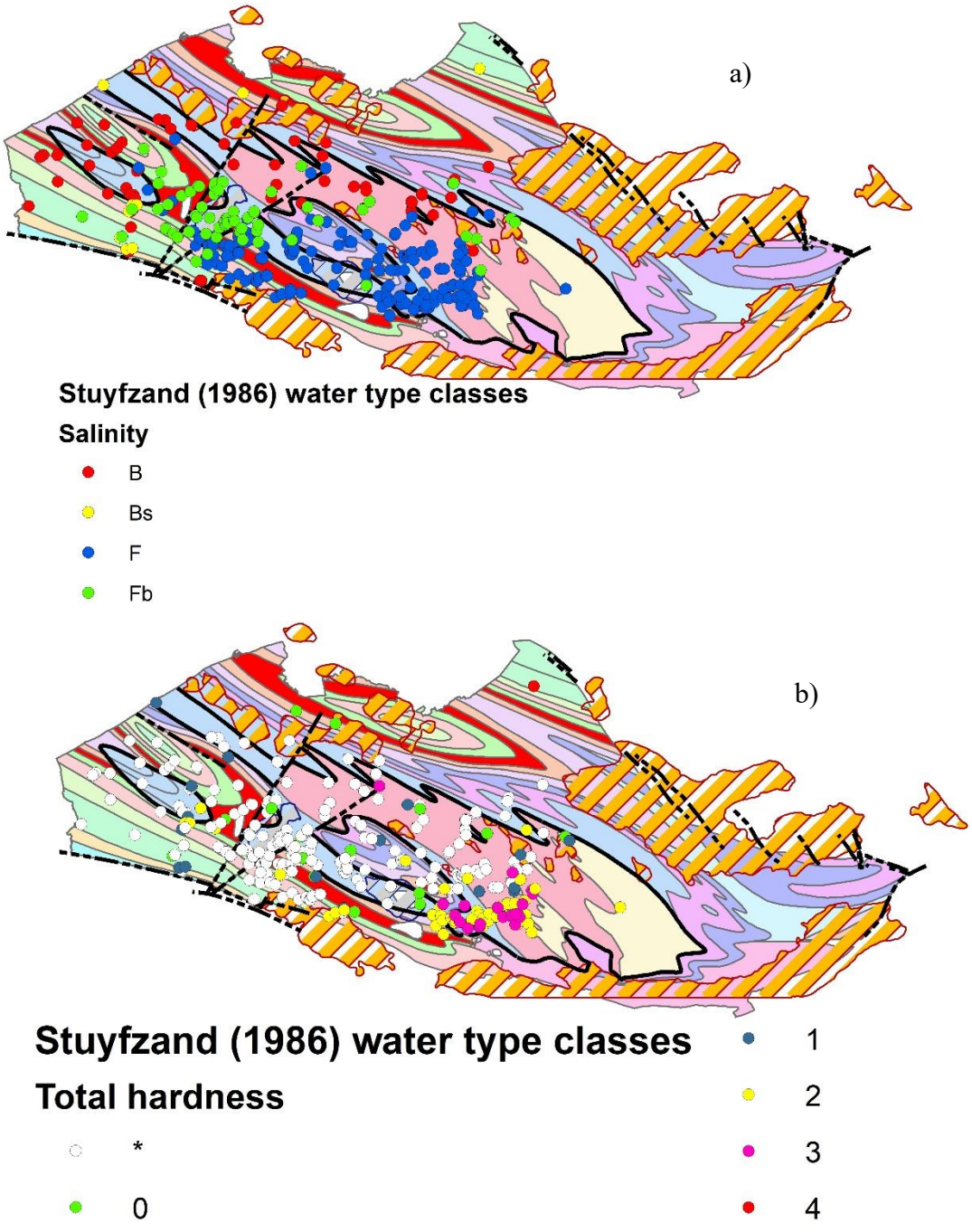

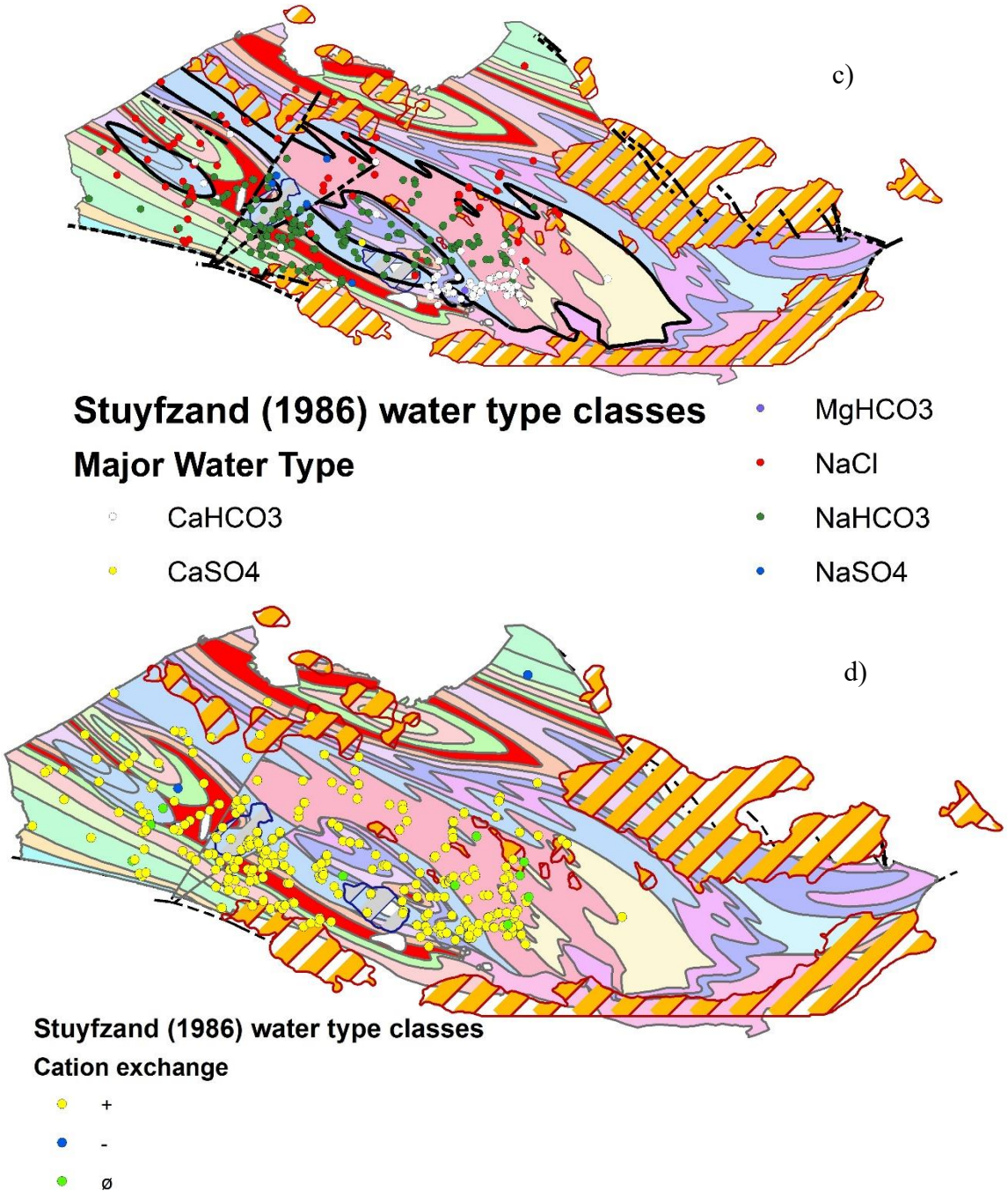

Figure 27. Individual parameters of the Stuyfzand (1986)-classification: salinity based on Cl^- concentration (a), total hardness (TH) in French hardness degrees (b), major water type based on dominant cation and anion (c), and cation exchange maps based on Stuyfzand (1986)'s classification system (d).

Moving towards the central part (more south and southeast) of the Brabant Massif (Figure 26), the water types begin to reflect transitional conditions. This is an area where freshening is underway, but not yet complete. The prevalent groundwater types here include Fb-$NaHCO_3$+, B0-$NaHCO_3$+, and B1-$NaHCO_3$+, which are intermediate in salinity but show a marked shift from chloride to bicarbonate dominance in anions. Na^+ continues to dominate among cations, but the presence of bicarbonate signals the increasing influence of recharge water. The recharging water might not be recent recharging water; rather, it could be old recharge water that is infiltrating through the thick overlying Cenozoic geological formations. The basement aquifers are hydrogeologically found at the deepest below the Cenozoic formations, being confined by several tens of meters of thick clayey confining

layers. These confining layers may considerably slow the recharge of the deep aquifer system, resulting in relatively old recharge water. These waters are not only the result of conservative mixing between salt and fresh water; rather, their chemical composition reflects cation exchange of Ca^{2+} by Na^{+}. As infiltrating water dissolves carbonates and displaces adsorbed marine cations, the water becomes enriched in Na^{+} and related cations (e.g., Li^{+}) and bicarbonate while remaining relatively soft. Going further upstream to the south and southeast, the water type changes into F*-NaHCO3+, F0-$NaHCO_3$+, F2-$NaHCO_3$+, and F1-$NaHCO_3$+, showing the dominance of freshwater, though still the cation exchange is determining the major water type as NaHCO3 instead of CaHCO3 (Figure 27c).

In the most southeastern part of the Brabant Massif, groundwater quality is markedly different. Here, the predominant water types are fresh and calcium-bicarbonate based, denoted by codes such as F2-$CaHCO_3$+, F3-$CaHCO_3$+, F2-$CaHCO_3$+, and F3-$CaHCO_3$ø. These water types suggest the influence of recharge zones. The dominance of Ca^{2+} as the principal cation, coupled with bicarbonate as the major anion, indicates that these waters have equilibrated with carbonate minerals in the aquifers. This part of the aquifer system has likely been fully flushed of older, more saline water, allowing the chemistry to reflect the modern meteoric type, while still showing evidence of the last stage of cation exchange, as shown in the types with (Na+K+Mg) surplus (+).

The hydrochemical sequence revealed by the maps (Figure 26 & Figure 27) follows a logical spatial progression from NaCl-type water in downstream parts of the aquifer through $NaHCO_3$-type waters in transitional zones, to $CaHCO_3$-dominated types in the most southerly recharge areas. This sequence is consistent with the conceptual model of groundwater freshening, where marine water is progressively displaced by rainwater infiltration. According to Walraevens (1997), the regional groundwater quality in the Brabant Massif, is controlled by two end-members. These are the marine conditions that occurred in the rock strata of the basement aquifers at the end of the Neogene marine transgression, on the one hand, and the fresh water from precipitation that infiltrated into the Cenozoic formations, and gradually percolated to the basement aquifers, on the other hand. Cation exchange plays a critical role in this process, especially in the early stages, by releasing dominantly Na^{+} from clay minerals into the water and elevating its concentration even in zones of freshwater. However, the spatial transition from NaCl to $NaHCO_3$ to $CaHCO_3$ water types from north to south and southeast is not entirely straightforward. As shown in Figure 26, there are fresh to fresh–brackish $NaHCO_3$ water types in the northwestern part of the area (around Tielt, Pittem, Torhout, etc.), where more brackish NaCl-type waters would be expected. This can be explained by the topography and related recharge zones shown in Figure 28. In these zones, infiltration through the thicker Cenozoic formations (which takes thousands of years by itself) locally provides a freshwater end member that enhances flushing and accelerates cation exchange for the aquifer water in the basement.

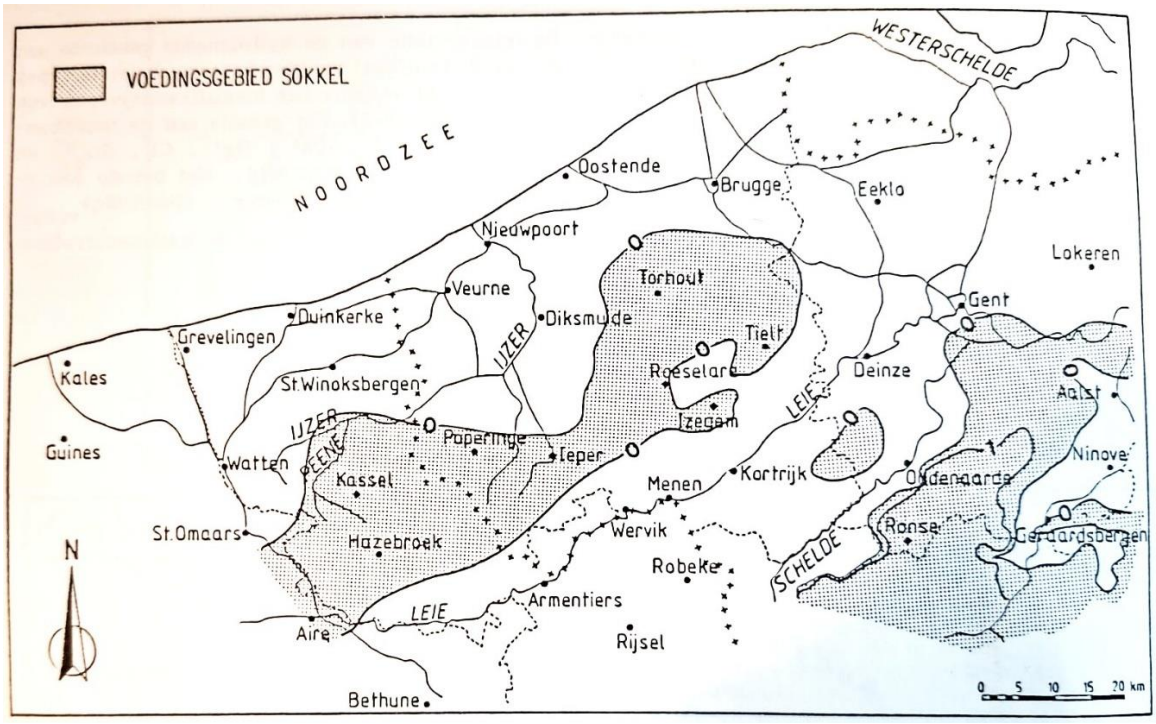

Figure 28. Groundwater recharge zones of the Flemish Massif, taken from Walraevens et al. (1989).

Even though the geographical distribution (2D location) of the sampled wells plays a major role in determining the chemical signature, the depth of the wells is also taken into consideration: deeper wells are supposed to be more mineralized (more marine), and freshening is expected to be less pronounced than in the shallower ones that are more affected by recharge processes. Thus, a box plot of depth for each water type is prepared (Figure 29).

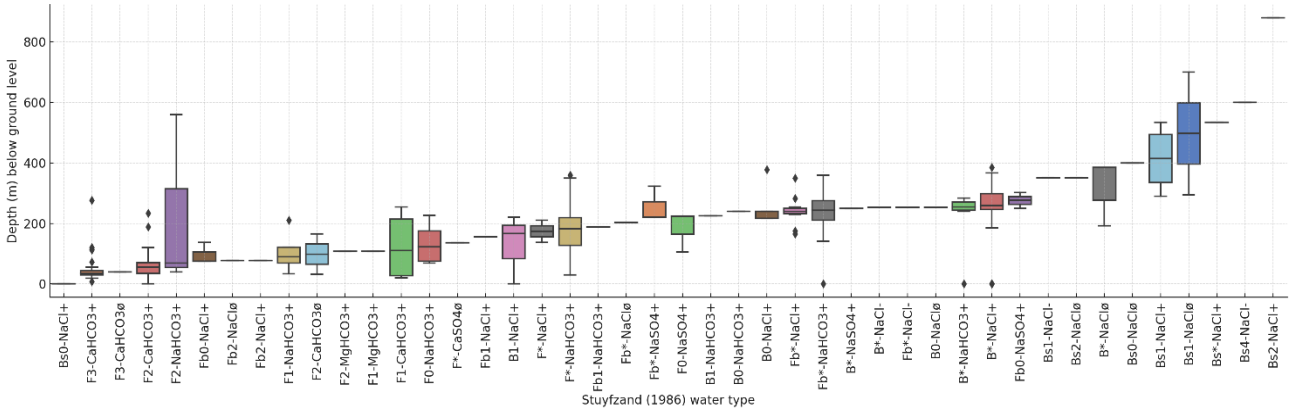

Figure 29. Box plot of depth of wells for each water type using Stuyfzand (1986).

Freshwater types such as F1-$CaHCO_3$+, F3-$CaHCO_3$ø, and F2-$NaHCO_3$+ are generally related to shallower depths. Brackish and brackish-salt types, like Bs1-NaCl+, Bs2-NaCl+, and Bs4-NaCl+, are clearly found at greater depths, indicating older groundwater with less flushed zones, i.e. where marine water could be preserved. Intermediate types such as Fb*-NaCl+ and Fb1-$NaHCO_3$+ lie between these two ends, representing transitional zones where freshening is ongoing but not complete. This depth trend supports the hydrochemical evolution model of the Brabant Massif: shallow groundwater is fresher, while deep groundwater retains saline characteristics due to limited flushing and the influence of fossil marine waters.

In general, the Stuyfzand (1986)-classification map offers valuable insight into the hydrogeochemical evolution of groundwater within the Brabant Massif. The spatial distribution of water types illustrates a clear transition from marine-influenced to meteoric water-dominated systems. The presence of NaCl and $NaHCO_3$ water types in the deeper and central areas of the Brabant Massif highlights ongoing freshening and cation exchange. The $CaHCO_3$ water type is found in the recharge zones, showing the freshwater end member of the system.

4.2.3 Piper-diagram

Additionally, the water types of the dataset are classified using the Piper-diagram, and both the distribution of water types according to the Piper-diagram and the Piper-diagram are shown in Figure 30. Similar to the Stuyfzand (1986)-classification, the Piper-plot shows the strong influence of the paleo seawater (most probably the connate seawater that intruded the aquifers during the Paleogene and Neogene marine transgression) on the groundwater chemistry. Also, the cation exchange of especially Na^+ by Ca^{2+}, played a significant role in the water chemical signature.

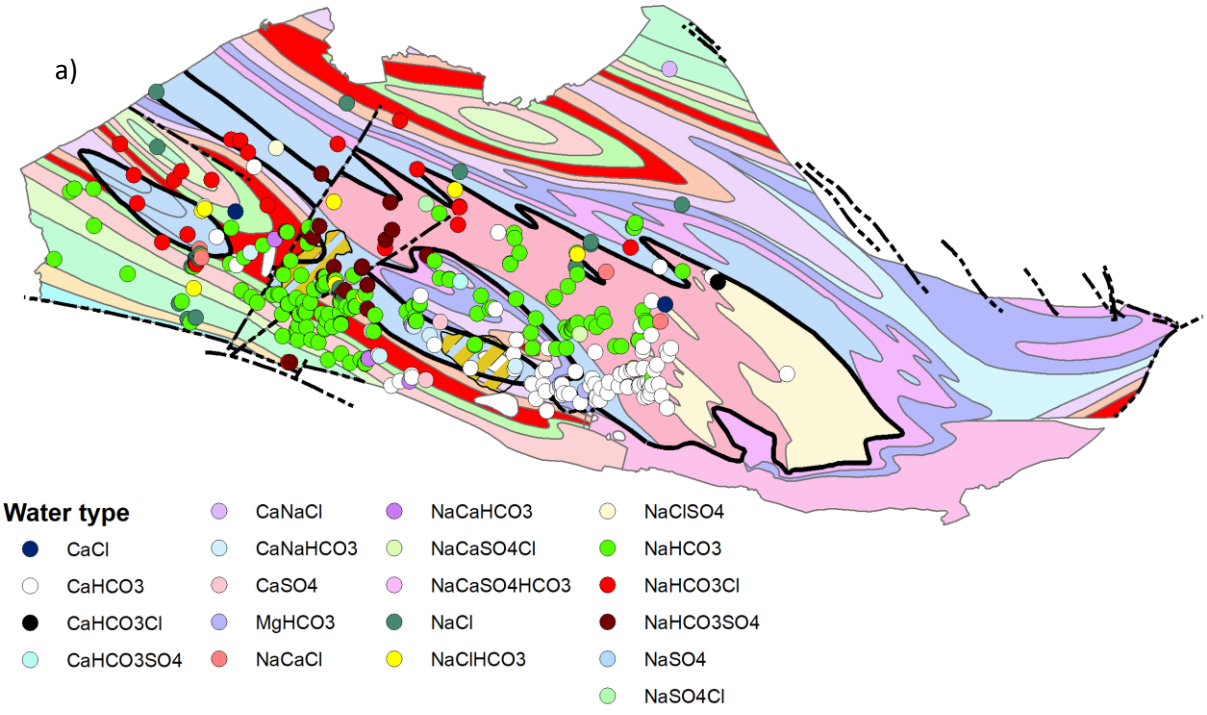

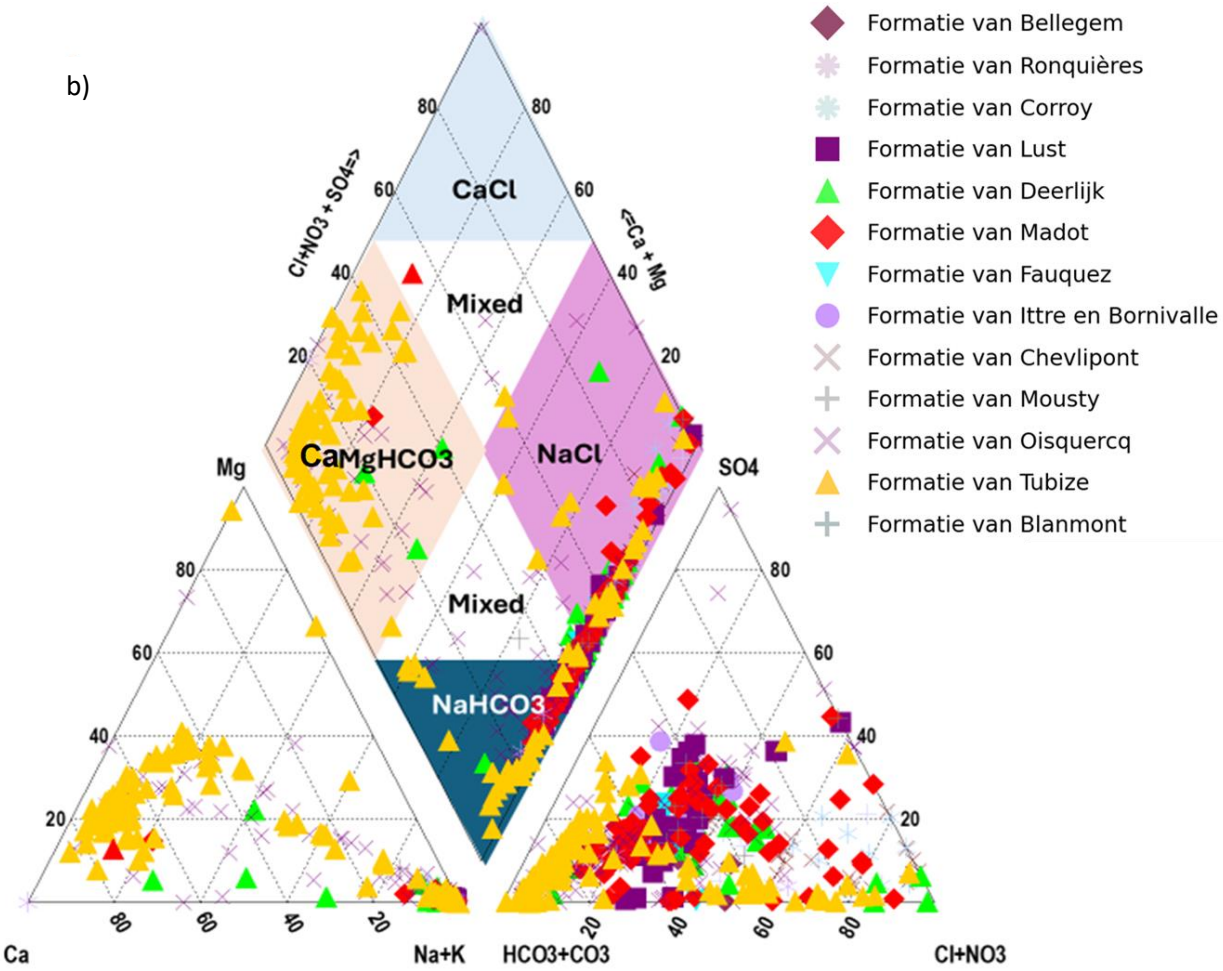

Figure 30. Distribution of the main water types (a) and Piper-diagram (b) of the groundwater in the aquifers of the Brabant Massif.

Figure 30a displays the spatial distribution of groundwater types across the study area, classified by dominant cations and anions (e.g., $NaHCO_3$, CaCl, NaCl). It shows that $NaHCO_3$ type waters dominate the central part of the region, indicating zones of ongoing freshening and cation exchange. In contrast, NaCl and $NaHCO_3Cl$ types are mostly located in the north zones, reflecting areas with strong residual marine influence. The $CaHCO_3$ waters, concentrated toward the southeastern part, suggest recharge type freshwater.

Figure 30b is a Piper-diagram that classifies water types hydrochemically with indication of geological formations. It shows that given water types are not necessarily associated with particular geological formations. A given geological formation can contain different water types. As one geological formation type consists of different lithologies, in addition to different parameters like depth and potential presence of fractures and faults, this association and further interpretation are found to be complicated. Together, the figures indicate a clear geochemical evolution from marine-influenced NaCl waters towards more fresh $CaHCO_3$ types driven by dilution from the freshwater that infiltrated from the overlying formations.

In conclusion, groundwater in the Brabant Massif exhibits significant hydrochemical diversity, reflecting the different hydrochemical processes: mainly salt-freshwater mixing, and cation exchange processes. Spatially, the groundwater evolved from marine-influenced NaCl type in the north and northwest to a fresh $CaHCO_3$ type in the south and southeast, driven by dilution and cation exchange.

4.3 SPATIAL VISUALIZATION OF HYDROGEOCHEMICAL DATA

In this chapter, hydrogeochemical data of the different analysed ions are visualized over the subcrop geological map of the Brabant Massif (VLA03-1.1, Piessens et al., 2005) and geophysical data (gravimetric Bouguer anomaly map for potential presence of granitic bodies at the subsurface, Everaerts and De Vos, 2012). The primary objective of this study is to spatially contextualize groundwater sample data in relation to regional and local geological frameworks using GIS software (ArcGIS). The spatial correlation of the major ions with Li and other CRMs, and CRMs to each other, has been studied, and possible geological and hydrogeological relationships are interpreted.

4.3.1 GIS mapping

The constructed groundwater database has been imported into ArcGIS, where the data were analysed within the geological framework of the Brabant Massif. Values below the limit of detection (LOD) were assigned LOD/2 for the visualization, and are totally omitted for correlation purposes; the latter is done in order to avoid bias on the correlation coefficient. As demanded by DOMG, this framework was the subcrop map of the Brabant Massif (VLA03-1.1) of Piessens et al. (2005). To enhance the interpretation of the hydrogeochemical data with the hypothesised granitic intrusion in the subsurface (see the detail in Piessens et al., 2005), a gravimetric Bouguer anomaly map was overlaid as well. Faults and fractures have also been mapped based on the Piessens et al. (2005) map. These geological and geophysical GIS layers were then used to examine the spatial relationship between groundwater chemistry, local geology (formation level), and geological structures.

The previous subcrop geological map of the Brabant Massif made by De Vos et al. (1993) (Figure 31) was remapped by Piessens et al. (2005) to a scale of 1:200,000 (Figure 25). The new map was prepared using new data captured between 1993 and 2001, in addition to the old database used in the previous mapping. Many geological structures are omitted in the new map, which is mainly based on drilling validation, unlike the old map, that was mainly based on the gravimetric and magnetic geophysical data interpretations. However, the concept of the Asquempont detachment system (Figure 25, Piessens et al., 2005) was kept..

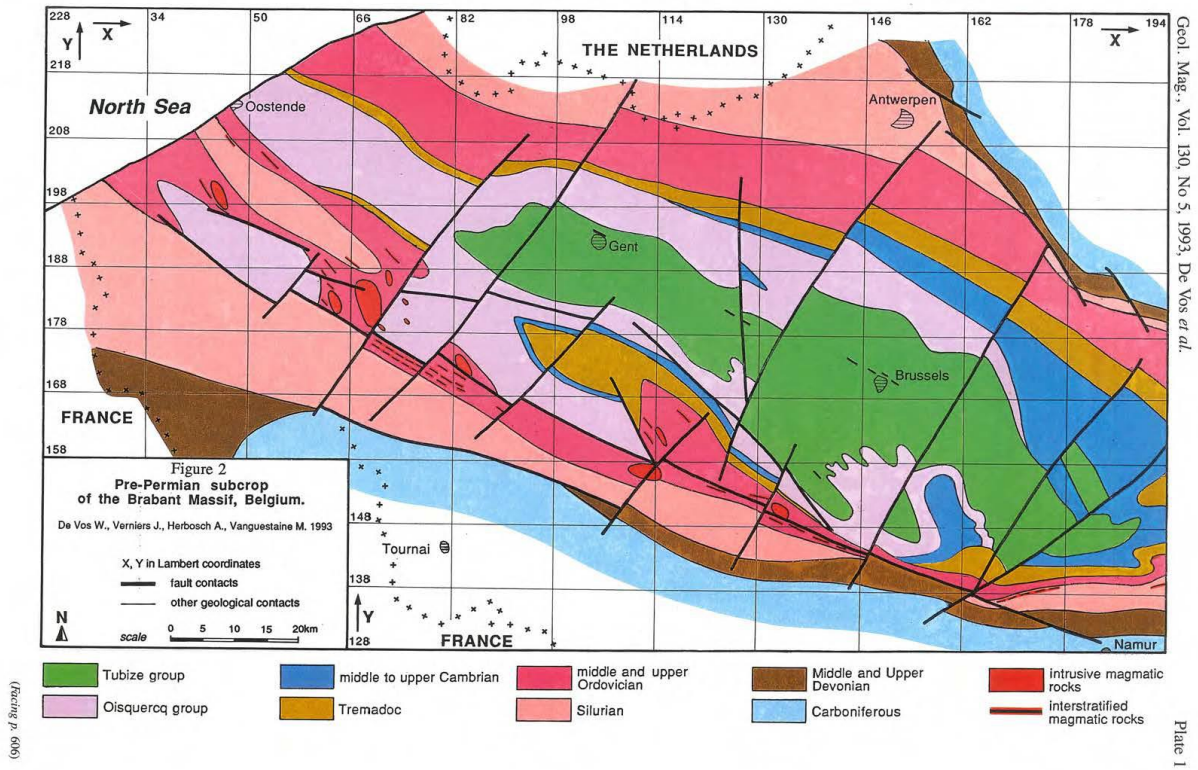

Figure 31. A previous version of the old geological map of the Brabant Massif, taken from De Vos et al. (1993).

4.3.2 Spatial distribution of lithium (Li)

The only data source for Li concentration distribution is the 49 newly analysed water samples by VMM-DOMG. Therefore, the spatial correlation for this element is limited to this data source. Still, these sampling points are distributed across the different geological formations and are more or less fairly distributed throughout the study area.

Before going into the detailed spatial association and correlation analyses, the average concentration of Li in groundwater has been reviewed from the scientific literature resources. The objective was to identify what should be considered as an anomalous Li concentration according to the geological context. According to the studies by Dugamin et al. (2021), Li et al. (2022), Lindsey et al. (2021), Lombard et al. (2024), and Zhang et al. (2022), the expected concentration of Li depends on the groundwater sources mentioned in Table 15. For example, Lindsey et al. (2021) mentioned that the Li concentration in the groundwater across the United States ranges from < 0.001 mg/l to 1.7 mg/l. The Li et al. (2022) study in Tibet found that concentrations higher than 5 mg/l are common in high-temperature geothermal zones. The latter study also found that most of the enrichment is due to magma degassing rather than leaching from the surrounding rocks by circulating groundwater. According to Zhang et al. (2022), high Li^+ concentrations in groundwater are usually related to mixing with fossil seawater and/or deep–seated processes, such as volcanic fluid input, magmatic–hydrothermal fluid influx, or leaching from Li-rich rocks. Thus, the correlation and interpretation of Li should take into account all these possible hydrogeochemical processes.

Table 15. Common concentration of Li in different groundwater groups and seawater compiled from different literature studies.

Source Type	Typical Li Concentration (mg/l)
Fresh groundwater (common range)	0.001- 0.020
Slightly mineralized groundwater	0.01- 0.05
Geothermal or deep aquifers	0.1-5.0 (sometimes much higher)
Seawater (for comparison)	~0.17

The Li^+ concentration in our database was analysed according to the categories of Table 15 and compared with the scientific literature mentioned above. The values in this study range from 0.002 mg/l to 0.1 mg/l, with a mean of 0.043 mg/l and a standard deviation of 0.028 mg/l. The dataset has a Q1 of 0.02, a Q3 of 0.07, and a median of 0.035 (Figure 32). According to Eurofins Analytico, the detection limit for Li^+ is 0.001 mg/l. As the lowest measured concentration is 0.002 mg/l, the reported values are above the detection limit, although the lowest concentrations remain relatively close to it. Therefore, these low values can be interpreted with reasonable confidence, while minor differences among the lowest concentrations should still be treated with some caution.

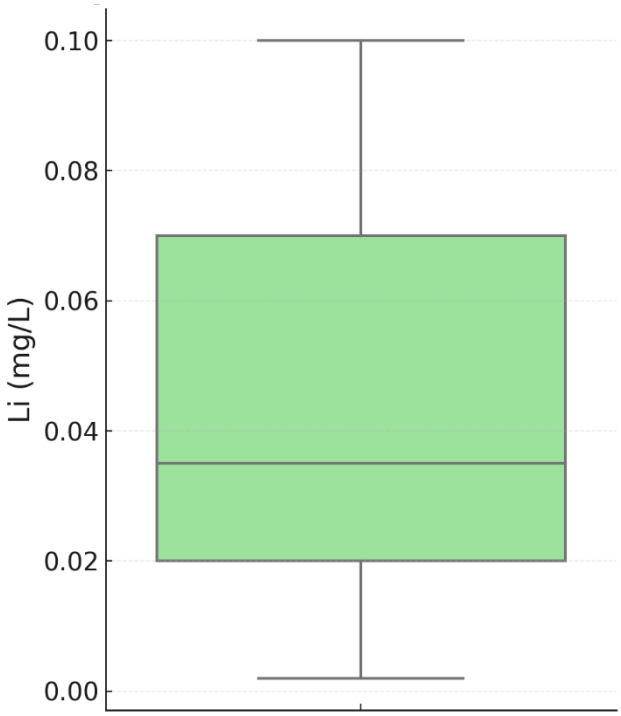

Figure 32. Box plots of the observed lithium concentrations in the VMM-DOMG data.

The concentration of Li^+ is generally low to medium (Table 15). There is no sample value that can be considered as a hydrochemical anomaly (that underwent abundant rock-water interaction) (Figure 32). The concentration of Li^+ is typically higher in the northwest and decreases towards the southeast of the Brabant Massif. Though the subsurface map only shows the formation of the upper part of the Brabant Massif, we have tried to see if there is any correlation between the concentration of Li^+ and the corresponding geological formation. However, there is no clear association with any of the formations (Figure 33).

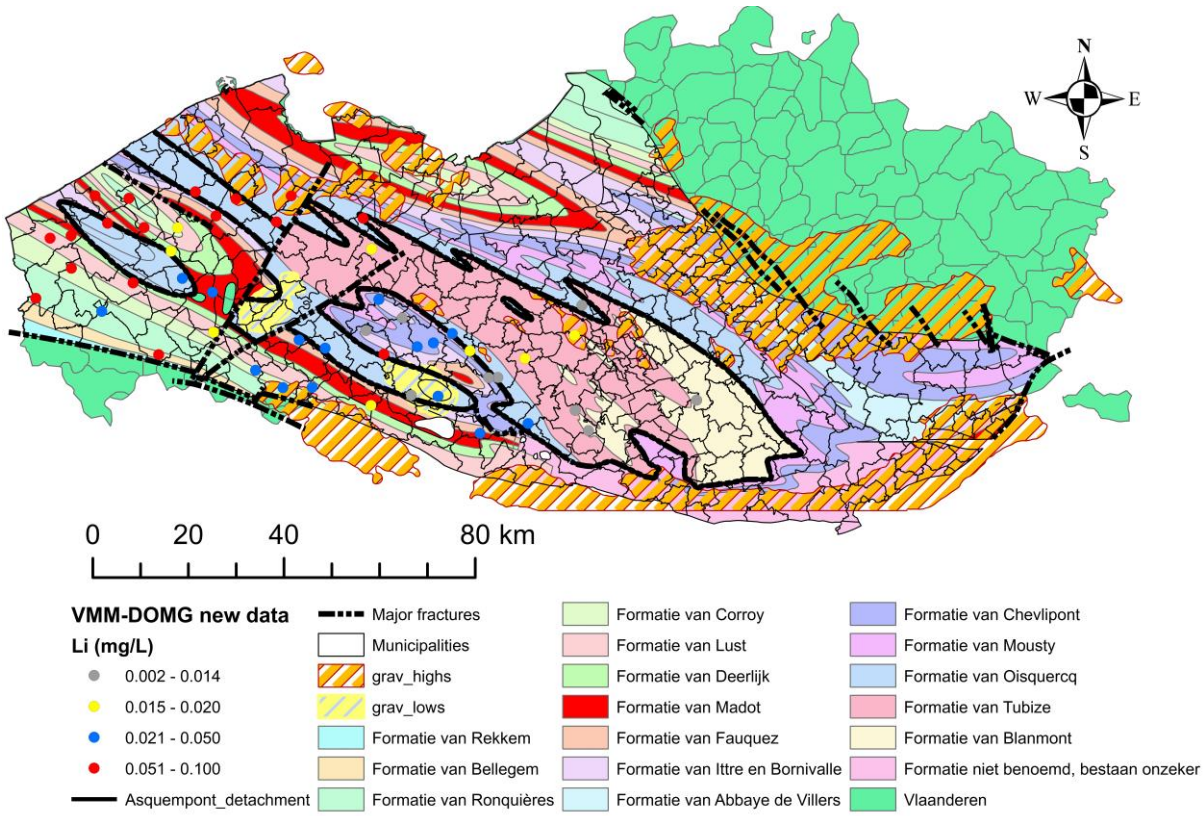

Figure 33. Concentration of Li overlaid over the Brabant Massif geological formations, mapped by Piessens et al. (2005). The gravity anomalies are included.

To understand the factors controlling the spatial distribution of Li^+ concentrations, it is essential to first examine its statistical correlation with major ions (Na^+, Ca^+, Mg^{2+}, K^+, Cl^-, HCO_3^{2-}, SO_4^{2-}). This correlation analysis serves as a foundation for interpreting the spatial relationships between Li^+ and these ions. Once these statistical associations are established, the spatial trends can be analysed in relation to the distribution of Li^+. Concentration of Li^+ is statistically fairly correlated with Na^+ and Cl^- (Figure 34a & b). Cl^- is assumed to be a conservative anion, inactive in water-rock reactions except in rare cases (e.g., presence of evaporite rock types such as halite). Its concentration can be used as a tracer for seawater intrusion and anthropogenic pollution, for example, from landfill leachate and wastewater. The moderate correlation between Li^+ and Cl^- points to mixing of fossil marine water in the Brabant Massif aquifers with fresh groundwater infiltrating from the overlying aquifers (see chapter 4.2). To see how the fossil seawater mixing controls the water chemistry, the seawater mixing line is added to the cross plots. The reference values for major ions of the end members were adapted from Walraevens and Van Camp (2004). As Figure 34b shows, there is a surplus of Li^+ compared to Cl^-, suggesting the presence of a non-marine source of Li^+. This could be due to cation exchange with Ca^{2+}. The infiltration of freshwater in recharge areas leads to both dilution and cation-exchange processes. At the onset of recharge, the resident saline groundwater is mainly diluted by mixing with infiltrating freshwater. With continued infiltration, cation exchange becomes increasingly important: marine cations (Na^+, K^+ and Mg^{2+}) adsorbed on clay-mineral exchange sites are progressively displaced by Ca^{2+} carried by the freshwater (Walraevens, 1997). Li^+, which is monovalent like Na^+ and can be relatively abundant in seawater, may also be released from exchange sites during this freshening process.

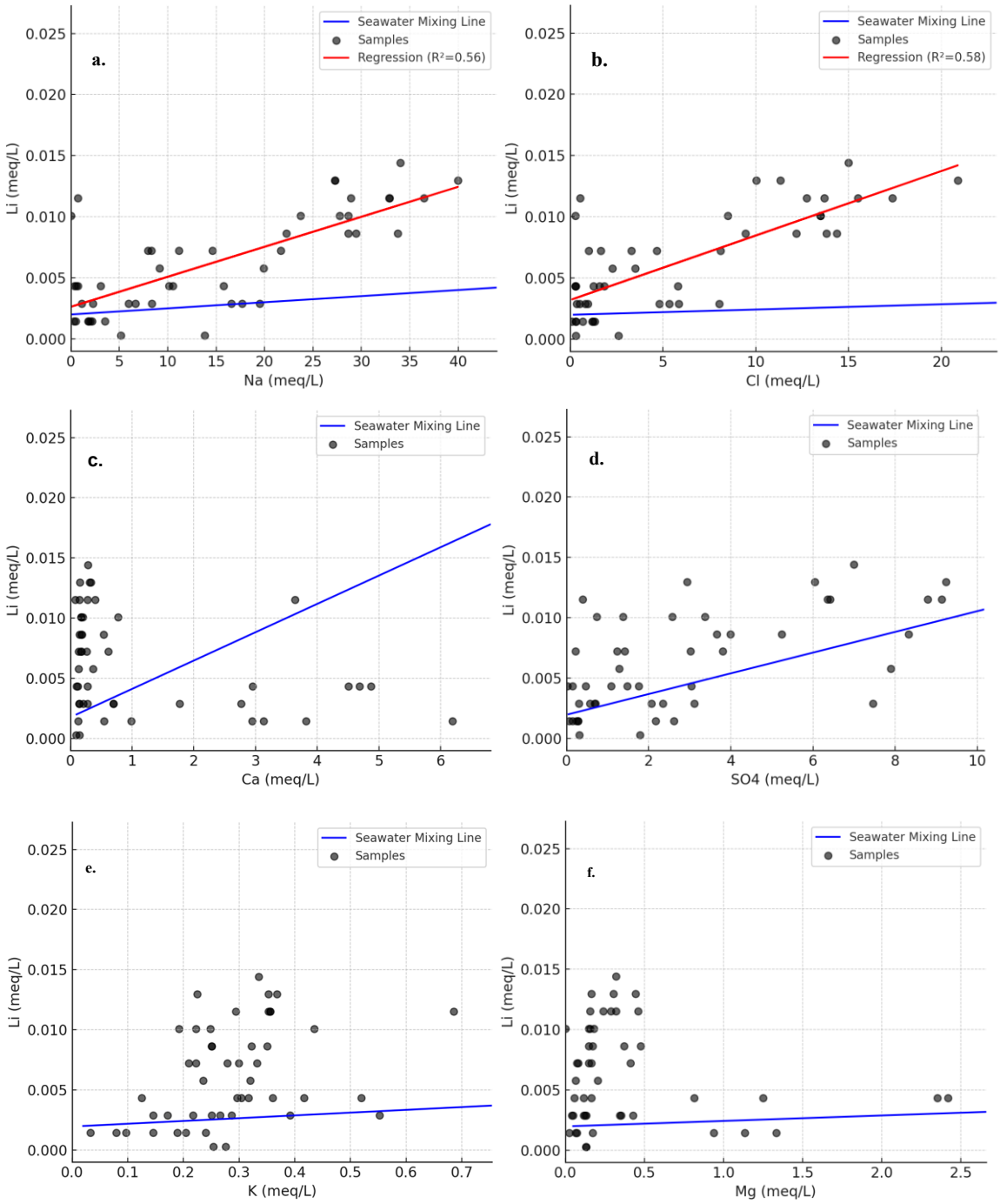

Figure 34. Statistical correlation of Li^+ versus major cations and anions with the seawater mixing line.

Both Cl^- and Na^+ are more or less spatially correlated with Li^+ (Figure 33 &

Figure 35). As it is noted by Bogaerts (1998), the concentration of Na^+ increases from south to north. Na^+, because of its position in the cation exchange affinity sequence, will be the first cation to undergo cation exchange with the Ca^{2+} from the infiltrated fresh water. Because this exchange has been occurring for a long time, a clear, increasing trend from south to north and northwest for Na^+ and a decreasing trend for Ca^{2+} can be seen in Figure 35a & c. However, the expected significant negative correlation for all of the data sets, both between Na^+ and Ca^{2+}, and Li^+ and Ca^{2+} (Figure 34c), is not observed. This must be due to the additional hydrogeochemical process of calcite dissolution that increases Ca^{2+} concentration without affecting both Na^+ and Li^+.

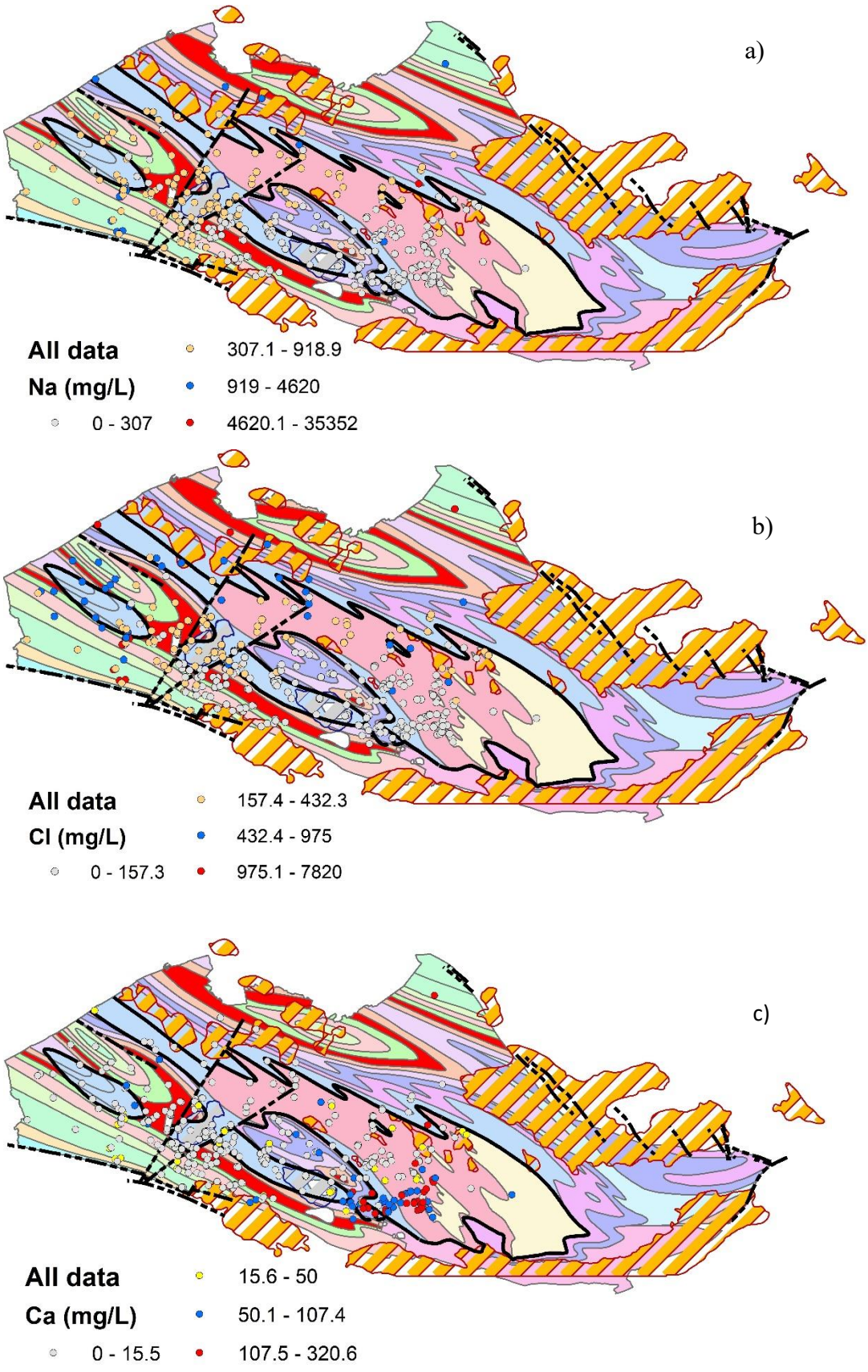
a)
All data
Na (mg/L)
0 - 307
307.1 - 918.9
919 - 4620
4620.1 - 35352
b)
All data
Cl (mg/L)
0 - 157.3
157.4 - 432.3
432.4 - 975
975.1 - 7820
c)
All data
Ca (mg/L)
0 - 15.5
15.6 - 50
50.1 - 107.4
107.5 - 320.6

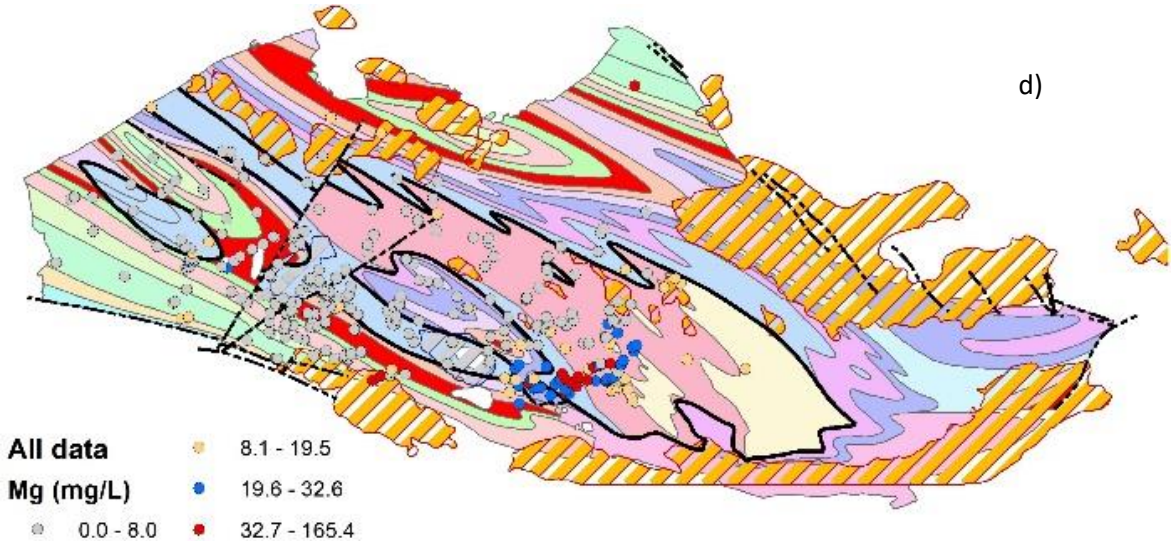
d)
All data
Mg (mg/L)
0.0 - 8.0
8.1 - 19.5
19.6 - 32.6
32.7 - 165.4

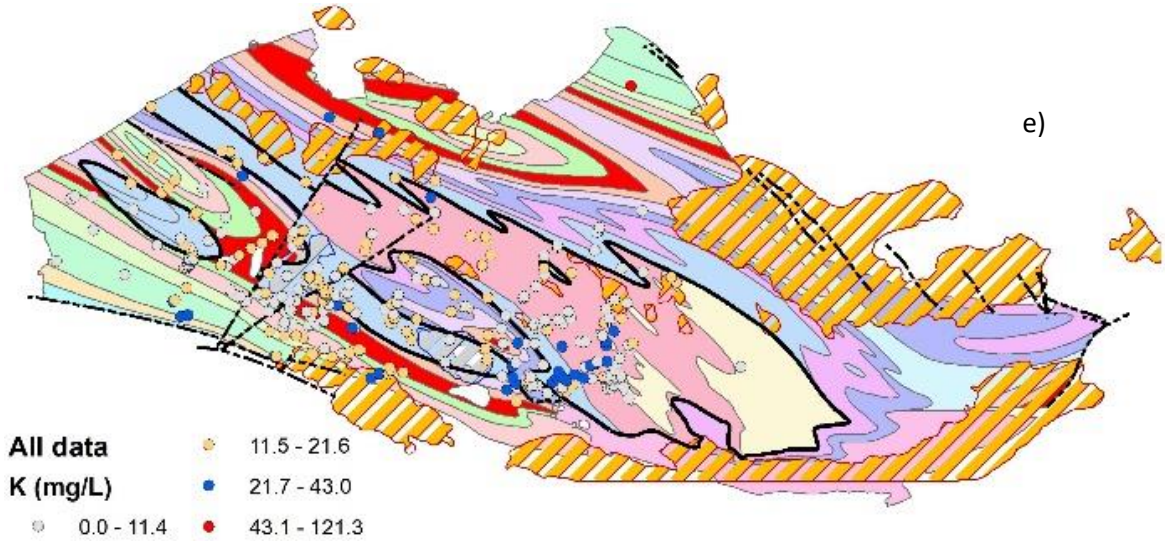
e)
All data
K (mg/L)
0.0 - 11.4
11.5 - 21.6
21.7 - 43.0
43.1 - 121.3

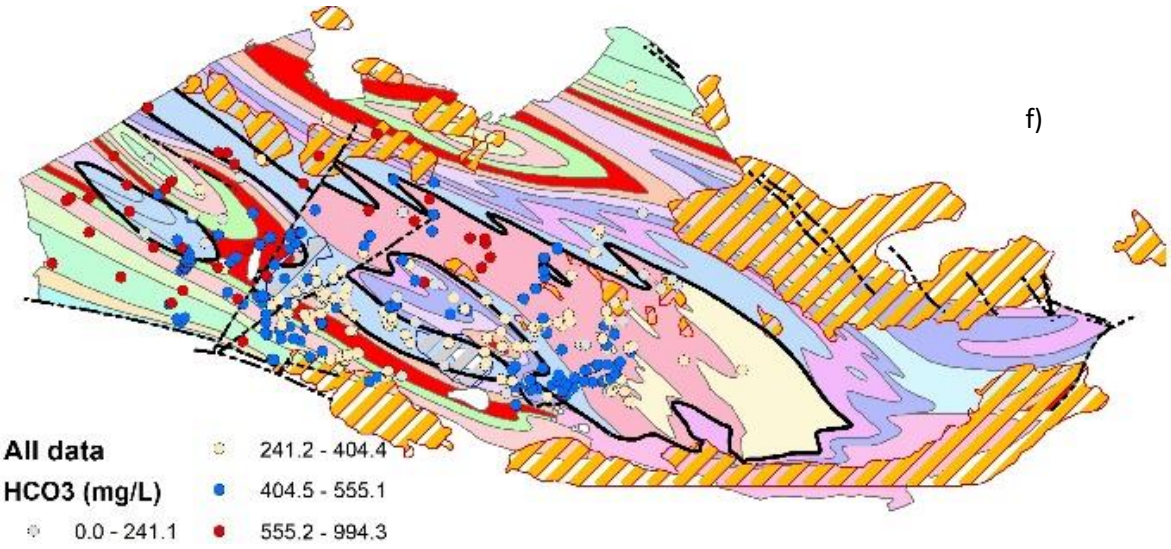
f)
All data
HCO3 (mg/L)
0.0 - 241.1
241.2 - 404.4
404.5 - 555.1
555.2 - 994.3

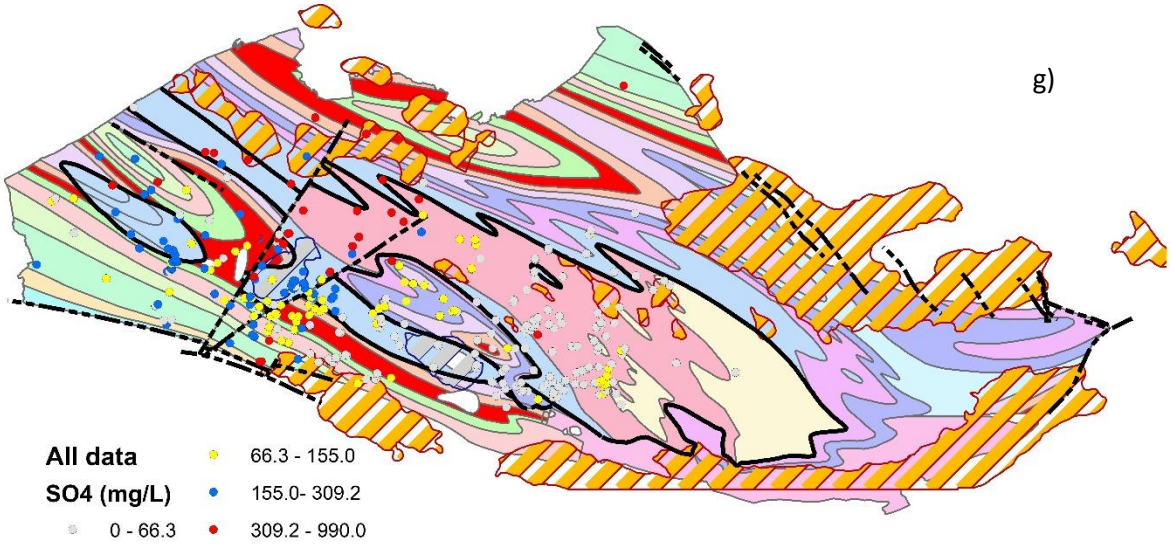

Figure 35. Concentration distribution of major cations and anions over the Brabant Massif.

One of the assumptions is that the presumed felsic magmatism, thought to be present at depth in the Brabant Massif, could be a source of Li. According to this hypothesis, higher hydrochemical concentration of Li in the deeper wells, especially where gravity lows are mapped, is expected. However, as it is shown in Figure 36 and Figure 37a, there is neither a good correlation with depth nor with interpreted gravity lows.

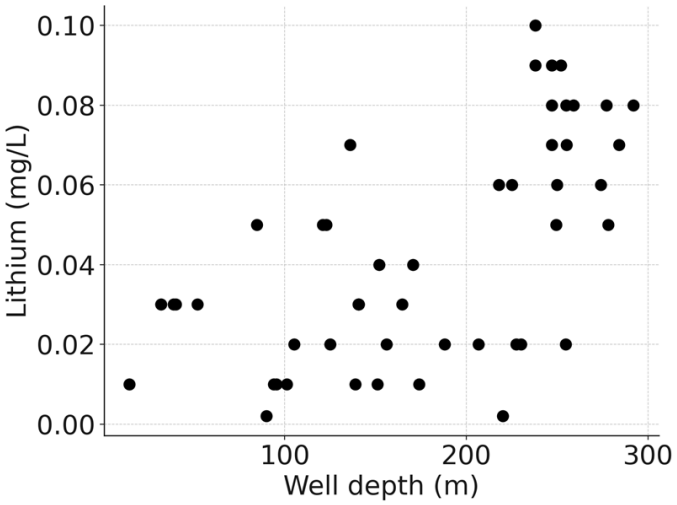

Figure 36. Concentration of Li^+ (mg/l) versus well depth for the 49 VMM-DOMG analyses.

B and Li are commonly associated elements in felsic magmatism (Trompetter et al., 1999). However, among the 49 new VMM-DOMG analyses, only 8 samples show values above the detection limit for B, which limits to do direct statistical correlation with Li^+. Nevertheless, sufficient B data from the other datasets used in this study are available to evaluate the spatial relationship between B and Li^+. As Figure 37 shows, the concentration distribution of B does not have a clear spatial trend compared to Li^+ (decreasing from northwest to southeast). This may reinforce the previous conclusion that Li^+ concentration in the groundwater of the Brabant Massif is mainly controlled by fossil seawater mixing and cation exchange rather than leaching of magmatic rocks.

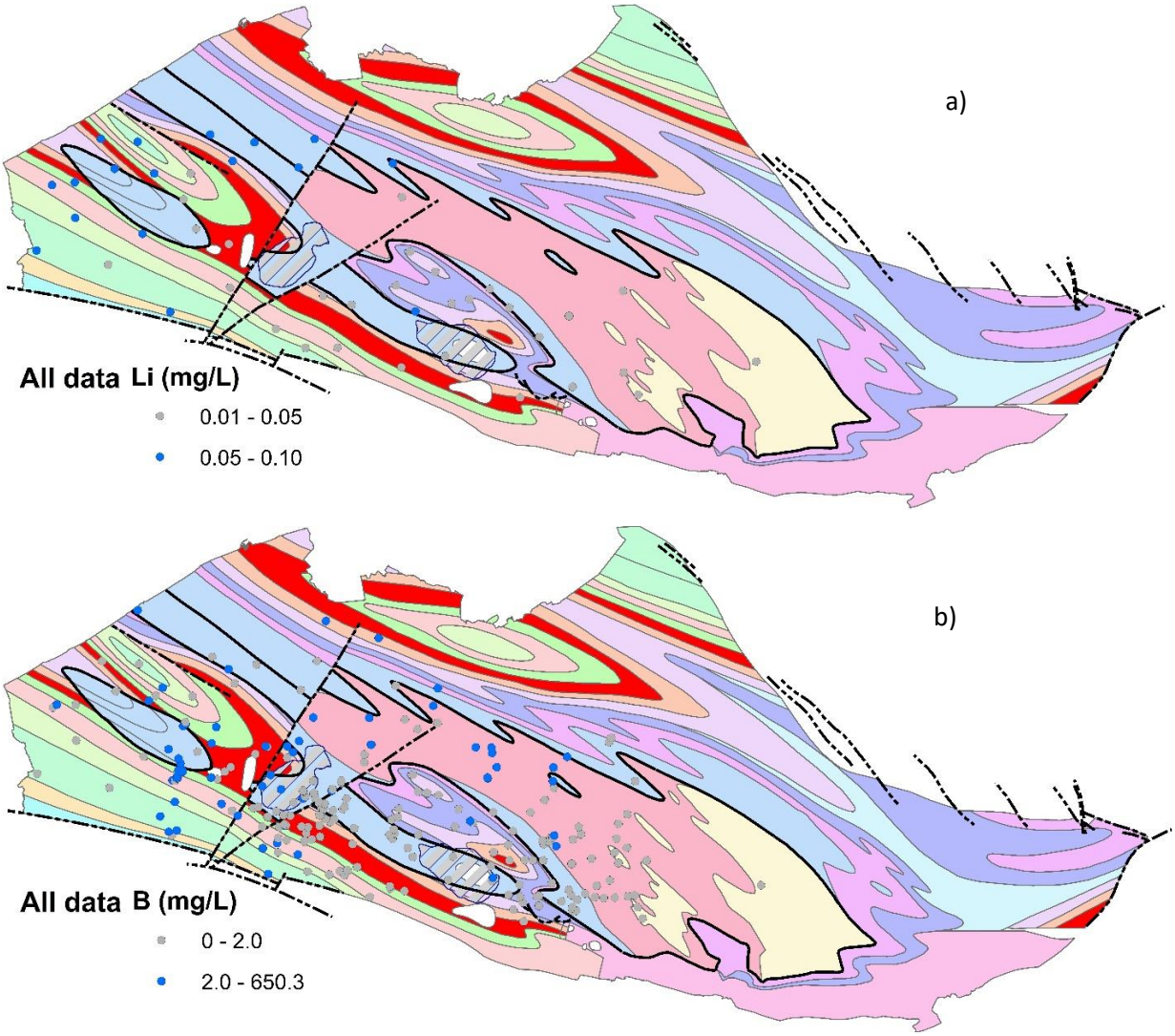

Figure 37. Concentration distribution of lithium and Boron. The upper value of the first range in the legend is the cutting point for the hydrochemical anomalies (see Table 16).

4.3.3 Distribution of other Critical Raw Materials (CRMs) and trace elements

Other critical raw materials and trace elements (such as Bi, Pt, Nb, Cd, Au, Sn, Co, Sb, W, Ni, As, Mo, Cu, Cr, Se, Ba, Zn, Sr, V) besides Li have also been considered in this study. The spatial correlation of these trace elements with each other and with major ions has been evaluated. Similar to what has previously been noted by Sterpin (1996) (Project VLA/94-3.5), no meaningful statistical correlations among the trace elements and with major ions were found in this study either. Sterpin (1996) attributed this to the predominance of low and very low concentration values, where relative analytical errors are significantly higher, and to the strongly logarithmic distribution of the data, particularly the presence of anomalous values that distort the correlation coefficient.

For the visualization of the concentration of each trace element on the GIS map, we first establish threshold values above which the concentration is regarded as hydrochemical anomaly. We set threshold values by studying the statistics of the data (e.g. their histograms) and using literature references (e.g. Sterpin, 1996) for determining thresholds in this study (Table 16). The range, mean, standard deviation, and the different percentiles are also included in Table 16. Furthermore, a histogram containing the concentration distribution of the different trace elements is presented in Figure 38. The histograms reveal important insights into the geochemical behaviour of these

constituents in groundwater. Most of the CRMs and trace elements, including Bi, Pt, Ag, Cd, Sn, Sb, Pt, Mo, Cu, Cr, Zn, Sr, Ba, Co, Ni, As, W and Nb, display strongly right-skewed distributions. This indicates that the majority of samples contain very low concentrations of these elements, while a small number of samples exhibit significantly elevated levels, suggesting the presence of localized hydrogeochemical anomalies. This is in line with the percentile values of Table 16 and studies by Sterpin (1996). Several elements, such as Sr, Zn, Ba, and Pb, exhibit particularly wide concentration ranges, which may reflect varying geological sources or processes, especially in the case of Sr, which reaches values up to 6000 ppb.

Most of the samples are below the determined threshold value, but there are anomalous values for all of the trace elements (Table 16 & Figure 38. Histogram concentration distribution of the trace elements discussed in the following paragraphs, as well as Li.). Most anomalies are limited to the upper percentile (90^{th}, $95^{th,}$ and 97.7^{th}), meaning that typically only a few samples display high concentrations. The mean values for the different elements are below the defined threshold except for Bi, Cd, and Pb.

Table 16. Threshold values of the different trace elements in groundwater and statistical measurements of the analysed data. Threshold values are determined by both adapting the threshold values of Sterpin (1996) and histograms of the data used in this study.

Element	Treshold values (ppb)	Measured range (ppb)	Measured mean (ppb)	St Dev (ppb)	10th Perc (ppb)	50th Perc (ppb)	90th Perc (ppb)	95th Perc (ppb)	97th Perc (ppb)
Bi	**0.01**	0.0 - 0.9	**0.09**	0.15	0.001	0.005	**0.25**	**0.3**	**0.48**
Pt	**0.03**	0.002-0.101	0.01	0.01	0.004	0.008	0.03	0.03	**0.05**
Ag	**0.04**	0.002 – 0.136	0.02	0.02	0.004	0.01	0.03	0.04	0.04
Nb	**0.08**	0.007 – 4.87	0.06	0.44	0.008	0.02	0.06	0.07	**0.11**
Cd	**0.2**	0.0 – 40.0	**0.72**	4.84	0.03	0.07	0.2	**0.48**	**1.21**
Au	**0.3**	0.022 – 3.72	0.18	0.37	0.04	0.09	0.29	**0.41**	**0.72**
Sn	**0.8**	0.0 – 4.0	0.32	0.5	0.03	0.09	0.7	**0.84**	**1.11**
Co	**0.8**	0.01 – 8.46	0.52	0.91	0.05	0.2	**1.1**	**1.64**	**2.64**
Sb	**0.8**	0.009 – 33.51	0.37	2.46	0.02	0.1	0.26	**0.81**	**1.54**
Pb	**1**	0.0 – 16.97	**1.48**	2.72	0.1	0.45	**4.2**	**6.3**	**10.91**
W	**3**	0.01 – 13.14	1.26	1.55	0.03	0.79	2.93	**3.25**	**3.8**
Ni	**7.5**	0.22 – 28.19	2.27	3.02	0.5	1.35	4	6.68	**10.32**
As	**8**	0.02 – 26.11	2.85	3.61	0.05	1.59	6.65	**8.55**	**14.43**
Mo	**10**	0.04 – 24.04	3.23	3.57	0.25	2.12	6.56	9.71	**12.68**
Cu	**10**	0.0 – 35.13	5.77	6.02	0.77	2.95	**13**	**15.42**	**20.71**
Cr	**10**	0.01 – 12.62	2.49	3.19	0.2	0.83	8.28	9.47	**10.63**
Se	**17**	0.0 – 30.64	5.8	6.37	0.1	2.79	14.06	**17.49**	**22.99**
Ba	**100**	1.11 – 1002.8	46.61	98.68	8.85	28.21	71.8	**135.9**	**250.2**
Zn	**200**	0.0 – 2426.3	79.92	201.62	3.62	19.1	199.7	**300**	**482.6**
Sr	**1000**	0.0 – 5829	337.08	602.54	31	138	849.5	**1041.3**	**1911.3**
Li	**100**	2.0 – 100.0	43	28.23	10	35	80	90	90

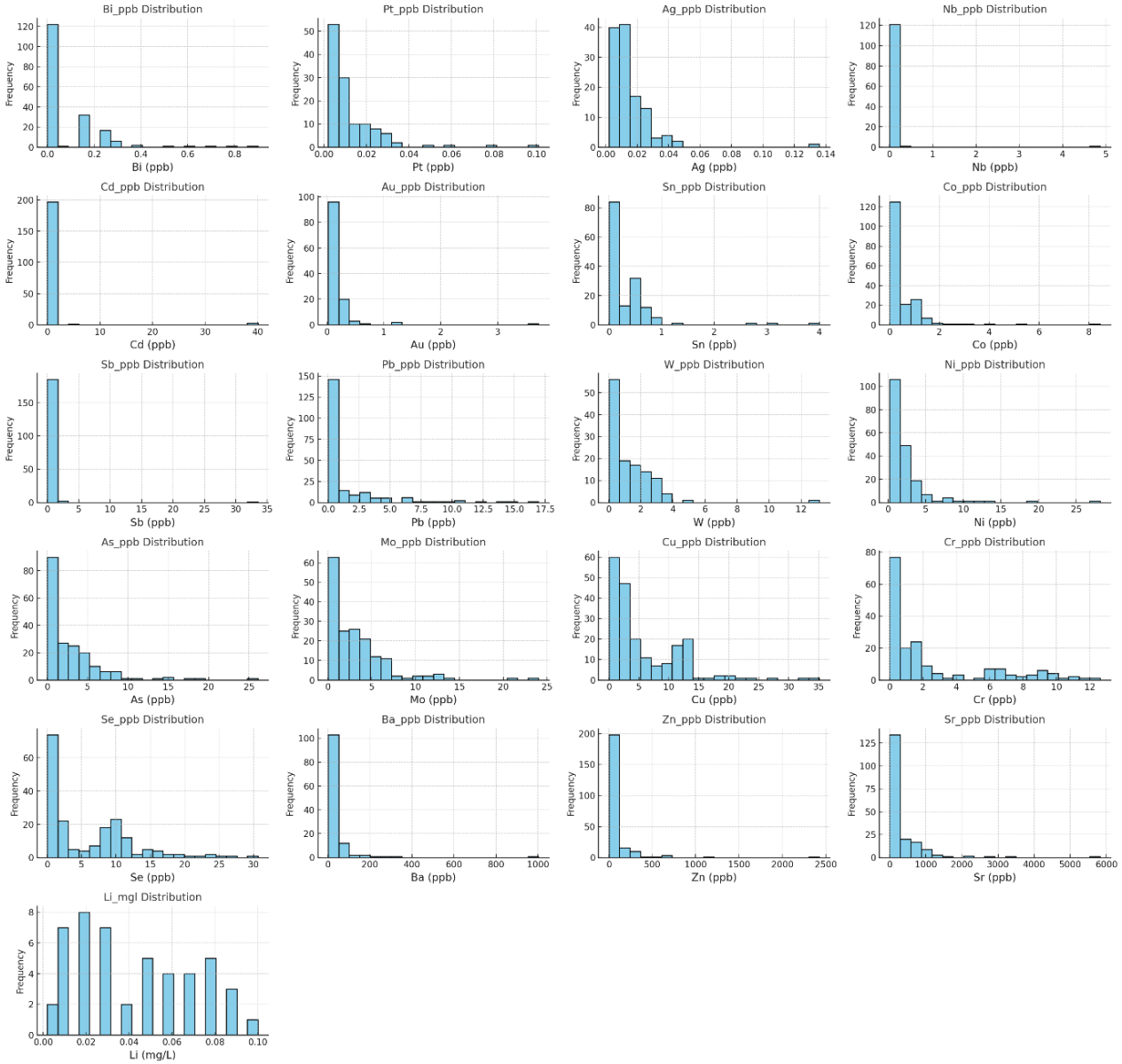

Figure 38. Histogram concentration distribution of the trace elements discussed in the following paragraphs, as well as Li.

The threshold values were used to classify the observed values into two classes for GIS mapping, and the interpretation focused on the spatial correlation of anomalous values with different geological features (formations, major fractures and faults). Most of the anomalies for trace elements are at Oostrozebeke-Waregem-Harelbeke-Deerlijk, which can be referred to as Zone 1 (Figure 39a). This zone is where the highest densities of anomalies are observed (e.g., Figure 39,
Figure 41, Figure 45). The other zone, where anomalies of some trace elements (such as Pb, Zn, Mn, Sn, Cd, to a certain extent Cu) are found, is the southeastern anomaly zone (Zone 2: area Oudenaarde-Brakel-Geraardsbergen) (Figure 39a). Other than these two, there is no geographical area that can be interpreted as a “broad” anomaly zone. However, there are areas where some anomalies are found for specific elements, such as in the southern Zonnebeke-Staden area, where anomalies such as for Zn and Bi are found, and the Oudenaarde-Brakel area, where anomalies for W and Mo have been observed. Besides, there are occurrences of scattered anomalies throughout the study area.

a)

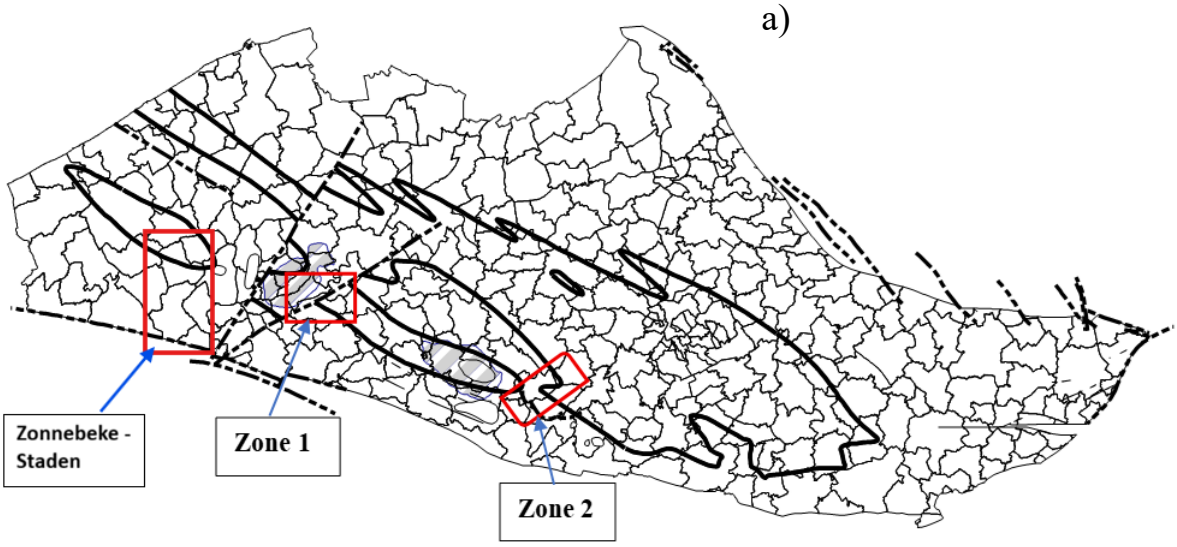
Zonnebeke - Staden
Zone 1
Zone 2

b)

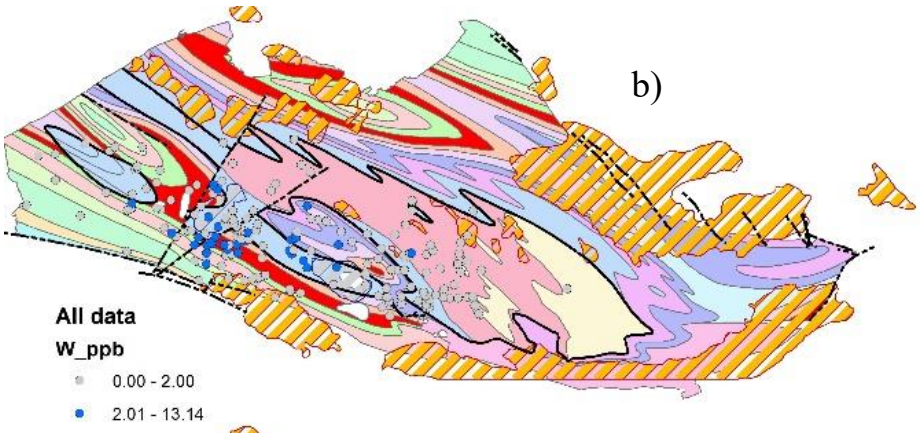
All data
W_ppb
0.00 - 2.00
2.01 - 13.14

c)

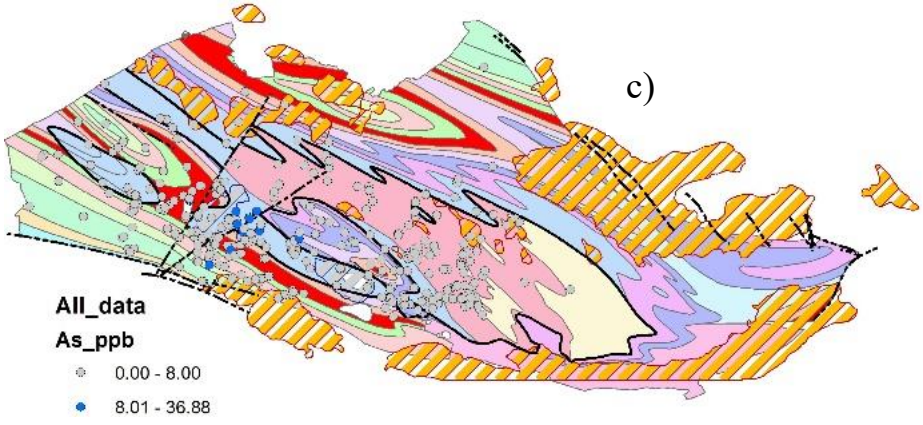
All_data
As_ppb
0.00 - 8.00
8.01 - 36.88

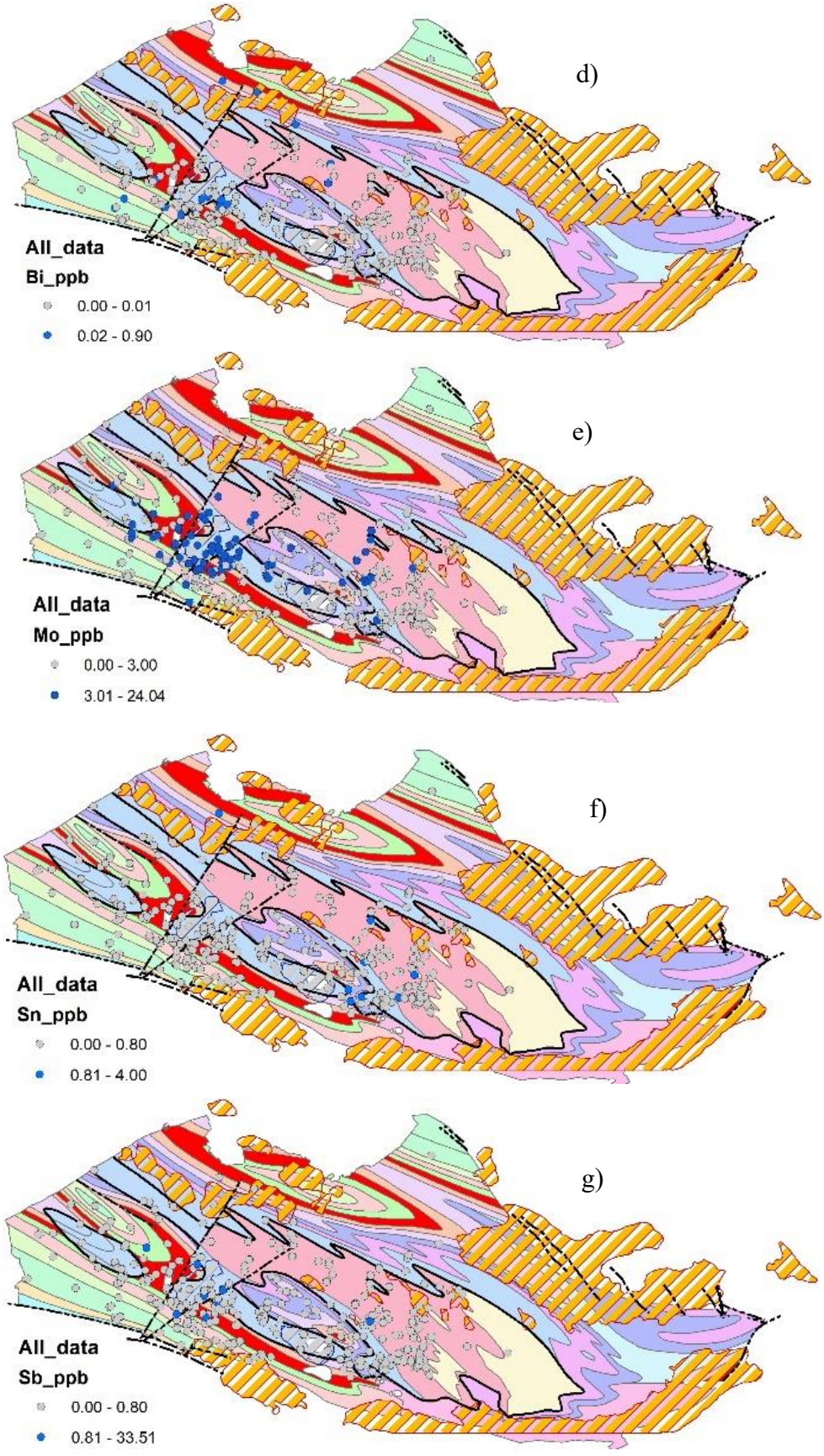

Figure 39. Concentration of some of the important trace elements. The anomalous values (see Table 16) are represented in blue. For the other elements, GIS-data is available in Appendix 5.

4.3.3.1 Tungsten (W), molybdenum (Mo), antimony (Sb), and tin (Sn)

Tungsten is one of the critical elements. There are a few samples with anomalous values of W (Figure 39b). These anomalous concentrations are concentrated in Zone 1 and a few samples in the Oudenaarde-Brakel-Geraardsbergen area. According to Thompson et al. (1999), W, Sn, Mo, and Sb can be found associated with intrusion-related mineralizations. As shown in Figure 39, in the Waregem area (Zone 1), anomalies of W, Mo, and Sb are spatially correlated. This has been also supported in Spearman's rank correlation (Figure 40), which show strong positive correlations between W and Mo ($\rho = 0.834$, $p < 0.001$, $n = 191$) and between W and Sb ($\rho = 0.793$, $p < 0.001$, $n = 191$), while Mo and Sb are also positively correlated ($\rho = 0.633$, $p < 0.001$, $n = 237$). Together, these spatial and statistical relationships support a possible link between these elements.This does not seem to be the case for Sn.

A statistical correlation of W with other major cations was made (Figure 40), and no meaningful correlation was found. Also, statistical correlation of W with other trace elements is not present (see Appendix 6).

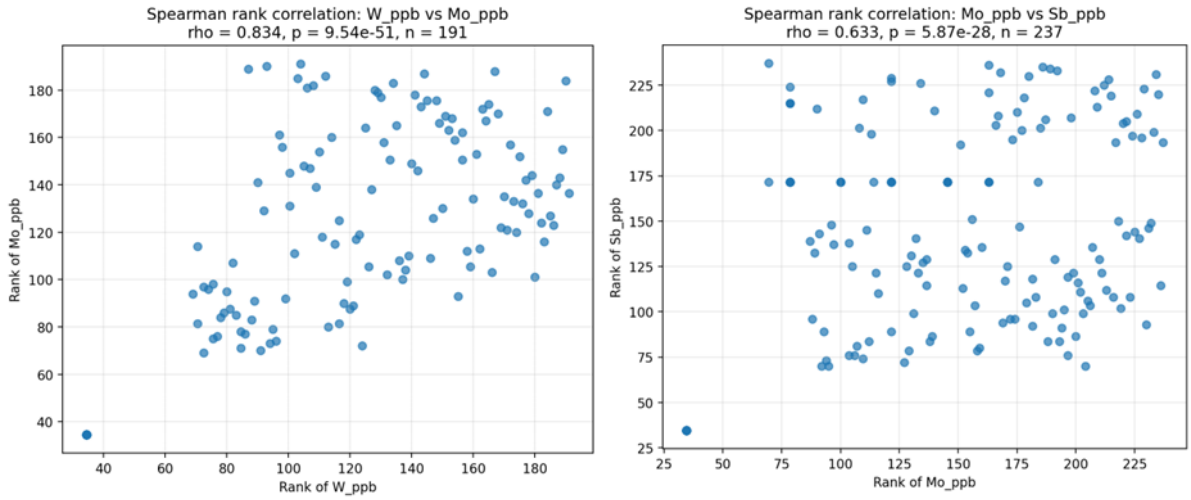

Figure 40. Spearman rank correlation among W, Mo and Sb.

Molybdenum is often assumed to be associated with selenium (Fitzgerald et al., 2008), e.g., in molybdenite ore. Thus, both the spatial and statistical correlations of Mo with Se and SiO_2 have been examined (

Figure 41 and Figure 42). From the histogram of Se (Figure 38), the anomalous value is set at 14.04 ppb, and the GIS map is prepared based on this threshold value. As can be seen in

Figure 41, Mo seems spatially well-correlated with Se. It has also a good spatial correlation with silica.

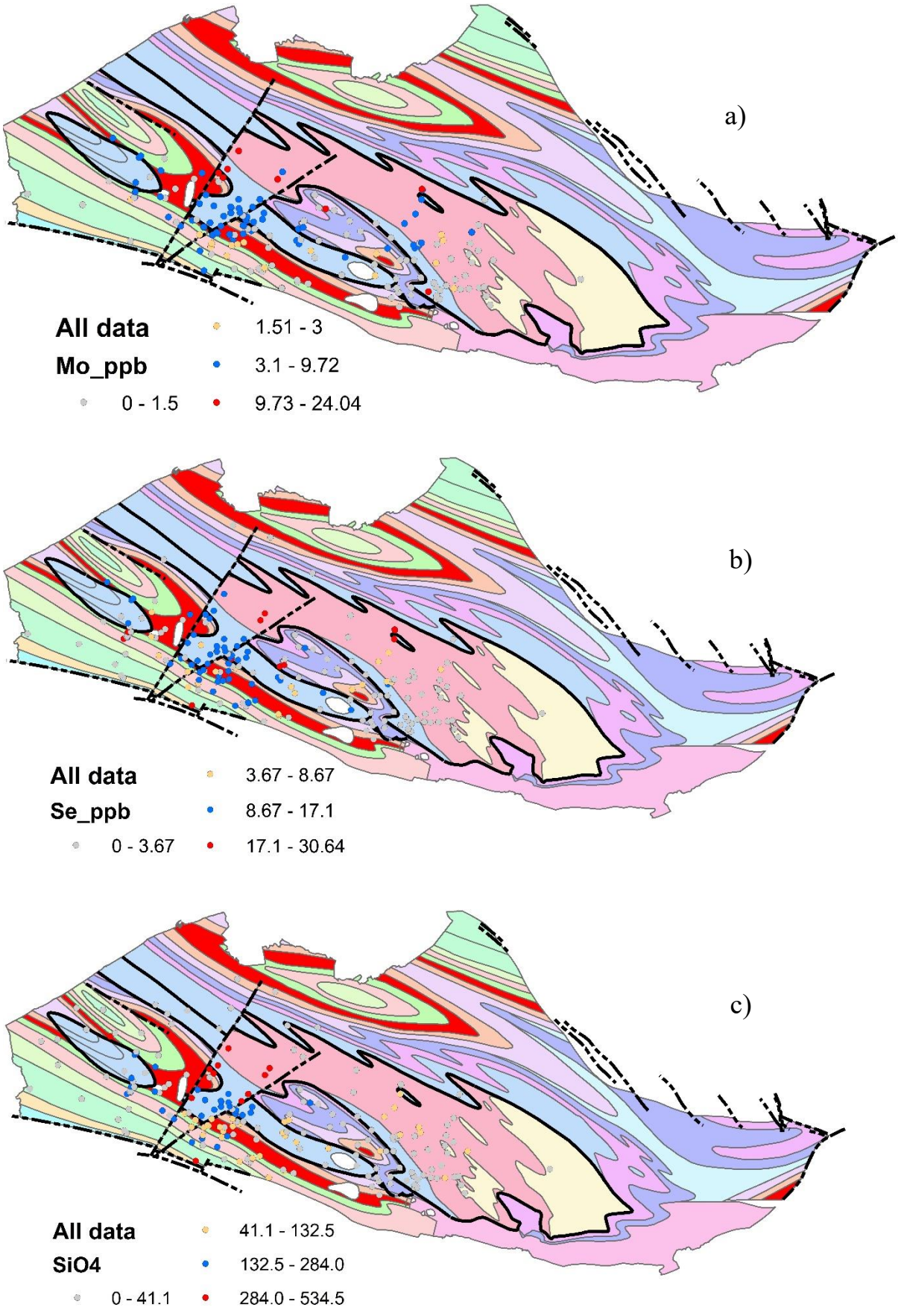

Figure 41. Spatial distribution of the concentration of Mo, Se, and silica.

Statistically, at most of the sampled wells, these elements have a fair correlation (Figure 42). However, due to outlier values at some of the wells, the R^2 values are low (approximately 0.4). This fair spatial and statistical correlation of Mo with Se and silica suggests that volcanic rocks (probably leached by hydrothermal activities in the fractures) could have played a role for the Mo and Se-concentrations observed.

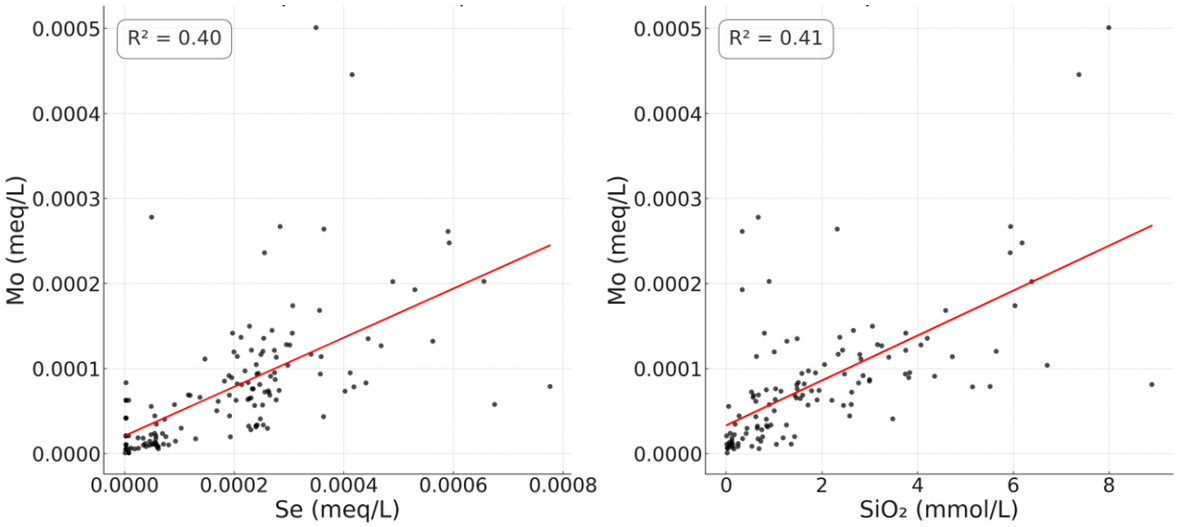

Figure 42. Statistical correlation of Mo with Se and silica.

4.3.3.2 Base metals

The other group of trace elements that are analysed and the target of exploration in this study is the base metal group, consisting of Cu, Pb, Zn, Fe, Mn, Ni, and Co. As shown in Figure 43, the anomalies for most of the base metals are concentrated in zones 1 and 2 (see also Figure 39a).
The distribution of base metals may reflect a complex interplay between lithology, geological structure, and geophysical anomalies (assumed intrusives at depth). Elevated concentrations of Cu, Pb, Zn, Fe, Mn, Ni, and Co are not randomly distributed in the Brabant Massif, but are instead spatially associated with specific hydrogeological phenomena and/or geological features.

Cu concentrations are highest in both Zone 1 and Zone 2 in the Brabant Massif as defined above (Figure 39a and Figure 43a). Pb is more diffusely distributed, with elevated levels also appearing in the southwest (Zonnebeke-Staden) area. Zn concentrations show strong spatial overlap with Pb and Cu, exceeding 1000 ppb in Zone 2, especially along the Asquempont detachment fault. Anomalous Fe concentrations are diffusely distributed and widespread throughout the Brabant Massif. On the other hand, anomalous Mn values are found in wells located in Zone 2. Anomalous Ni concentrations are found in Zone 1, and the highest concentration was analysed at a well located further southeast. The anomalous values of Co are found in Zones 1 and 2 (Figure 39a and Figure 43g), and also in the Zonnebeke-Staden area. Co shows a strong spatial correlation with Pb and Zn anomalous values.

The anomalies in Zone 1 are spatially correlated with a major depression cone (see Figure 43 and Figure 44). The groundwater exploitation that started more than a century ago, and intensified since the 1950th industial period, has led to substantial declines in piezometric levels in the deep aquifer system of the region, including the Paleozoic aquifers. As a result, regional depression cones, with drawdowns reaching up to 200 m, have developed in the aquifers of the Brabant Massif (Van Camp and Walraevens, 2009) (Figure 44). Piezometric levels have dropped dramatically below the top of the

Basement Aquifer. Walraevens et al. (1994) reported groundwater quality deterioration attributed to both the upcoming of more saline, deeper groundwater and the oxidation of minerals due to this substantial water level drop and the entry of air along wells. When oxygen gains access along the well annulus or inside the well, Fe-sulphides such as pyrite can oxidise, releasing dissolved Fe together with associated trace metals that occur as minor constituents in sulphide minerals. This mechanism is therefore expected to be spatially limited: the highest concentrations occur in the immediate vicinity of wells where oxygen entry is possible, whereas further from the wells oxygen is rapidly consumed and sulphide oxidation is inhibited, leading to lower trace-element concentrations in the groundwater. Overall, this well-induced aeration can be a primary control on the mobilisation of trace elements such as As, Pb, Cu, Zn, Ni, Co and Mn through the oxidation of sulphide phases.

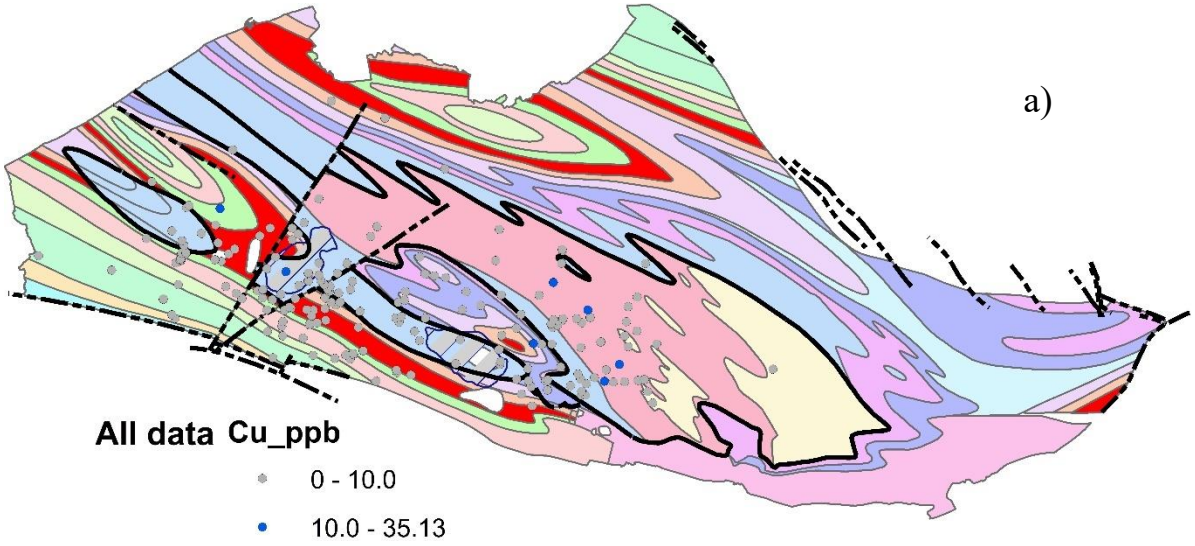

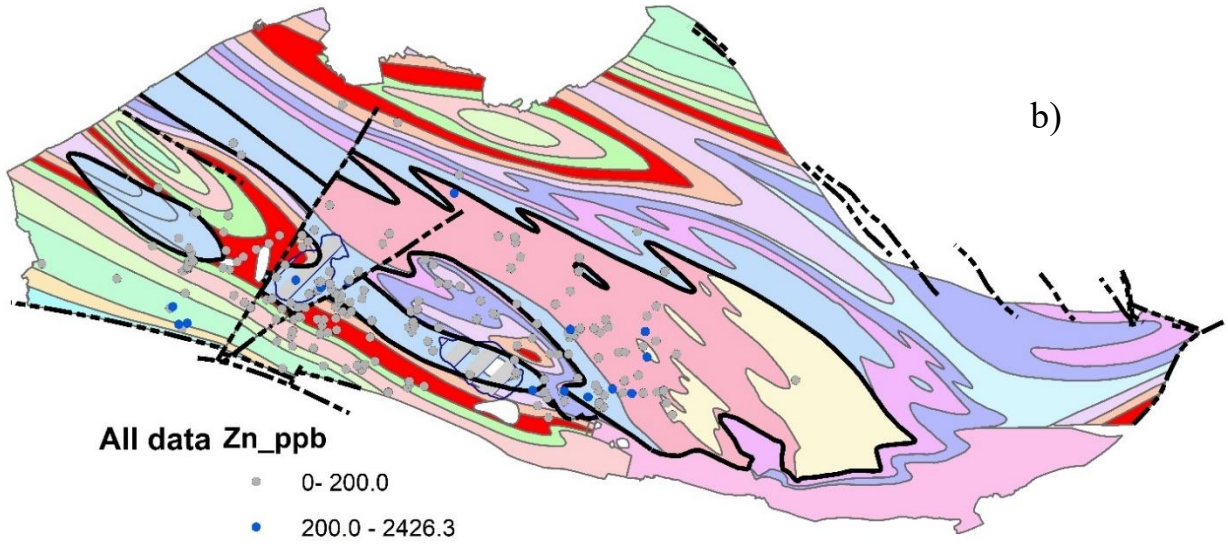

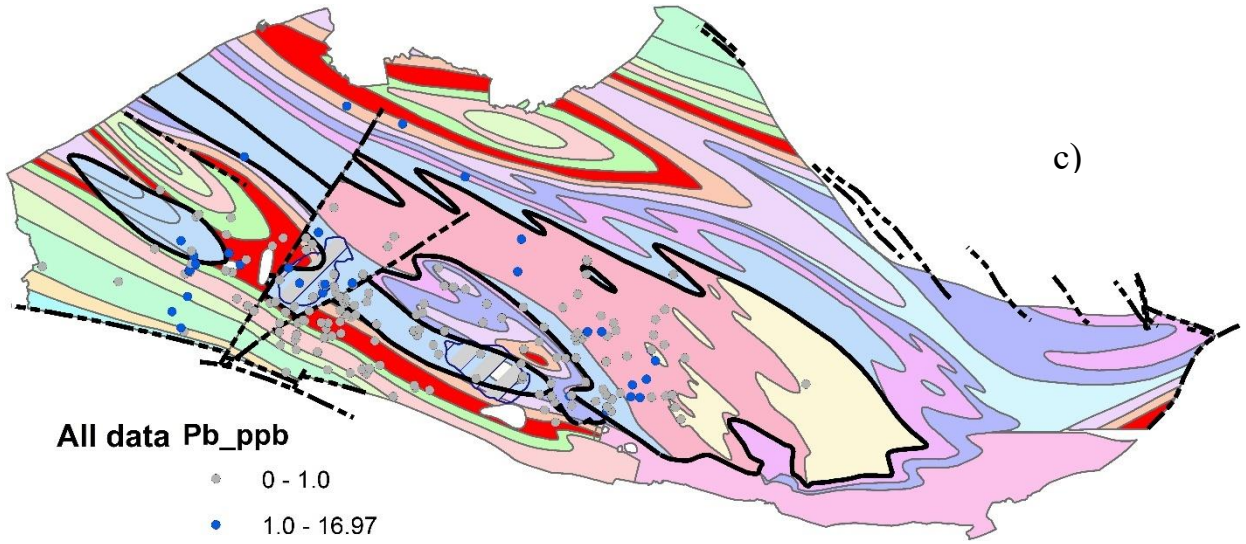
c)
All data Pb_ppb
0 - 1.0
1.0 - 16.97

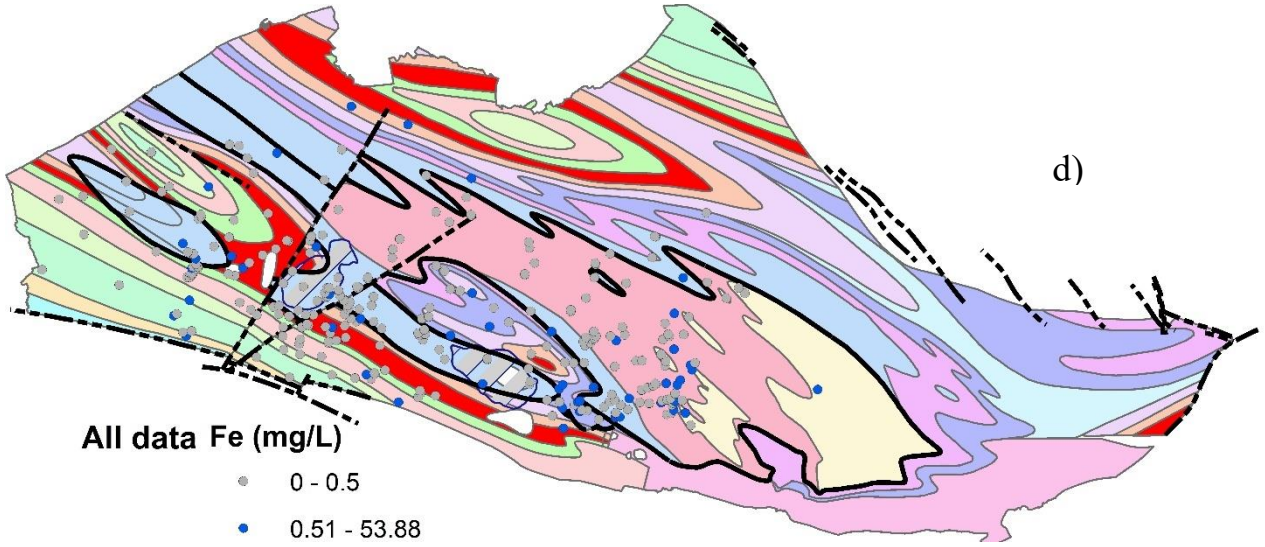
d)
All data Fe (mg/L)
0 - 0.5
0.51 - 53.88

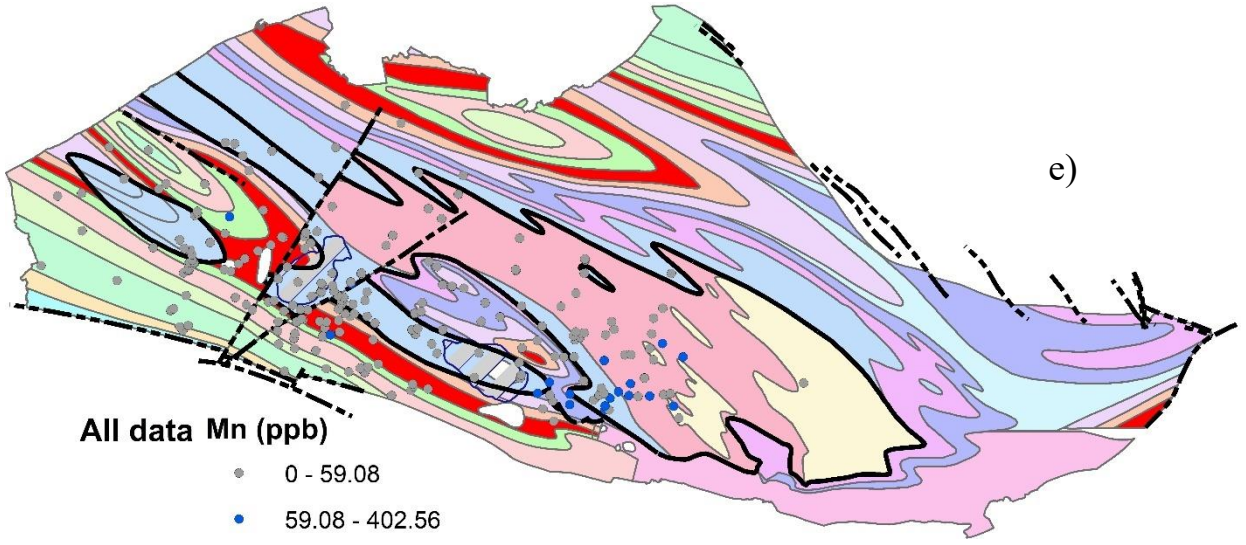
e)
All data Mn (ppb)
0 - 59.08
59.08 - 402.56

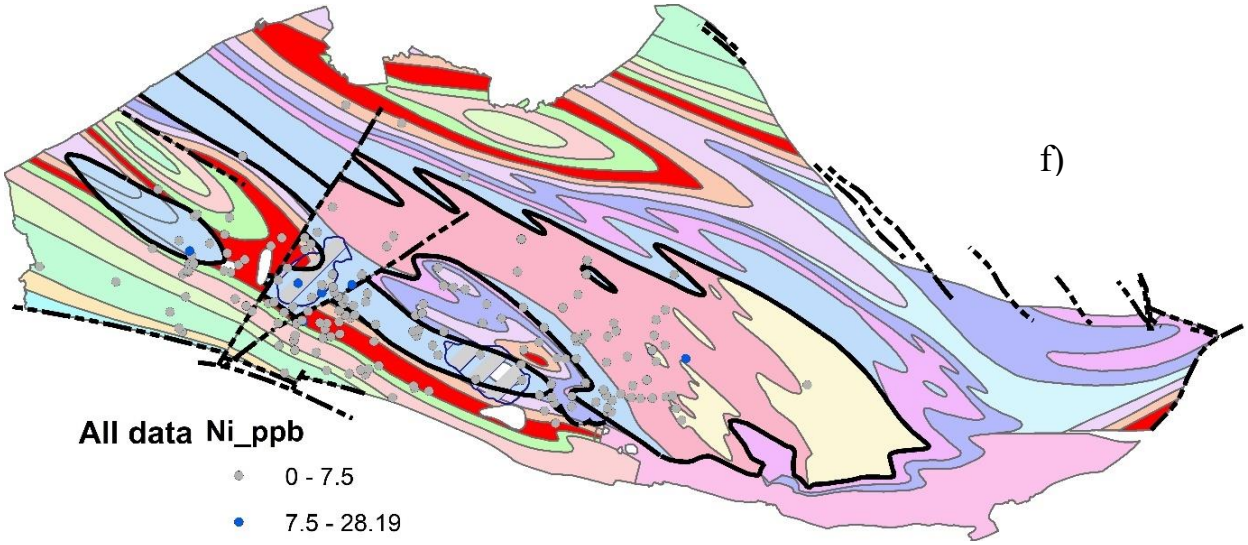

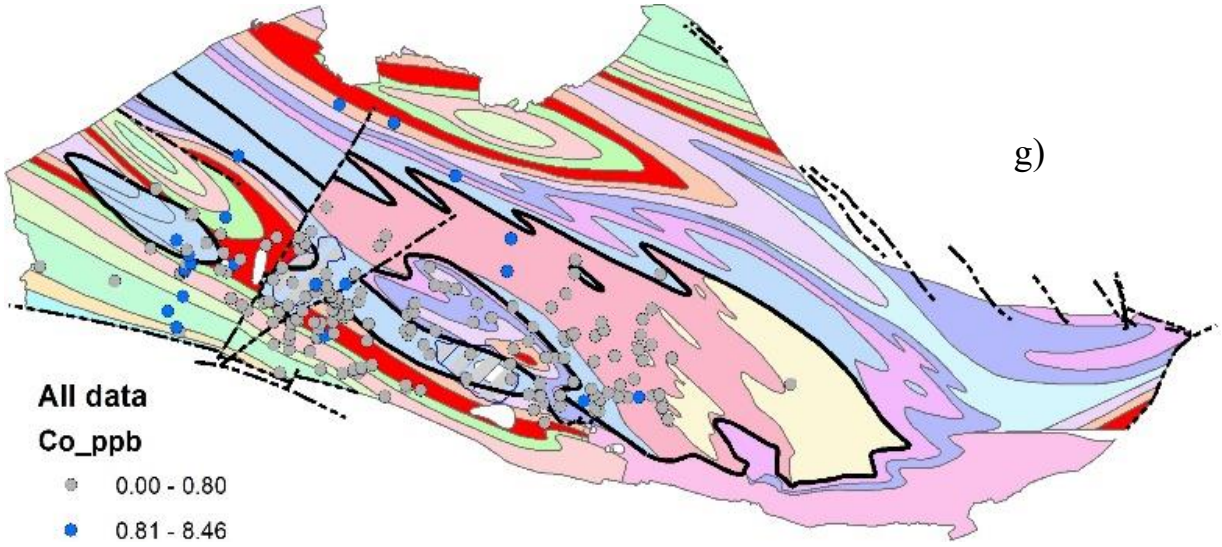

Figure 43. Concentration of base metal in the Brabant Massif. The anomalous values (see Table 16) are represented in blue.

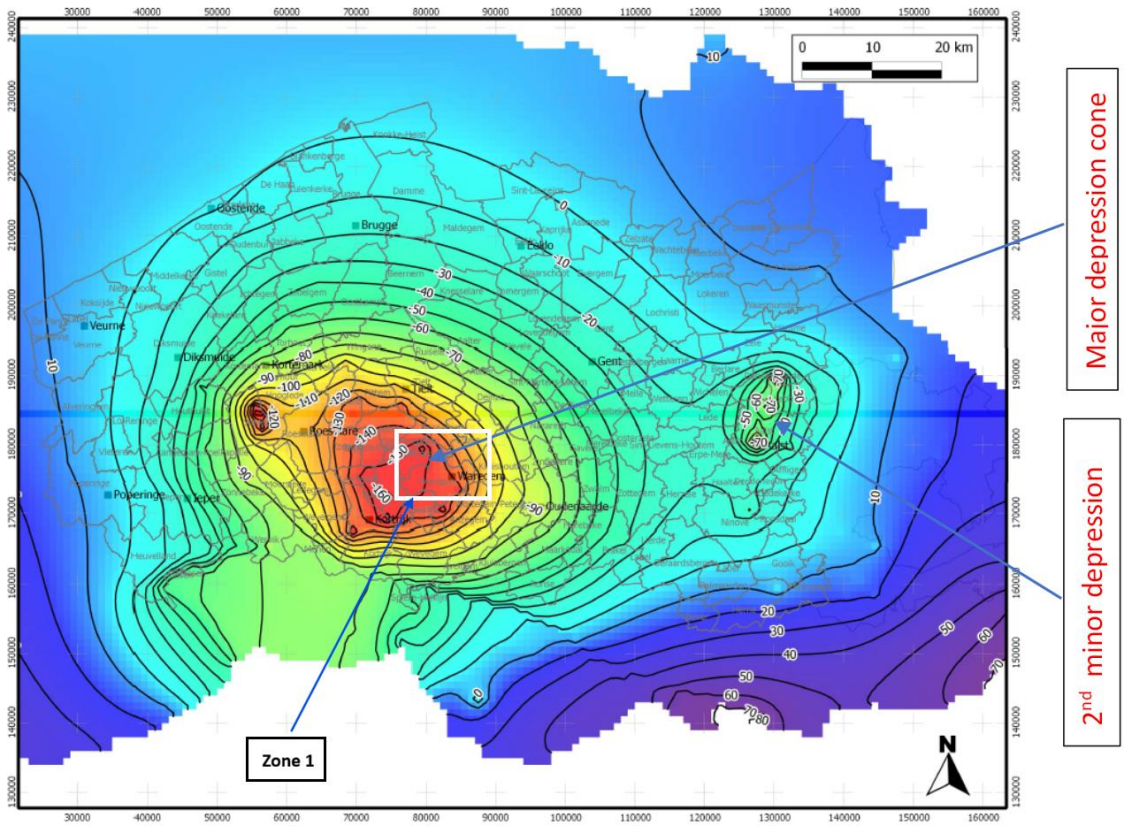

Figure 44. A piezometric map produced by the water level measurements of the wells in the year 2000 by Melger (2018).

The geology may play a role in shaping these hydrogeochemical patterns. However, in this study, there is no clear association of trace metal anomalies with a particular lithostratigraphic formation.

Major fault zones cut the Brabant Massif (Figure 25), which might likely channelled mineralizing fluids. Gravity lows, interpreted as granitic intrusions (Figure 25), align with the main anomalous zone (Zone 1) (Figure 39). In the second zone with a gravity low, anomalies are less pronounced. The co-occurrence of fractures, gravity anomalies, and pumping-related drawdown (Figure 44) complicates the interpretation and association of these anomalies with one of the causative factors. However, given the shallow depth of the groundwater samples compared to the expected depth of the granite intrusion, the chance of the intrusion being the source for the trace elements anomalies is low, and the depression cone that changes the redox condition and thus the mobility of the trace elements likely is the main factor.

4.3.3.3 Antimony (Sb), bismuth (Bi), and arsenic (As)

Another group of associated elements consists of Sb, Bi, and As. The association of these elements is often used as a pathfinder for the geochemical exploration of base metal sulphide mineralisation (Cu, Pb, Zn) (Hale, 1981). The spatial distribution of Bi, Sb, and As across the Brabant Massif reveals clear hydrochemical anomalies that strongly correlate with the central groundwater depression cone in Zone 1 (Figure 44 & Figure 45). Bi is also found in the southern Zonnebeke-Staden area, and at some wells of the central Brabant Massif. This shows that there is a clear association between Sb and As, and with Bi to a degree. There is elevated concentration of SO_4 in both Zone 1 and 2 (see Figure 35g) but it is difficult to quantify the contribution of the remnants of seawater and of the oxidation effect.

Therefore, it cannot be deducted with certainty if this association of Sb, Bi and As indicates the presence of Cu, Pb and Zn sulphide ore minerals at depth.

Anomalous Bi, Sb, and As values are concentrated along fault-bound structural corridors and gravity lows, particularly within or adjacent to the depression cone. These zones of drawdown create dynamic redox conditions that enhance the mobilization of redox-sensitive elements (Walraevens, 1997). As pumping continues, the piezometer level drops and air may enter through wells, pyrite minerals often containing traces of Cu, Zn, As, Pb, Sb, Bi, Co, Cd oxidize and release trace constituents such as As, Sb, and Bi into solution. At the same time, the induced vertical flow may draw in deeper, metal-rich fluids or leach trace elements from sulphide-bearing formations intersected by fault systems. This could be the reason for the distributions of Bi in the southwest (Zonnebeke-Staden area) (Figure 45).

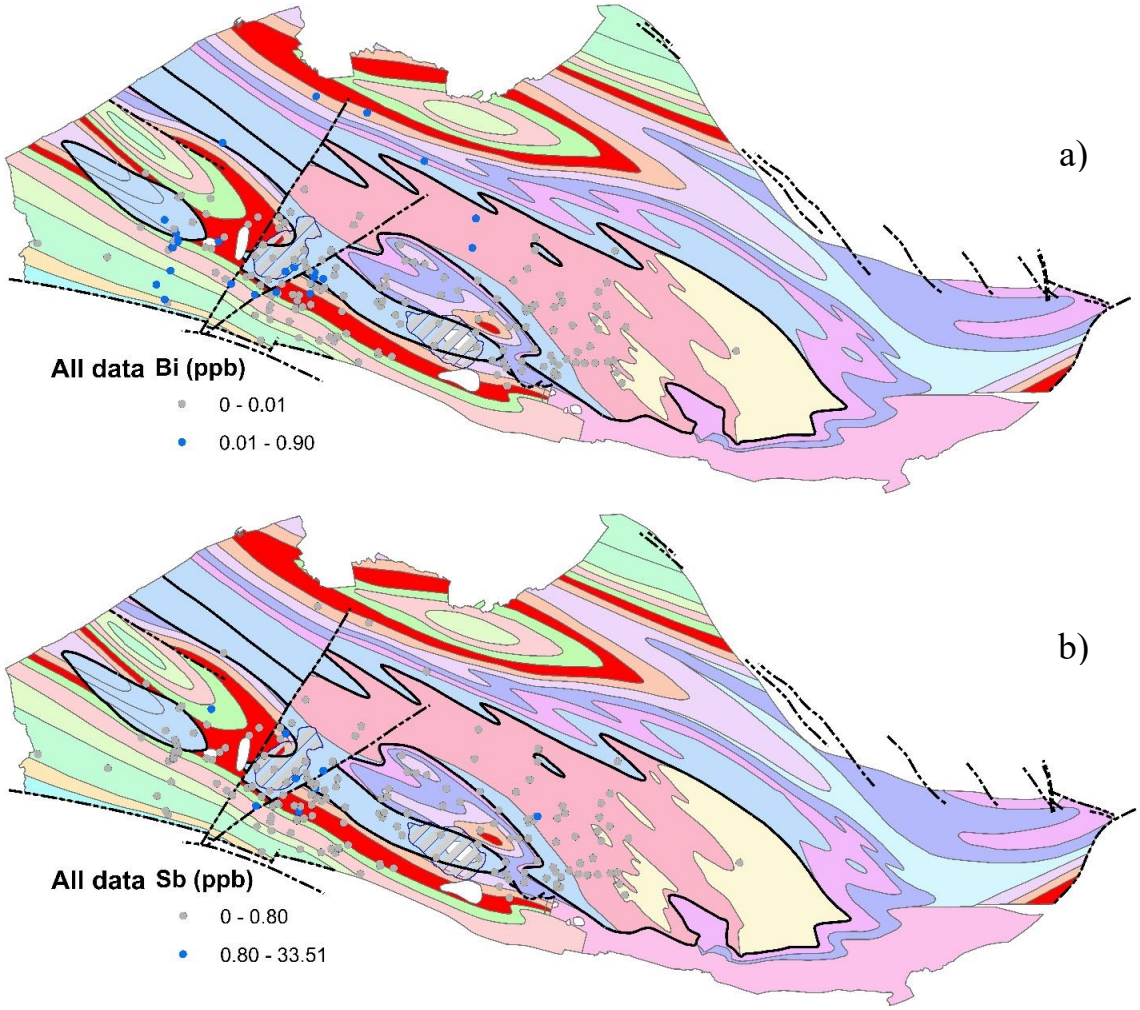

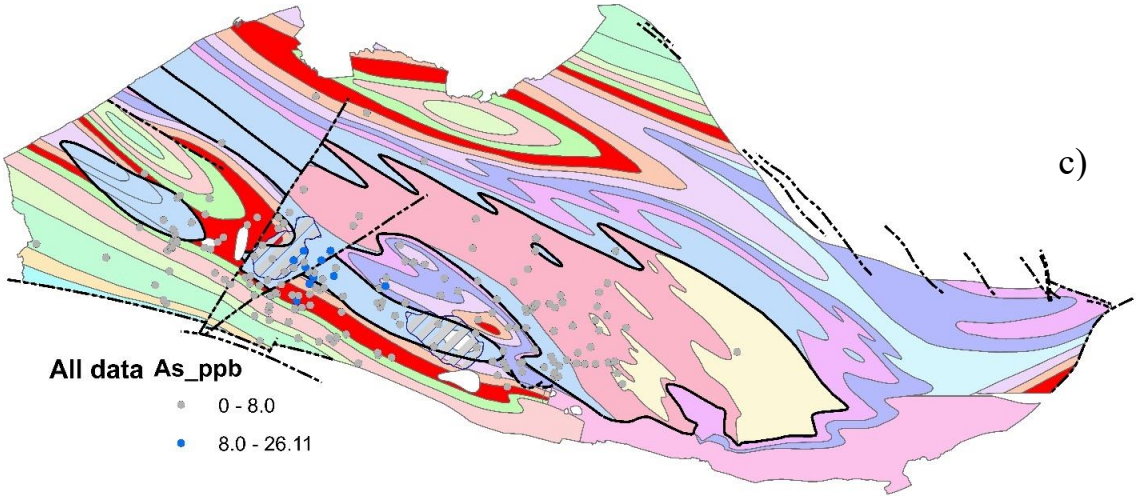

Figure 45. Concentration distribution of Bi, Sb, and As. The anomalous values (see Table 16) are represented in blue.

However, there is no meaningful statistical correlation among these trace elements (Figure 46). This is due to the dominance of the many low values of analysed concentrations in the correlation analysis, as already mentioned earlier (Table 16 and Figure 38).

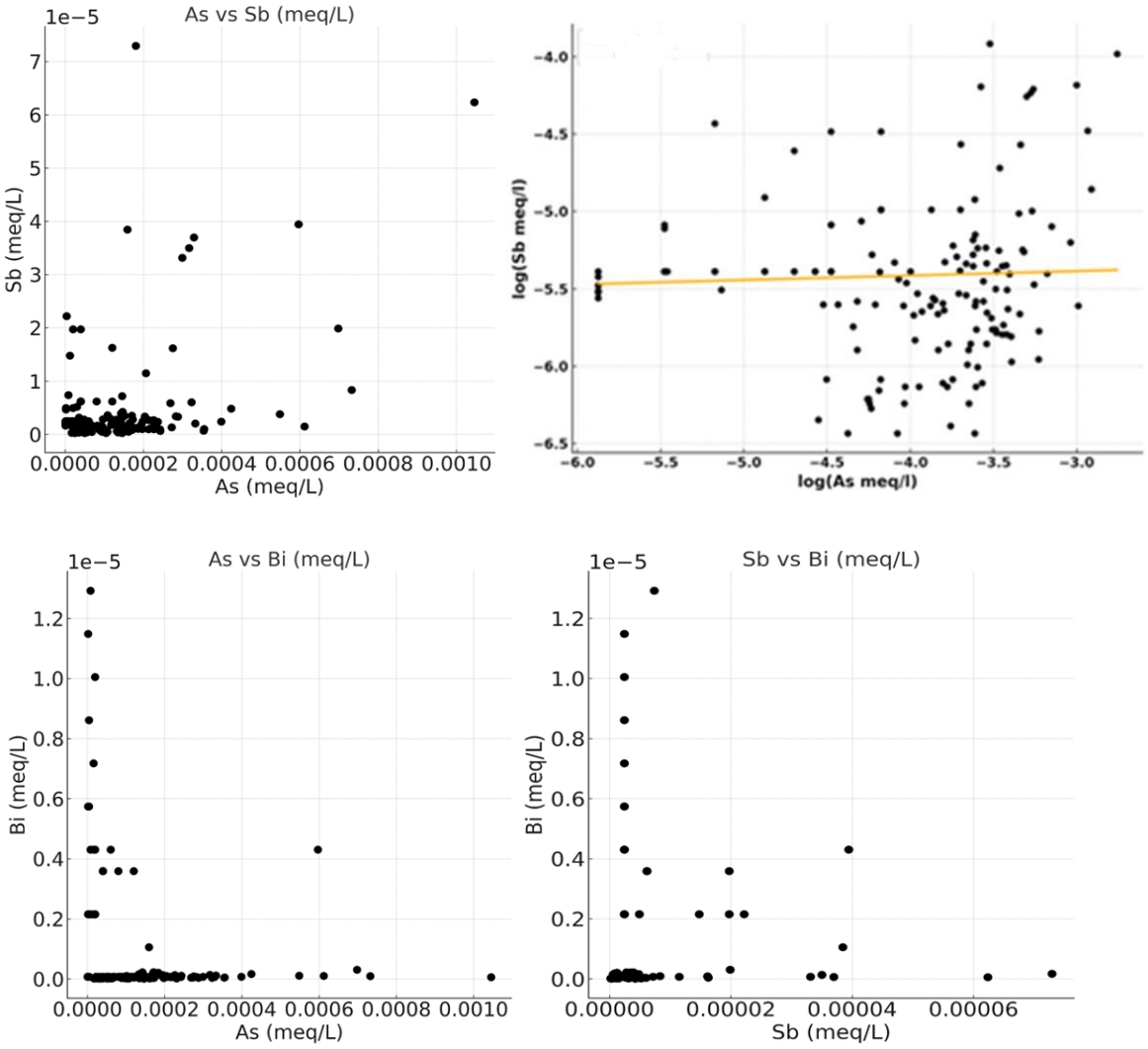

Figure 46. Statistical correlation among Bi, Sb, and As.

4.3.3.4 Tantalum (Ta) and titanium (Ti)

The spatial distribution of tantalum (Ta) and titanium (Ti) in groundwater of the Brabant Massif is found to be well correlated with the zone 1 anomaly, co-located with the main groundwater depression cone (Figure 44 and Figure 47). Especially the Ta anomalies are found to be well correlated with this zone.

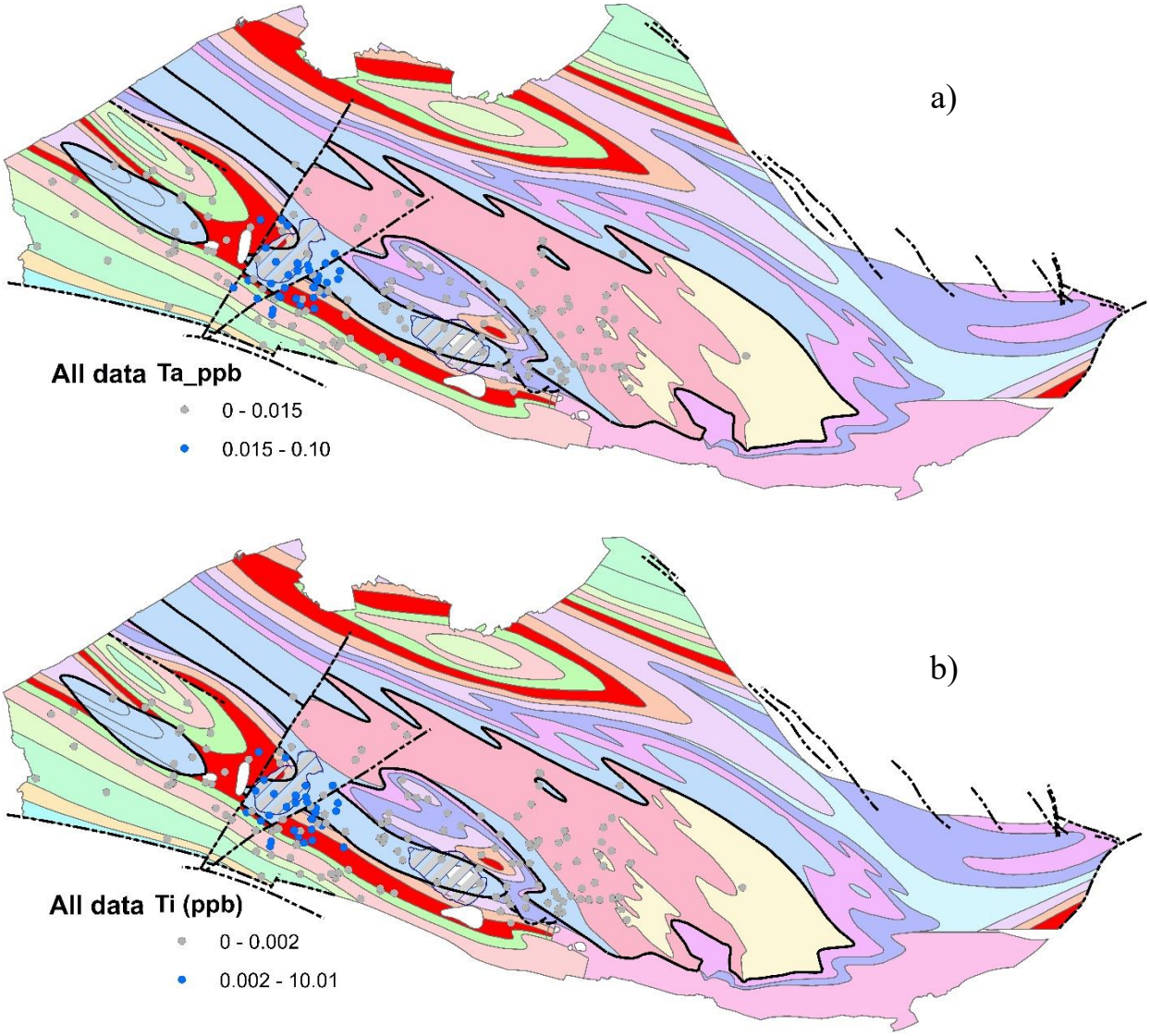

Figure 47. Concentration distribution of Ta and Ti in the Massif Brabant of Belgium. The anomalous values (see Table 16) are represented in blue.

4.3.3.5 Cadmium (Cd) and zinc (Zn)

Cadmium (Cd) can be an important component of zinc ore. The association of both elements might be an indication of polysulphide mineralization at depth (Dewaele & Muchez, 2005). The correlation of their anomalies is evaluated in this study (Figure 48a & b). There is some co-occurrence of anomalies, especially in Zone 2 and near the main depression cone (Zone 1) (Figure 39a). Similar to pyrite, sphalerite (Zn-sulphide) oxidizes when air enters via a well in depression cones. There is no statistical correlation between the elements.

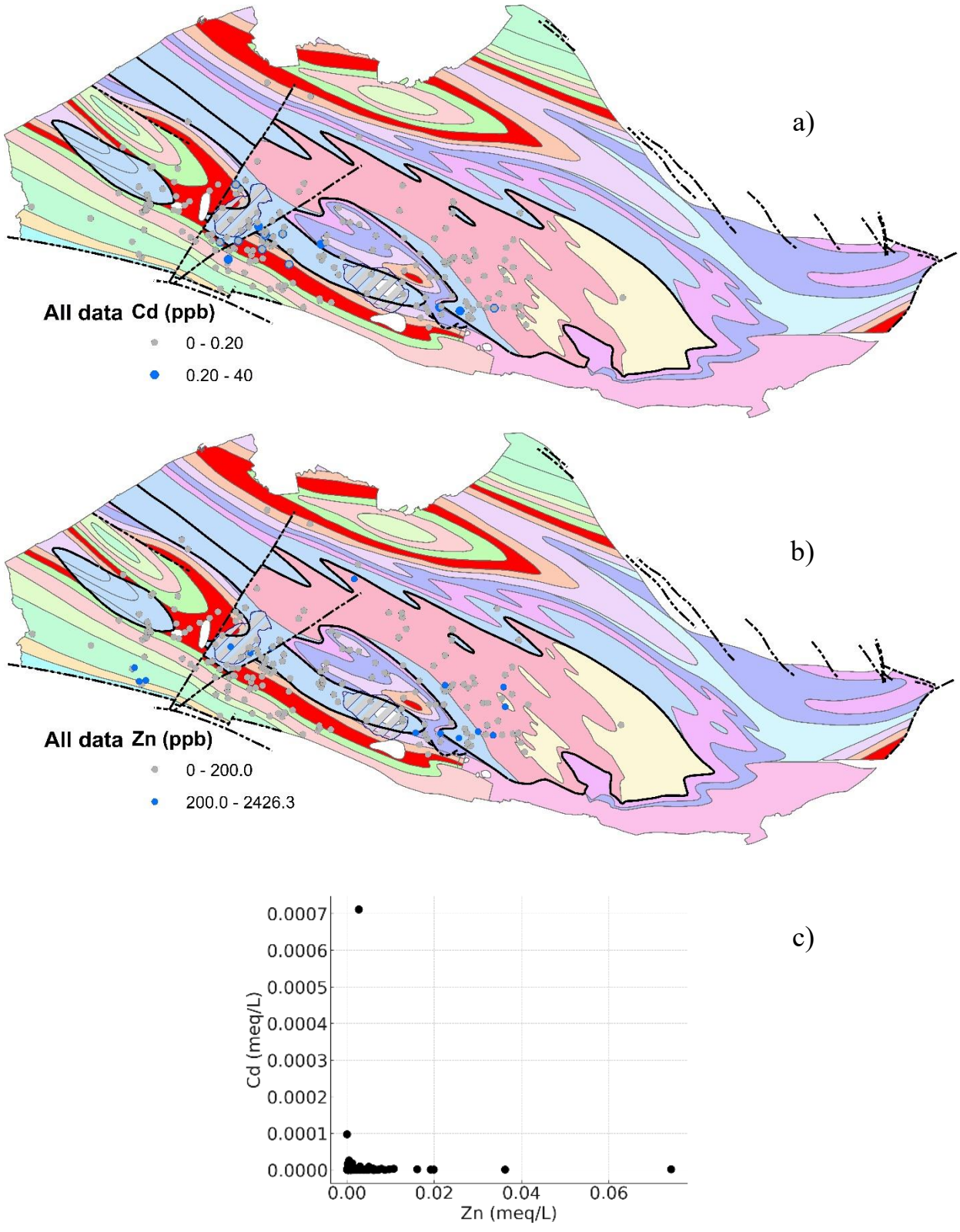

Figure 48. Concentration distribution of Cd and Zn, showing their spatial and statistical correlations. The anomalous values (see Table 16) are represented in blue.

4.3.3.6 Chromium (Cr) and precious metals (Pt, Au and Ag)

As there are only limited anomalies of Pt and Cr, it is difficult to evaluate their spatial correlations. There is only one well (at the central region of the Brabant Massif) (Figure 49a & b), with both Pt and Cr anomalies. Other anomalies for each are only found at a few locations and seem sparsely dispersed throughout the Brabant Massif. Some of the anomalies seem to occur along fractures (and gravity lows) and lithological contacts. That would imply that discontinuities may possibly facilitate the leaching of Cr from ultramafic or mafic lithologies and mobilization through fluid pathways. Due to very few anomaly values of Ag, it is not possible to evaluate the spatial correlation with this element in detail. In general, few anomaly values of the precious metals are observed and they are widely distributed. Therefore, it is not possible to correlate them with specific hydrogeological and geological characteristics of the area.

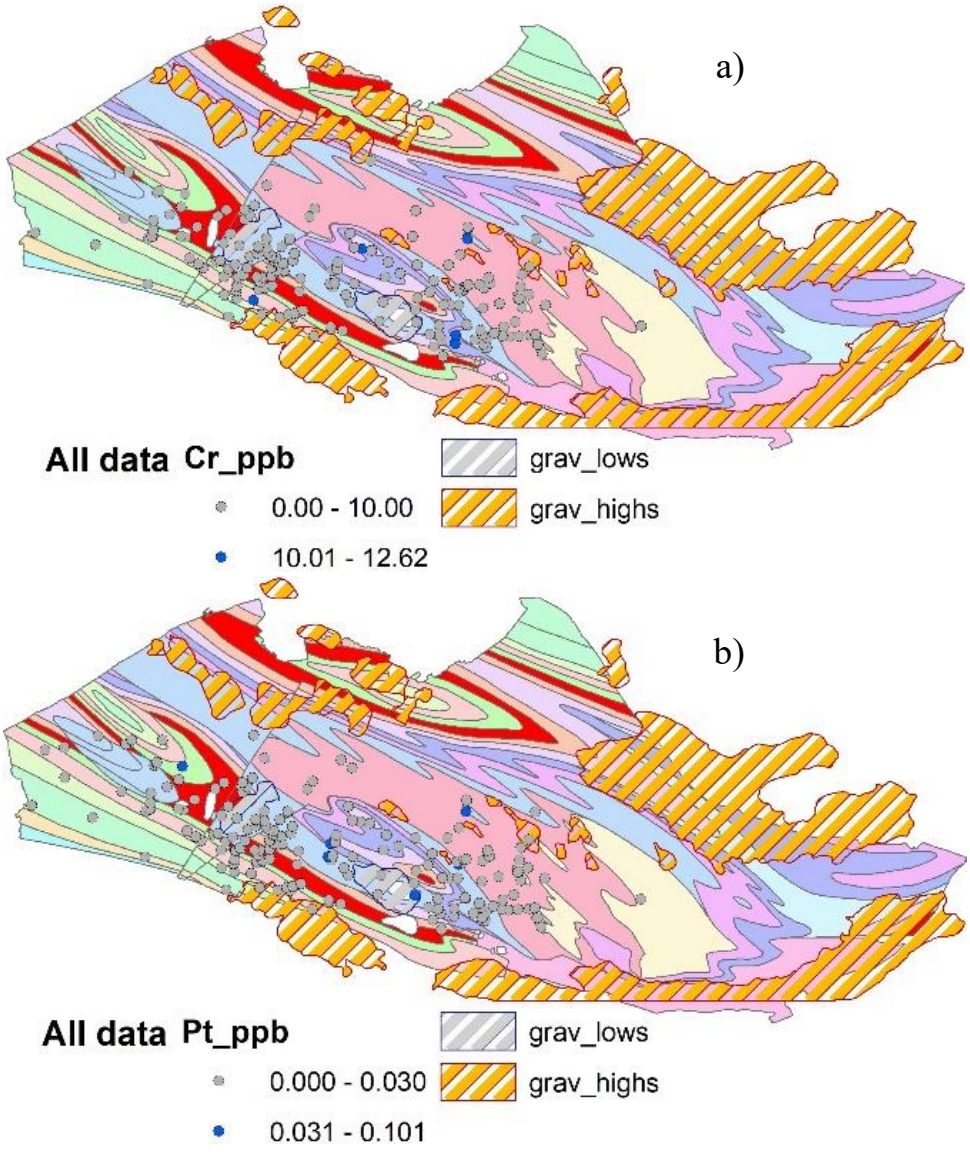

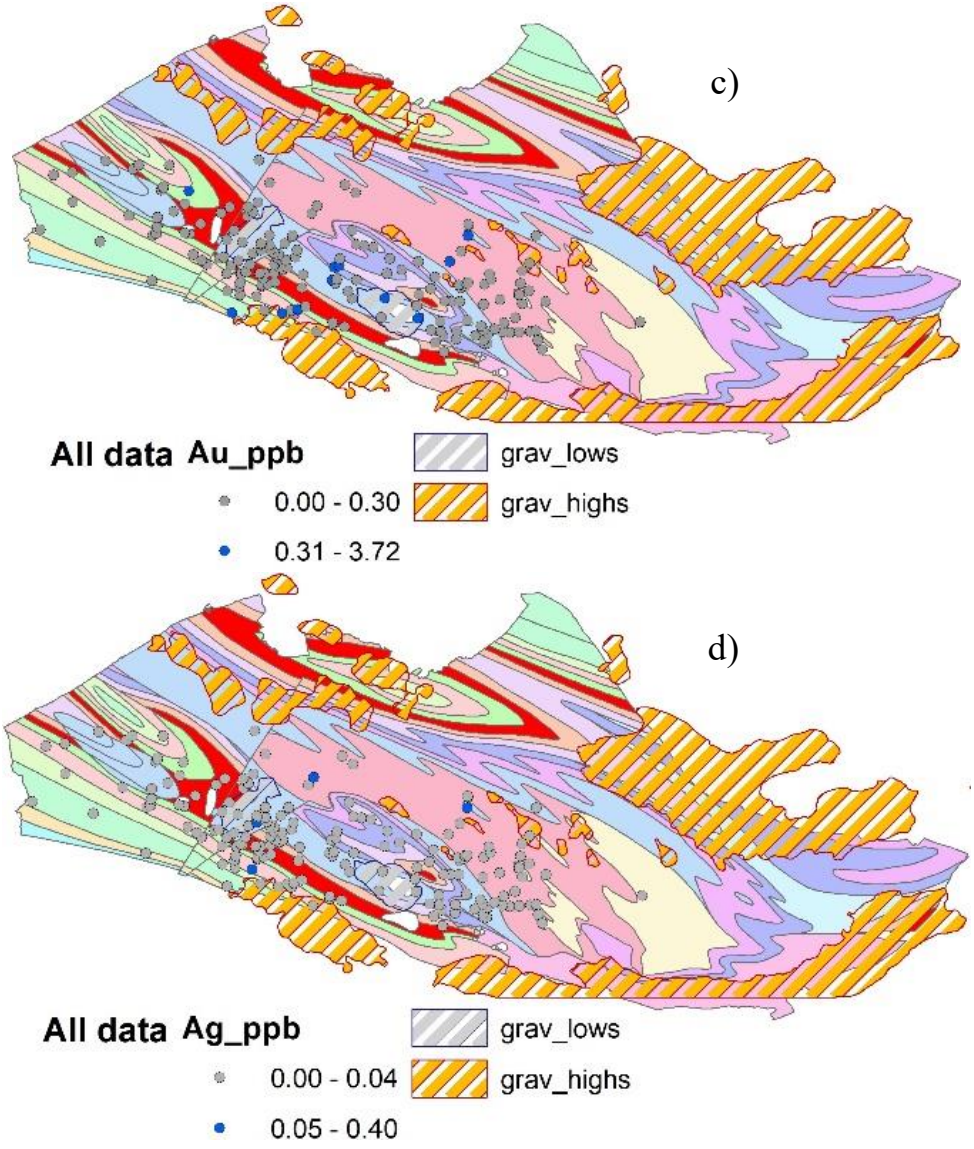

Figure 49. Concentration distribution of Cr, Pt, Au, and Ag. The anomalous values (see Table 16) are represented in blue.

4.3.3.7 Barium (Ba) and strontium (Sr)

Anomalies of Ba (>200 ppb) are observed in the southern part of the Asquempont detachment fault near the gravity low (Zone 2), whereas Sr shows a broader anomaly distribution, with concentrations above 1000 ppb stretching across a wider region (north, northwest, south, and southeast). There is no anomaly in Zone 1, unlike many of the anomalies of the other trace elements (Figure 50b).

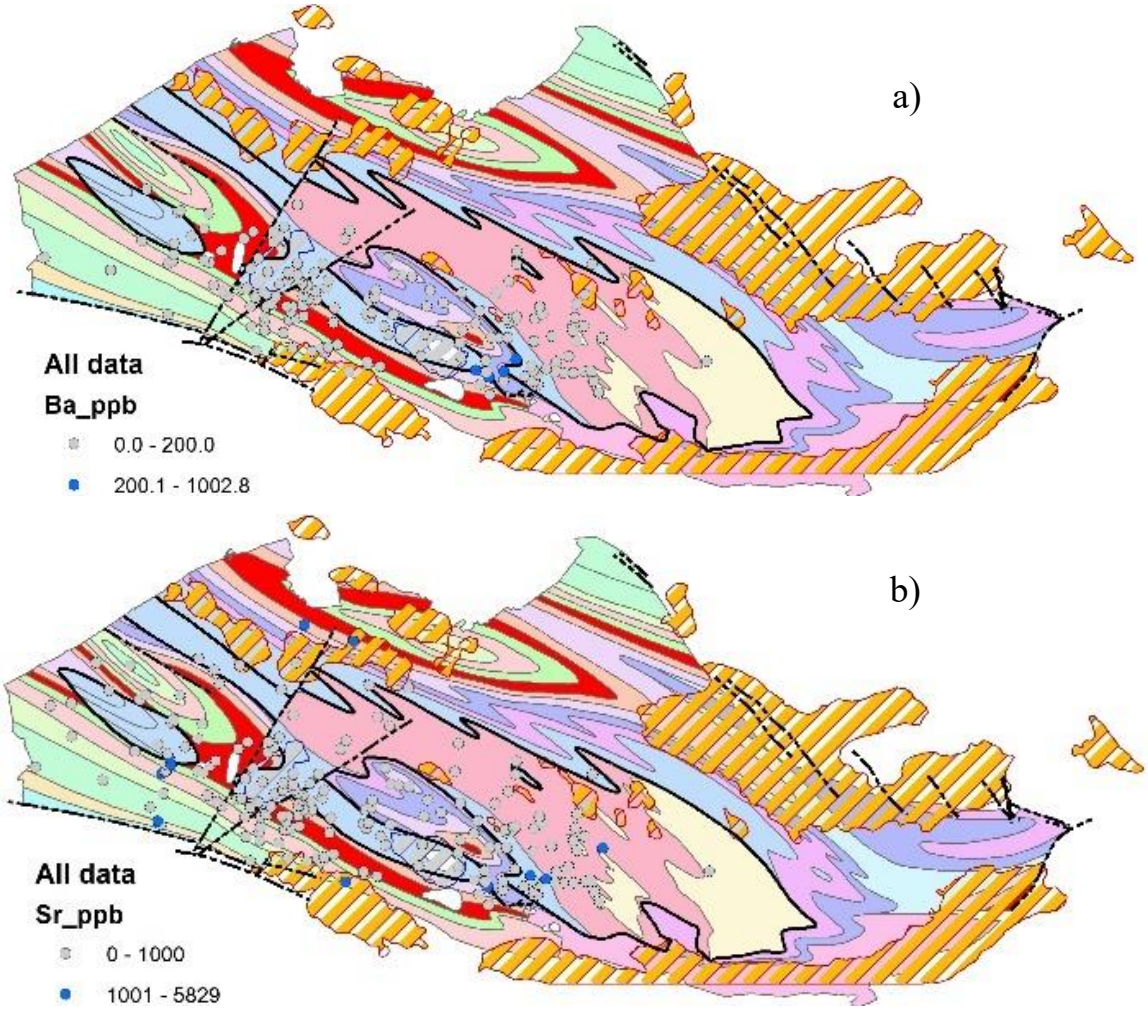

Figure 50. Concentration distribution of Ba and Sr elements in the Brabant Massif. The anomalous values (see Table 16) are represented in blue.

4.3.3.8 Antimony (Sb), lead (Pb), zinc (Zn), and silver (Ag)

Sb, Pb, Zn, and Ag are often found together in polymetallic sulphide mineralization. The extent of the spatial correlations of these metals may be an indication for the possible presence of metamorphic sulphide mineralization in the Brabant Massif related to the Brabantian orogeny (Dewaele and Muchez, 2005). However, weak spatial correlation exists among these elements (Figure 51).

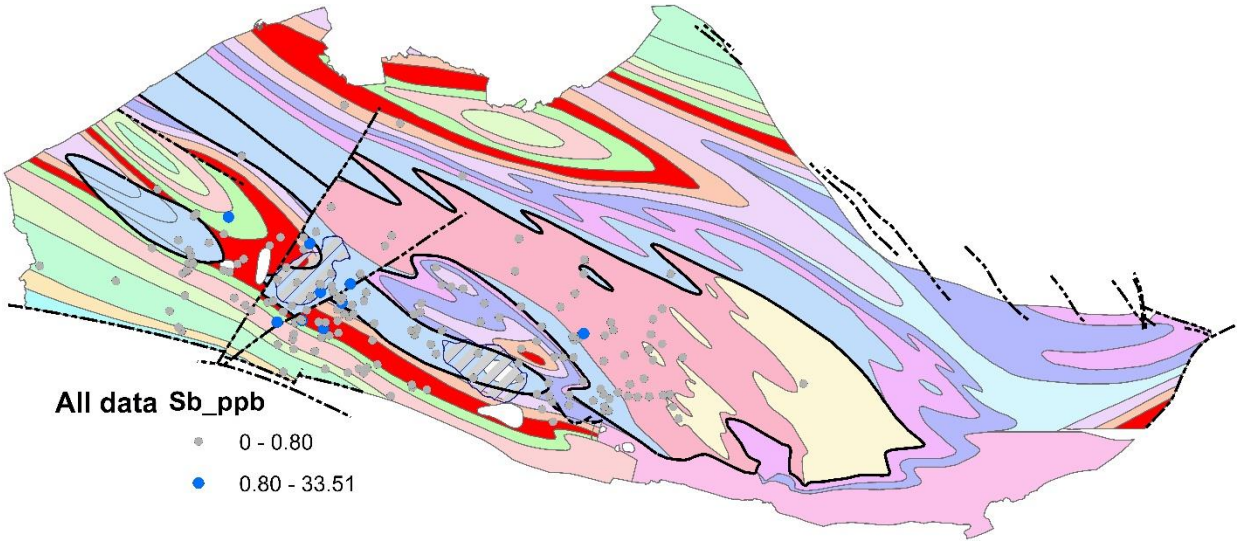
All data Sb_ppb
0 - 0.80
0.80 - 33.51

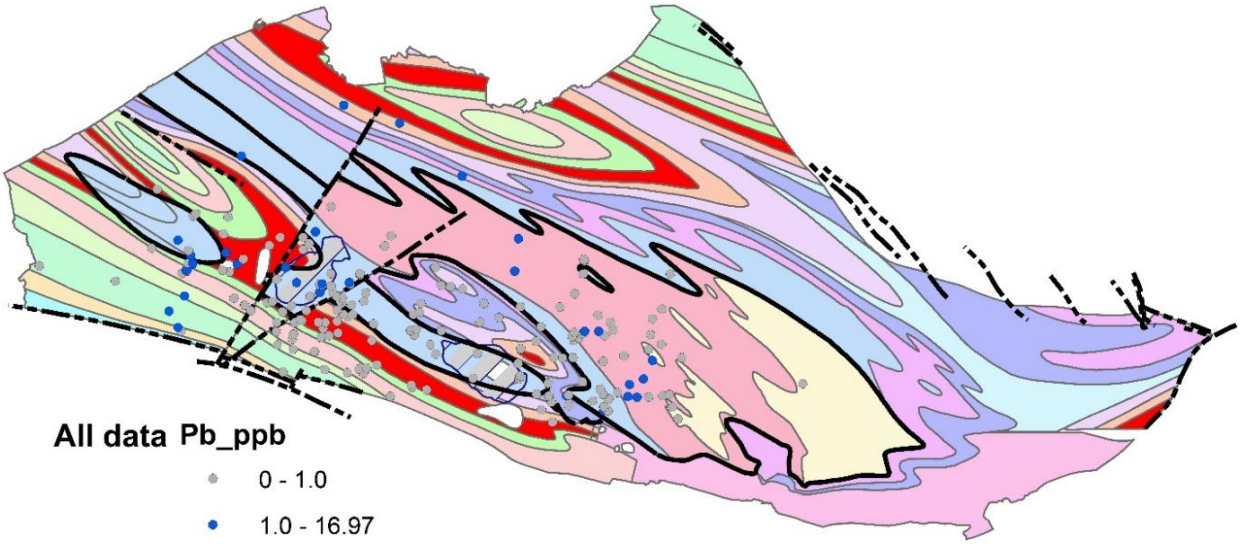
All data Pb_ppb
0 - 1.0
1.0 - 16.97

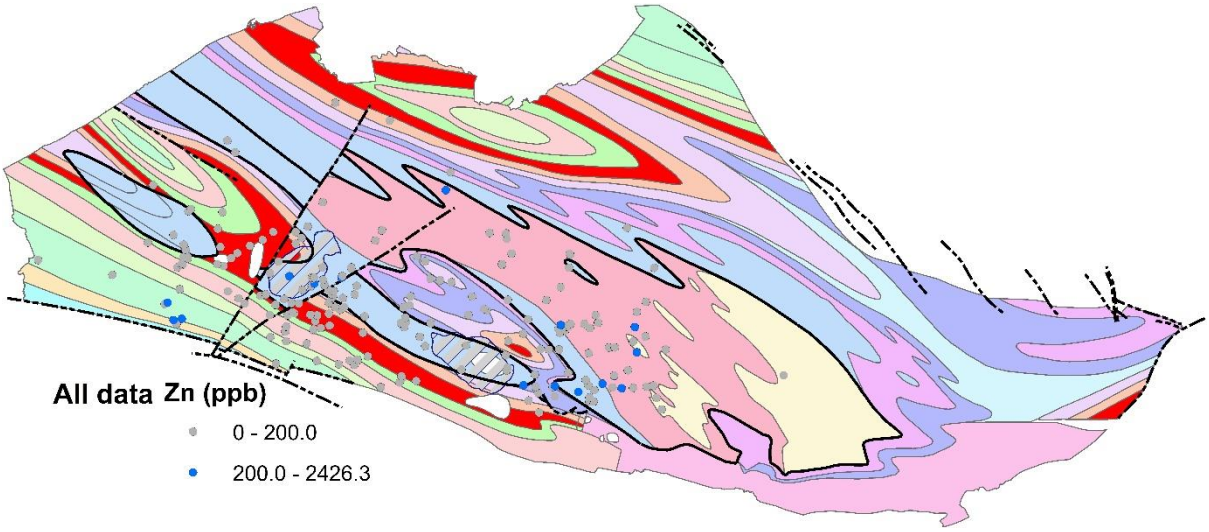
All data Zn (ppb)
0 - 200.0
200.0 - 2426.3

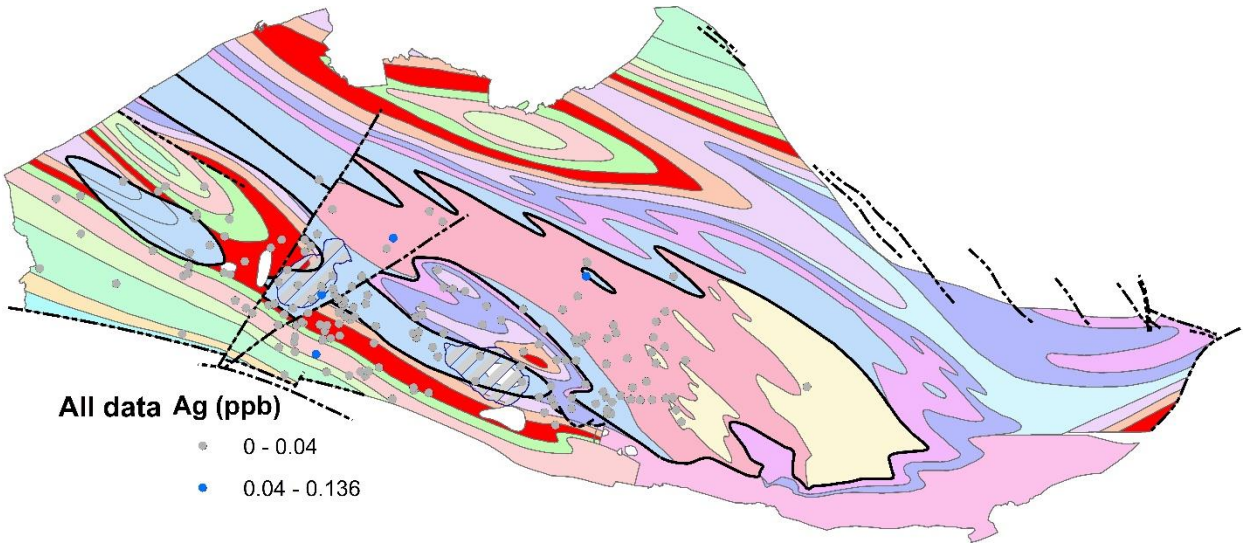

Figure 51. Concentration distribution of Sb, Pb, Zn, and Ag. The anomalous values (see Table 16) are represented in blue.

4.3.3.9 Vanadium (V)

Next to Li, vanadium also has concentrations above the detection limit in the wells sampled by VMM-DOMG. At about 19 (out of 49) wells, concentration values were measured above the detection limit, but with most of them below the anomalous threshold.

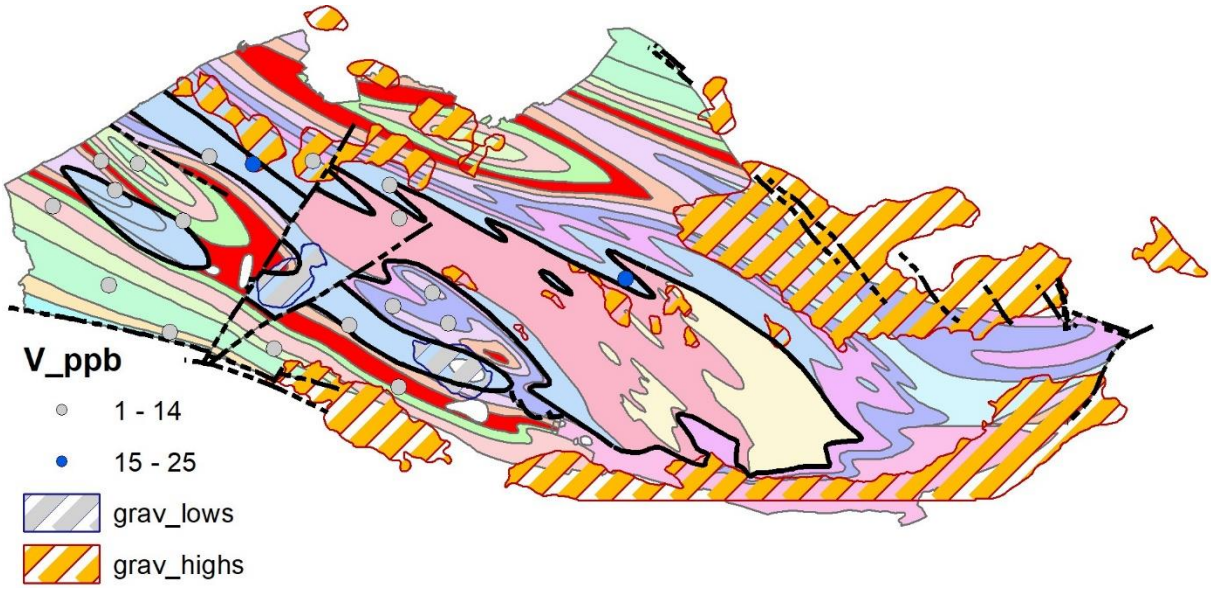

Figure 52. Vanadium concentration in 19 wells sampled and analysed of VMM-DOMG. The anomalous values (see Table 16) are represented in blue.

In conclusion, Li^+ is found to be controlled by the cation exchange for Ca^{2+} and mixing with old seawater that was connate or remained from the last transgression. There is no correlation of Li^+ with other trace elements and major ions, except Na^+ and Cl^-. The spatial correlation of Li^+ is controlled by the distance from the recharge area, where freshening took place. Locally, however, elevated Li^+ together with B and a Na–K–As–SO_4–HCO_3 signature near the Asquempont detachment fault (e.g.,

W3-0502a) suggests that structural pathways may enhance water–rock interaction and/or sulphide oxidation along this corridor. However, distinguishing these effects from simple mixing/cation exchange remains uncertain with the current dataset. The anomalies for most of the trace elements (Figure 39,
Figure 41, Figure 43, Figure 45, and Figure 47) are correlated with the depression cone developed by the overexploitation of the groundwater since the industrial period, which also overlaps to some extent with the gravity anomaly and the presence of fracture zones (Zone 1). On the other hand, Zone 2, the southeastern anomaly zone, is characterized by anomalous values in Pb, Zn, Mn, Sn and Cd (and locally Cu and Ba). Some of the trace elements, for example, Fe and precious metals, are widely dispersed. There is no statistical correlation found among other trace elements due to the dominance of very low to low values at many sampling points (see Appendix 6).

4.4 INTERPRETATION OF THE TRACE ELEMENT HYDROCHEMICAL CONCENTRATIONS AND COMPARISON WITH LITERATURE

In this chapter, Li, other critical raw materials (CRMs) and some other trace elements in groundwater within the Brabant Massif region are compared with existing literature on known ore deposits and mineralization types. Geological insights of the Brabant Massif, particularly its expected history of mineralization, are essential to interpreting the hydrogeochemical anomalies identified in groundwater analyses. As discussed in the previous chapters, hydrochemical anomalies of many (critical) trace elements are observed, although they represent only a small proportion of all the samples analysed in the Brabant Massif. In addition, several spatial associations among them could be noted.

It should be mentioned, as discussed in chapter 4.2, that the water chemistry of the area is dominantly controlled by paleo-seawater mixing and cation exchange. Some of the aquifer layers might also host ore minerals. In addition, trace elements might have been transported upwards by hydrothermal water from deeper-seated mineralization. Therefore, it is not straightforward to make a link between anomalies and the potential presence of mineralization of CRM's.

According to Dewaele and Muchez (2005), the Brabant Massif had a complex geodynamic history, including magmatic and metamorphic events, which suggests potential for multiple types of mineralization.

Important magmatic activity occurred during the lower Palaeozoic, indicated by the widespread occurrence of volcanic layers in the stratigraphic section. In addition, based on geophysical modelling, granitoid rocks are presumed to be present at depth. Thus, granite-related mineralization could be expected in such a geological setting. Magmatic-hydrothermal fluids are often associated with elements such as Sn, W, Nb-Ta, Be, and Li. The presence of the supposed granitoids and the potentially associated mineralization could be spatially correlated with zone 1 (Figure 39g), as discussed in chapter 4.3. This zone, however, also corresponds to the zone where there was a decrease in water levels resulting from groundwater extraction, resulting in local oxidation of the subsurface. As mentioned above, during this oxidation, specific elements present in sulphides could have been liberated (mainly base metals and their associated trace elements), and join into the groundwater.

Dewaele & Muchez (2005) distinguished different sulphide generations in the Brabant Massif: **pre-cleavage pyrite** uniformly dispersed in metamorphosed sedimentary and igneous rocks, and **syn-**

deformational sulphides linked to cleavage and veins. The latter polysulphide mineralization has been linked to metamorphic fluid circulation during the Brabantian orogeny, which was identified along the entire southern margin of the Brabant Massif. This mineralization is particularly enriched in Cu–Zn–Pb–As–Sb (Dewaele and Muchez, 2005). The metamorphic fluids that are thought to be formed in the Cambrian core of the main fold moved along shear zones at depth, and mineralized the southeastern margin of the Anglo-Brabant fold belt (Marcq-Asquempont, Bierghes, and Dongelberg). Unfortunately, these shear zones, except the Asquempont detachment fault system, are excluded from the new geological map (see Figure 25 and Figure 31). Still, different hydrochemical anomalies are found in the southern part of the Brabant Massif, especially in the Zonnebeke-Staden area.

Compared to what is regarded as anomalous values in the groundwater of a deep aquifer system in bedrock comprising weathered and fractured granitoids and mafic rocks in southern India (Sarath et al., 2023), many of the higher values in our study could be considered anomalous values. These authors have analysed many trace elements (Sr, Li, Ba, Al, V, Cr, Mn, Fe, Co, Ni, Cu, Zn, As, Se, Cd, Ag, Au, Te, Pb, Re, and PGEs) in the groundwater, and considered Sr (489.6 ppb), Ba (226 ppb), Li (11.76 ppb), Mn (396.8 ppb) and Ni (68 ppb) as anomalous values. Li values in our study range from 2 to 100 ppb. However, different Li-values have been mentioned in other literature sources. According to Sharma et al. (2022), the concentration of Li in the drinking groundwater in the United States ranges from 0.9-16.1 ppb (average 13.9 ppb), where the higher values in the range observed in the southwest states are related to the granitic, pegmatite, and lithium brine deposits. Balaram et al. (2024) found that Li concentration in hydrothermal water is (on average) 8.2 ppb, and in geothermal waters 77,310–99,400 ppb. According to Kostik et al. (2014), Li concentrations in groundwater may range from 16,000 to 49,100 ppb if Li-bearing minerals are present. Dugamin et al. (2021) did a systematic analysis of published Li concentration in about 3000 samples of groundwater from 48 sedimentary basins worldwide and found concentrations mostly between 500 and 37,000 ppb. Compared to these literature values, some of the Li concentration values in this study could be anomalous according to Sharma et al. (2022), but seem not to fall within anomalous values compared to the other literature values. However, as it is already mentioned in chapter 4.3, the Li concentrations in our study are more likely related to hydrogeochemical processes of seawater mixing and cation exchange with Ca^{2+} , though some dissolution from minerals might also be occurring. Distinguising Li originating from mineral dissolution and cation exchange/seawater intrusion is not possible with the current limited data set. In addition, it should be mentioned that the geological composition of the Brabant Massif is also different from that described in the different studies mentioned above.

Seo et al. (2023) have investigated Li in deep groundwater across South Korea using 555 thermal water samples. High lithium levels (above 90^{th} percentile: >0.94 mg/l) were linked to three hydrochemical types: Na(Ca)Cl from seawater intrusion and cation exchange; Ca(Na)SO_4, from volcanic clays in Cretaceous basins; and low-pH Ca(Na)-HCO_3 from rock weathering enhanced by deep CO_2. Even though the Li concentration in our data set is much smaller (90^{th} percentile: 0.08 mg/l in this study vs 0.94 mg/l in Seo et al., 2023), a similar correlation with water type is possible. The higher values in our study are correlated with Na(Ca)Cl water type, favouring similar hydrochemical processes of seawater intrusion and cation exchange as the dominant processes.

Some elements (e.g. Hg, Hf, Nb, V, Au, and Pt) are mostly present at or near detection limits and have only very few samples above the threshold values, which does not allow any interpretation. It should also be mentioned that the sampling depth is much shallower (< 300 m; Figure 36 for the new VMM-DOMG sampling wells) compared with the supposed depth of the inferred granite intrusion (top at 1 km depth or deeper; Everaerts et al. 1996). This could be the main limiting factor to draw conclusions about potential mineralization based on the groundwater samples.

In general, the element distributions reflect a groundwater system influenced by natural geological and hydrogeological processes, with sporadic inputs of certain trace elements possibly linked to mineralized zones and hydrogeological processes due to a changing redox system (overexploitation). However, it does not mean that sulphide minerals are only found at such hydrodynamic depression cones. They might be widely distributed at many locations, but due to the hydrochemical environment (reducing conditions with stable sulphide minerals), their concentration in the groundwater is lower than where groundwater extraction contributed to their mobilization.

Sterpin (1996) concluded that anomalies in zone 1 (regarded as Paragenesis A in their study) have a genetic connection with the inferred granitic intrusion at depth, as it is in close proximity to the negative gravity anomaly of Oostrozebeke (Figure 25). Also, they concluded that the traversing main fractures are playing a role in hosting mineralized zones, e.g. for Mo, Ni, As, Bi, Sb, Co, and W. However, according to our study, oxidation of sulphide minerals, due to the regional depression cone (Van Camp and Walraevens, 2009), would have played a more important role. The proximity of the depression cone with this gravity low and traversing main fractures makes it difficult to draw a conclusion, especially considering the relatively shallow depth of the groundwater samples.

In conclusion, there is no clear evidence for the presence of Li ore minerals in the Brabant Massif rocks based on the groundwater analysis data used in this study. Correlations of Li with Na and Cl are in line with other studies and show paleo seawater and cation exchange as a reason for higher concentrations in the northwest region, rather than mineral dissolutions. However, relatively higher concentrations at a few wells in the southeast region may indicate some enrichment due to the dissolution of ore minerals deposited by hydrothermal flow or in the host rocks themselves. Elevated concentrations of elements like Sb, As, and Bi potentially indicate the presence of polysulphide orogenic mineralization. These findings align with historical metallogenic models and reinforce the importance of continued hydrogeochemical and geological investigation in the region.

4.5 GENERAL CONCLUSIONS FOR THE BRABANT MASSIF

Generally, the Li concentration in groundwater of the Brabant Massif is found to be low and cannot be considered anomalous. The analysed data bear no concrete evidence that Li is added from the dissolution of Li-bearing minerals. However, it does not mean that Li-bearing minerals could not exist at depth, especially at the assumed granite/pegmatite sources inferred by gravity lows, which are assumed to be much deeper than the sampled depths.

Additionally, the hydrochemical dataset revealed several wells with anomalous concentrations of different CRMs or other trace elements. No meaningful relationship based on a statistical and spatial correlation was found, neither between trace and major elements, nor between trace elements themselves. The main ore minerals that might have been sources of the hydrochemical anomalies are sulphide minerals. It is observed that the concentration of trace elements that are typically present in sulphide minerals has been enhanced by oxidation of these sulphides at depression cones resulting from groundwater extraction from the Brabant Massif aquifers. The Piessens et al. (2005) geological map has been used as base for the correlation of geology and the potential occurrence of geochemical anomalies. As many geological structures are excluded in this geological map (compare Figure 25 and Figure 31), a detailed spatial correlation between hydrochemical anomalies and these omitted geological structures was not possible.

At the same time, the clustering of several anomalous elements, especially in Zone 1 (e.g., W, Mo, Sb, Cu, Ni, Co, Bi, As, Ta, Ti, Cd, Zn), should be retained as a significant observation. Although the broad extent of the depression cone and the associated local oxidation processes prevent a straightforward attribution of this clustering to geology alone, the spatial coincidence of Zone 1 with the inferred intrusion/gravity low and the main fault and fracture corridors remains noteworthy and is consistent with the interpretation previously proposed by Sterpin (1996). The present results therefore do not invalidate the previous geological hypotheses; rather, they show that, with the currently available methods, the relatively shallow depth of the groundwater dataset compared to the assumed intrusion, and the overprinting effect of pumping-induced redox changes, such geological relationships are difficult to demonstrate conclusively.

5 RADIOISOTOPES AND NORM

5.1.1 Context

Zukin et al. (1987) studied the presence of naturally occurring radioisotopes (NOR) in brine from the Salton Sea Geothermal field. The brine proved to be enriched in ^{226}Ra, ^{228}Ra, ^{210}Pb and ^{212}Pb compared to the source rocks. One of the first analysis of NORs in deep formation waters is Europe was for the Merksplas-Beerse geothermal well (Vandenberghe et al., 2000). The brine proved to be slightly radioactive. Detected NORs were ^{226}Ra (74 Bq/l) and ^{222}Rn (22 Bq/l). The authors explained their presence due to contact of the brine with the radioactive shales of the overlying Chokier formation. Since then, data from geothermal plants in Germany, Denmark, France, and Belgium pointed out that the occurrence of NORs in deep formation waters is widespread. The main radioisotopes found in deep formation waters are ^{226}Ra, ^{228}Ra, ^{224}Ra, ^{222}Rn and ^{210}Pb.
The primary source of the NORs are rocks with which the groundwater comes into contact. Decay of ^{238}U and ^{232}Th are the primary sources. Despite the low concentrations of these radioisotopes in crustal rock and their low solubility under most reservoir conditions, daughter isotopes can be fractionated and mobilized, resulting in their enrichment in secondary minerals and in groundwaters. Residence times, water-rock interaction processes and mixing of different fluids explain the large number of radionuclide species and their activity concentrations in geothermal brines (Kölbel et al., 2020).

The presence of NORs in the deep formation fluids can result in the generation of NOR-containing materials (NORM) during processing of the fluids in e.g. geothermal installations or oil-gas production installations. NORM-generation in geothermal installations was only recently brought to attention in Central and West-Europe. Radioisotopes found in scales and filter residues from geothermal plants include ^{226}Ra, ^{228}Ra, ^{224}Ra, ^{210}Pb and ^{210}Po (Degering & Köhler, 2015; Eggeling et al., 2013; Kölbel et al., 2020, 2022; Olivarius, 2018.; Regenspurg et al., 2014; Pauwels, 2021).

Deep formation waters from the Campine Basin show an elevated concentration of natural radioactive elements. Other mineralized formation waters may also contain high concentrations of radioactive isotopes. On the one hand, this poses a risk regarding the treatment of the formation waters and the processing of residues. On the other hand, the isotope ratio is partly determined by interactions between the formation water and the rock with which it is in contact, and it could potentially be used as a proxy for the presence of mineralisation in the deep subsurface.

As part of this study SCKCEN determined the radioactivity and uranium isotopes in five groundwater samples from the Lower Carboniferous Limestone Group. With a view to further exploration of Li and other CRMs, we will discuss the potential risks associated with the treatment of these deep formation waters and any residues. Additionally, we evaluated to what extent uranium isotopes can be used as a proxy for mineralisation.

5.1.2 Measurements

Radiological analysis on the new samples taken during this study in the Campine Basin is performed at SCKCEN as described below and in Vasile et al., 2017.

Gamma-ray spectrometry is performed by high-resolution detectors for which reference efficiency calibrations are set up using multi gamma sources prepared in the reference geometry using a water matrix (acidified) and filled at the reference filling height and with an energy range covering the desired working range. The reference efficiency calibration is corrected for true coincidence summing.

The reported radionuclides using this approach are ^{40}K and ^{226*}Ra. Analysis of ^{226}Ra is based on the measurement of its daughters in a radon-tight sample container after secular equilibrium is installed between mother and daughter nuclides or using the direct gamma-ray emission line at 186 keV. When the activity of ^{226}Ra was derived from daughter nuclides under the assumption of equilibrium, this is indicated by reporting the radionuclide as ^{226*}Ra (using the asterisk symbol).

Alpha-particle spectrometry is performed using PIPS (Passivated Implanted Planar Silicon) detectors on a source obtained after electrodeposition using a stainless disk. The water samples were pre-concentrated by $Fe(OH)_3$ co-precipitation. Uranium isotopes were separated using UTEVA® resin (Horwitz et al., 1992), measured by alpha-particle spectrometry using PIPS semiconductor detectors and counting times of 250,000 s. The samples for total U concentration determination are measured with the iCAP RQ ICP-MS of Thermo Fisher Scientific.

5.1.3 Discussion of results and relation to regulations

5.1.3.1 Results

The analysed U-isotopes were in almost all groundwater samples below the detection limit of 0.0005 Bq/l. The low U concentrations are in line with the reducing conditions encountered in the lower Carboniferous and physical properties that do not favour U dissolving into the groundwater. The ^{226}Ra results, on the other hand indicate that ^{226}Ra levels and hence also total activity of all measured samples exceed the exemption level of 3.6 Bq/l ^{226}Ra as given in annex IX (ARBIS) for liquid samples. This indicates that (i) these samples are classified as NORM-residues, (ii) their treatment and disposal need to be in agreement with regulation as described in ARBIS, (iii) measures as described in article 20.3 need to be taken to protect people and prevent exposures exceeding 1 mSv/y and any activities with this material follow a declaration file to the regulator (FANC), as written out in article 9 (ARBIS).

The high Ra activities can be explained by complexation with Cl in the brine, which increases mobility of this element. Likely, sources for ^{226}Ra and ^{228}Ra are ^{238}U and ^{232}Th in the overlying shales of the Chockier and Souvré formations and ^{238}U associated with organic limestone beds in the Goeree and Loenhout Formations. Except for the sample from DZH24, the ground water samples have similar ^{226}Ra activity levels. The reason why the sample from DZH24 is anomalous is unclear. This similarity between the other samples indicates that there is little difference in the U-Ra fractionation between the locations, and therefore little difference in water-rock interaction, mixing and migration time.

Table 17. ^{226}Ra using gamma-ray spectrometry, value is given ± uncertainty. 1: Vasile et al., 2017, a: Radon-emanation technique, b: Gamma-ray spectrometry

wellname	Ra-226 (Bq/l)	Sampling depth (m MD)
DZH14	84 ± 6	1315
DZH15	129 ± 9	1325
DZH23	148 ± 10	1485
DZH24	540 ± 80	1395
Beerse-GT-01a	65 ± 6	surface
VITO-geothermal[1,a]	109 ± 7	surface
VITO-geothermal[1,b]	95 ± 18	surface

Table 18. ^{238}U, ^{235}U and ^{234}U isotopes using alpha particle spectrometry and total U concentrations using ICP-MS. Analyses above the detection limit value are given ± uncertainty. '-' indicates that U_{tot} was not measured.

wellname	U-234 (Bq/l)	U-235 (Bq/l)	U-238 (Bq/l)	U tot (µg/l)
DZH14	<0.0005	<0.0005	<0.0004	<0.5
DZH15	0.0033 ± 0.001	<0.0005	0.0005 ± 0.0004	-
DZH23	<0.0007	<0.0007	<0.0005	-
DZH24	<0.0005	<0.0005	<0.0003	-
Beerse-GT-01a	<0.0005	<0.0007	0.0007 ± 0.0004	<3

5.1.3.2 Regulation

As stipulated on the website of the Federal Agency of Nuclear Control (FANC), the presence of NORM e.g. in residues may pose health risks to exposed individuals and can have non-negligible environmental impact. Therefore, industries (including geothermal installations) when classified as NORM-industries need to declare their activities to FANC as regulator and take precautionary measures to limit the risk to people and environment. Belgian radiological protection regulations are defined in the Royal Decree of July, 20th 2001 (Algemeen Reglement op de Bescherming van de bevolking en van de werknemers tegen het gevaar van Ioniserende Stralingen, ARBIS). This decree transposes European Council directives (formerly 96/29/Euratom, now 2013/59/Euratom) and incorporates Radiation Protection 122 Part II (EU 2002). For NORM, Articles 42, 93, and 20.34 of ARBIS are particularly relevant. Article 4 defines "professional activities using natural radiation sources" for which there is a risk of exposure to natural radioactive substances. It concerns these activities where radioactivity concentrations exceed either the total quantity of 1 tonne or the activity levels specified in annex VIII for solid sources or annex IX for liquid sources. For these professional activities a declaration file to FANC (defined in section 9 of ARBIS) is mandatory. Based on its expertise and operational feedback, FANC identifies sectors likely to fall under this regulation.

5.1.3.3 Safety measures

The safety measures for working with NORM need to ascertain that exposures do not exceed 1 mSv/y and that doses follow the ALARA principle (As Low As Reasonably Achievable). Given the activity concentrations in table 17 safety measures include wearing appropriate personal protection equipment, occupational hygiene measures, use of filters to limit exposure to the environment, and adequate ventilation of rooms in which the liquid is handled to prevent Rn accumulation. In general, for the given activity concentrations, the same type of safety measures as for laboratories handling chemical pollutants (e.g. metals) apply. The most important process contributing to the formation of NORM in installations in contact with deep formation waters in the Campine Basin is the formation of deposits (known as "scaling") in the pipes and crucial components such as filters, heat exchangers and pumps. If lithium production is considered in geothermal plants or in dedicated plants, next to these known risks, the possible accumulation of NORM in the extracted lithium-rich fluids should be studied. The formation of these NORM-deposits is subject to changes in physical parameters including changes in temperature and pressure. Hence care must be taken when replacing or cleaning or handling any parts of the installation. If degassing of the pumped water occurs in some way, radon can accumulate in the buildings of the installation.

Within the framework of exploring circular economical options of geothermal water, including extraction of components of interest like Li, it is possible that radioactive elements start accumulating e.g. in filters or different parts of these installations as well. This warrants further investigation. Additionally, as the radioactivity levels of the geothermal water exceed the exemption levels defined in annex IX (ARBIS) for Ra, changes in the processing and use of the geothermal water are also subject to declaration to FANC. Finally, if the geothermal water for some reason cannot be returned to the

underground repository, it will become a NORM-residue that needs to be disposed following the procedures for NORM-residues defined in ARBIS. Technical guideline 5 for handling of NORM-residues is available at the FANC website. Depending on the activity concentration and the potential dose and quantity, this will normally be towards a disposal site cat 1. However, this is case by case dependent and needs additional declaration and approval by FANC.

6 RECOMMENDATIONS

Based on the hydro-chemical analysis of deep formation waters, three zones can be delineated where anomalies occur (Figure 53). The first zone covers a large part of the Campine Basin. The other zones are in the Brabant Massif. Here, the most important is the Oostrozebeke-Waregem-Harelbeke-Deerlijk zone; The other zone lies further to the southeast, in the Oudenaarde-Brakel-Geraardsbergen region.

The deep groundwater samples from the Campine Basin are rich in lithium. The water chemistry points to cation exchange as the main cause of the elevated Li concentrations. High concentrations of strontium and local enrichment of copper and zinc are attributable to chemical interaction between the formation water and the host rock.

The Brabant Massif is known for sulphide mineralisations. The trace elements related to this are found in the dataset of this study. However, they are often associated with oxidation caused by groundwater extraction, making it difficult to definitively determine which geological aspects regarding the critical raw materials are at play.

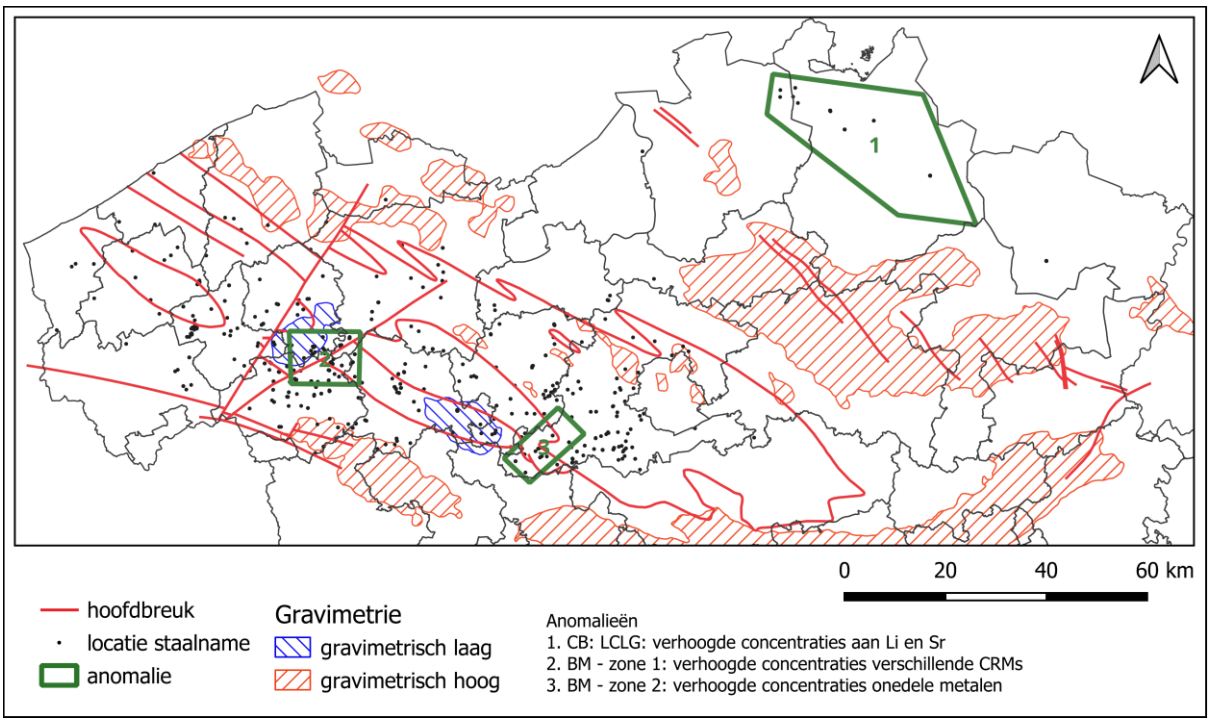

Figure 53: Delineation of zone with anomalous trace element concentrations in deep ground water. LCLG stands for Lower Carboniferous Limestone Group.

6.1.1 Campine Basin

The conceptual model for lithium enrichment of deep formation water in the Campine Basin can be verified by a mineralogical and geochemical study of the reservoir rock and the over- and underlying formations. This analysis can be supplemented with isotopic analyses (lithium, boron, and oxygen) as proxies for the origin of the formation water and the contribution of organic material.

The available data relate to a limited number of locations. Geochemical data from additional locations could help provide a more complete picture of compositional changes throughout the basin. Permit

holders of deep geothermal projects in the Campine Basin could be requested to provide water analyses. To ensure the quality of the data collected in this way, it is recommended to establish guidelines for sampling methods and to compile a list of minimum parameters to be measured. Elements such as Br, B, I, and F provide important information about the origin and evaluation of the formation water but are not routinely measured.

Lastly, it is recommended to compile a database of rock samples analyses (now only available for a limited number of rock samples on material from VITO Geothermal (Vasile et al., 2017, Pauwels, 2020) including mineral composition and geochemical analysis. Mineral composition and geochemical data for the reservoir rocks will allow to model the specific rock-water interactions in more detail to define the origin of Li enrichment and other element concentrations.

6.1.2 Brabant Massif

The Li concentration in groundwater of the Brabant Massif is found to be low and cannot be considered anomalous. Additionally, the hydrochemical dataset revealed several wells with anomalous concentrations of different CRMs or other trace elements. However, no meaningful relationship based on a statistical and spatial correlation was found. To enhance the interpretation and mapping of Li, it is recommended that additional groundwater sampling be conducted, particularly at deep(er) wells which are situated in the areas of the gravity anomalies and zones where most elements have anomalous values (e.g., Zone 1). A further extensive groundwater sampling campaign for Li analysis, targeting wells that show anomalies of its genetically related cations like Na, and those further southeast where the effect of seawater intrusion and cation exchange is expected to be insignificant, would be valuable. The use of inductively coupled plasma mass spectrometry (ICP-MS) is recommended for its high sensitivity and accuracy in detecting trace concentrations of these elements.

Besides Li, the current dataset is found to be insufficient for elements such as V, Hf, Hg, Pt, and Au. Additional groundwater samples across underrepresented zones and geological features may be done to improve spatial coverage and geochemical resolution. For instance, there are no analyses available of Li at wells in anomalous Zone 1 (the assumed granite/pegmatite intrusive) and along the main geological faults traversing the folds. Furthermore, carrying out a deep drilling in the anomalous zones is recommended. Subsequent mineralogical and petrographic analyses of the core samples will provide critical insights into mineral assemblages and alteration patterns. The deep borehole(s) should be subjected to geophysical well logging and be equipped as wells, in order to allow for hydrogeological (including sampling) and geophysical (including temperature logging) follow-up. Detailed geochemical modelling should also be taken into consideration, since many of the trace elements are redox reaction sensitive. In addition, where feasible, a more detailed review of lithology and drilling logs can be carried out for individual wells to identify the specific aquifer interval(s) from which the sampled water was collected. This effort could be further strengthened by integrating geophysical methods, such as gravity and transient EM or magneto-telluric surveys, to assist in refining subsurface interpretations and targeting.

REFERENCES

Angeli, B.N., 2005. Platinum group minerals in eastern Brazil. Platinum Metals Review, 49(1), pp.41-53.

Appelo, C.A.J., 1994. Cation and proton exchange, pH variations, and carbonate reactions in a freshening aquifer. *Water resources research*, *30*(10), pp.2793-2805

Araoka, D., Kawahata, H., Takagi, T., Watanabe, Y., Nishimura, K. and Nishio, Y., 2014. Lithium and strontium isotopic systematics in playas in Nevada, USA: constraints on the origin of lithium. *Mineralium Deposita*, *49*, pp.371-379.

Balaram, V., Santosh, M., Satyanarayanan, M., Srinivas, N., Gupta, H., 2024. Lithium: A review of applications, occurrence, exploration, extraction, recycling, analysis, and environmental impact. Geosci. Front. 15, 101868. https://doi.org/10.1016/j.gsf.2024.101868

Begaerts, N., 1998. Geochemische studie van het grondwater in het Massief van Brabant. Universiteit Gent.

Boni, M., Bouabdellah, M., Boukirou, W., Putzolu, F. and Mondillo, N., 2023. Vanadium ore resources of the African continent: State of the Art. *Ore Geology Reviews*, *157*, p.105423.

Bos, S. & Laenen, B., 2017. Development of the first deep geothermal doublet in the Campine Basin of Belgium. European Geologist 43, pp. 16-20.

Bralia, A., Sabatini, G. and Troja, F.J.M.D., 1979. A revaluation of the Co/Ni ratio in pyrite as geochemical tool in ore genesis problems: Evidences from southern Tuscany pyritic deposits. Mineralium Deposita, 14, pp.353-374.

Coffey, D. M., Munk, L. A., Ibarra, D. E., Butler, K. L., Boutt, D. F., & Jenckes, J., 2021. Lithium storage and release from lacustrine sediments: Implications for lithium enrichment and sustainability in continental brines. Geochemistry, Geophysics, Geosystems, 22, e2021GC009916. https://doi.org/10.1029/2021GC009916

Cuadros, J., Afsin, B., Jadubansa, P., Ardakani, M., Ascaso, C., & Wierzchos, J. (2013). Pathways of volcanic glass alteration in laboratory experiments through inorganic and microbially-mediated processes. Clay Minerals, 48(3), 423–445. https://doi.org/10.1180/claymin.2013.048.3.01

Decarreau, A., Vigier, N., Pálková, H., Petit, S., Vieillard, P. and Fontaine, C., 2012. Partitioning of lithium between smectite and solution: An experimental approach. *Geochimica et Cosmochimica Acta*, *85*, pp.314-325.

Dewaele, S., Boven, A. and Muchez, P., 2002. 40Ar/39Ar dating of mesothermal, orogenic mineralization in a low-angle reverse shear zone in the Lower Palaeozoic of the Anglo-Brabant fold belt, Belgium. *Applied Earth Science*, *111*(3), pp.215-220.

Dewaele, S., Muchez, P., 2005. Geochemical characteristics of pyrite formed during the evolution of an orogenic fold belt: A case study from the Lower Palaeozoic Anglo-Brabant fold belt (Belgium). Appl. Earth Sci. (Transactions Institutions Min. Metall. Sect. B) 114. https://doi.org/10.1179/037174505X62848

Dewaele, S., Muchez, P.H. and Banks, D.A., 2004. Fluid evolution along multistage composite fault systems at the southern margin of the Lower Palaeozoic Anglo-Brabant fold belt, Belgium. *Geofluids*, *4*(4), pp.341-356.

Dostal, J., 2016. Rare metal deposits associated with alkaline/peralkaline igneous rocks.

Dugamin, E.J.M., Boiron, M., Cathelineau, M., Richard, A., Peiffert, C., Lebreton, A., Banks, D.A. & Despinois, F., 2024. Brine-granite interaction and lithium leaching in a continental rift (Soultz-sous-Fôrets, Rhine Graben, France. LITHOS 478-479 107604.

Dugamin, E.J.M., Cathelineau, M., Boiron, M., Richard, A., Despinois, F., 2023. Lithium enrichment processes in sedimentary formation waters. Chemical Geology 635 121626.

Dugamin, E.J.M., Richard, A., Cathelineau, M., Boiron, M.C., Despinois, F., Brisset, A., 2021.

Groundwater in sedimentary basins as a potential lithium resource: a global prospective study. Sci. Rep. 1–10. https://doi.org/10.1038/s41598-021-99912-7

Eggeling, L., Genter, A., Kölbel, T., & Münch, W. (2013). Impact of natural radionuclides on geothermal exploitation in the Upper Rhine Graben. Geothermics, 47, 80–88. https://doi.org/10.1016/j.geothermics.2013.03.002

European Commission: Directorate-General for Communication. (2023). *European Critical Raw Materials Act.* Publications Office of the European Union. https://data.europa.eu/doi/10.2775/741940

European Parliament, & Council of the European Union. (2024). *Establishing a framework for ensuring a secure and sustainable supply of critical raw materials and amending Regulations.* (EU) No 168/2013, (EU) 2018/858, (EU) 2018/1724 and (EU) 2019/1020. Official Journal of the European Union.

Ferket, H., 2007. Opstellen van een sluitende begravingsgeschiedenis voor het Kempens Bekken. In Dreesen, R. & Laenen, B., VLAKO - Technology Watch 2006. Studie uitgevoerd in opdracht van ALBON, VITO-rapport 2007/MAT/R/014

Fitzgerald, D., Nicholson, R.V. and Regoli, L., 2008. Environmental management criteria for molybdenum and selenium: a review relevant to the mining industry.

Fontes, J.Ch., Matray, J.M., 1993. Geochemistry and origin of formation brines from the Paris Basin, France. Chemical Geology 109, pp.149-175.

Garuti, G., Proenza, J.A. and Zaccarini, F., 2007. Distribution and mineralogy of platinum-group elements in altered chromitites of the Campo Formoso layered intrusion (Bahia State, Brazil): control by magmatic and hydrothermal processes. *Mineralogy and Petrology*, *89*, pp.159-188

Garuti, G., Zaccarini, F., Proenza, J.A., Thalhammer, O.A. and Angeli, N., 2012. Platinum-group minerals in chromitites of the Niquelândia layered intrusion (Central Goias, Brazil): Their magmatic origin and low-temperature reworking during serpentinization and lateritic weathering. Minerals, 2(4), pp.365-384

Gourcerol, B., Sanjuan, B., Millot, R., Rettenmaier, D., Jeandel, E., Genter, A., Bosia, C., Rombaut, A., 2024. Atlas of lithium geothermal fluids in Europe. Geothermics 119.

Grew, E.S., 2020. The minerals of lithium. Elements*:* An International Magazine of Mineralogy, Geochemistry, and Petrology, 16(4), pp.235-240.

Hale, M., 1981. Pathfinder applications of arsenic, antimony and bismuth in geochemical exploration. In Developments in Economic Geology (Vol. 15, pp. 307-323).

Helsen, S. and Langenaeker, V., 1999. Burial history and coalification modeling of Westphalian strata in the eastern Campine Basin (Northern Belgium). Professional paper 1999/1, n°289, 23 pp., Geol. Survey of Belgium, Brussels, Belgium.

Herrington, R. J. (2024). The Raw Material Challenge of Creating a Green Economy. *Minerals, 14(2)*, 204. https://doi.org/10.3390/min14020204

Hofmann, M. H., & Sherry, M. C. (2025). Synchronous authigenic albite and dolomite formation in carbonates. Sedimentology, 72(7), 2393–2423. https://doi.org/10.1111/sed.70045

Hofmann, M., Hagelüken, C., & Hool, A. (2018). Critical raw materials: A perspective from the materials science community. *Sustainable Materials and Technologies, 17*, e00074. https://doi.org/10.1016/j.susmat.2018.e00074

Horwitz, E.P., Dietz, M.L., Chiarizia, R., Diamond, H., Essling, A.M., Graczyk, D., 1992. Separation and preconcentration of uranium from acidic media by extraction chromatography. Analytica Chimica Acta, Volume 266, Issue 1, pp.25-37. https://doi.org/10.1016/0003-2670(92)85276-C

Jancsek, K., Janovszky, P., Galbács, G. and Tóth, T.M., 2023. Granite alteration as the origin of high lithium content of groundwater in southeast Hungary. *Applied Geochemistry*, *149*, p.105570

Kerr, A., Walsh, J.A., Sparkes, G.W. and Hinchey, J.G., 2013. Vanadium potential in Newfoundland and

Labrador: a review and assessment. *Newfoundland and Labrador Department of Natural Resources, Geological Survey*, *13*, pp.137-165.

Kharaka, Y. K., & Mariner, R. H. (1989). Chemical Geothermometers and Their Application to Formation Waters from Sedimentary Basins. In Thermal History of Sedimentary Basins (pp. 99–117). Springer New York. https://doi.org/10.1007/978-1-4612-3492-0_6

Kölbel, L., Kölbel, T., & Fechner, D. (2022). Radiochemical monitoring of geothermal systems: Case study Bruchsal (Upper Rhine Graben). Applied Geochemistry, 147, 105509. https://doi.org/10.1016/j.apgeochem.2022.105509

Kölbel, L., Kölbel, T., Sauter, M., Schäfer, T., Siefert, D., & Wiegand, B. (2020). Identification of fracture zones in geothermal reservoirs in sedimentary basins: A radionuclide-based approach. Geothermics, 85, 101764. https://doi.org/10.1016/j.geothermics.2019.101764

Kompanchenko, A.A., Voloshin, A.V. and Balagansky, V.V., 2018. Vanadium mineralization in the Kola region, Fennoscandian Shield. *Minerals*, *8*(11), p.474.

Leonardi, F., Venoso, G., Bogi, A., Bucci, S., Caldognetto, E., De Stena, A., La Verde, G., Luzzi, L., Nuccetelli, C., Picciolo, F., Pratesi, G., Trotti, F., Ugolini, R., Pugliese, M., Trevisi, R., & Peroni, I. (2024). Review of NORM occurrence and application of a tailored graded approach for the radiation protection in geothermal plants. The European Physical Journal Plus, 139(2), 195. https://doi.org/10.1140/epjp/s13360-024-04917-6

Leybourne, M.I. and Cameron, E.M., 2010. Groundwater in geochemical exploration. Geochemistry: Exploration, Environment, Analysis, 10 (2): 99-118. https://doi.org/10.1144/1467-7873/09-222

Leybourne, M.I., Cameron, E.M. and Milkereit, B., 2007. Groundwaters in geochemical exploration: methods, applications, and future directions. In *Proceedings of Exploration* (Vol. 7, pp. 201-221).

Li, Jiexiang, Wang, X., Ruan, C., Sagoe, G., Li, Jianlin, 2022. Enrichment mechanisms of lithium for the geothermal springs in the southern Tibet, China. J. Hydrol. 612, 128022. https://doi.org/10.1016/j.jhydrol.2022.128022

Lillo Ramos, F.J., 1992. *Geology and geochemistry of Linares-La Carolina Pb-ore field (southeastern border of the Hesperian Massif)* (Doctoral dissertation, University of Leeds)

Lindsey, B.D., Belitz, K., Cravotta III, C.A., Toccalino, P.L. and Dubrovsky, N.M., 2021. Lithium in groundwater used for drinking-water supply in the United States. *Science of the Total Environment*, *767*, p.144691

Loftus-Hills, G. and Solomon, M., 1967. Cobalt, nickel and selenium in sulphides as indicators of ore genesis. *Mineralium deposita*, *2*, pp.228-242

Lombard, M.A., Brown, E.E., Saftner, D.M., Arienzo, M.M., Fuller-thomson, E., Brown, C.J., Ayotte, J.D., 2024. Estimating Lithium Concentrations in Groundwater Used as Drinking Water for the Conterminous United States. https://doi.org/10.1021/acs.est.3c03315

Nath, B., Jean, J.S., Lee, M.K., Yang, H.J. and Liu, C.C., 2008. Geochemistry of high arsenic groundwater in Chia-Nan plain, Southwestern Taiwan: possible sources and reactive transport of arsenic. *Journal of Contaminant Hydrology*, *99*(1-4), pp.85-96.

Nicholson, K., 2012. Geothermal fluids: chemistry and exploration techniques. Springer Science & Business Media.

Olivarius, M. 2018. Source and Occurrence of Radionuclides in Geothermal Water: With Focus on the Margretheholm Geothermal Plant.

Pauwels, J., 2021. Chemical and radiological assessment of deep brine-type geothermal groundwaters. PhD Dissertation, KU Leuven, 160p.

Piessens, K., De Vos, W., Beckers, R., Vancampenhout, P & De Ceukelaire, M., 2005. Opmaak van de pre-Krijt subcropkaart van het Massief van Brabant voor invoering in de Databank Ondergrond Vlaanderen. Studie uitgevoerd in opdracht van het Ministerie van de Vlaamse Gemeenschap (VLA 03-1.1), 94p.

Piessens, K., Muchez, P., Dewaele, S., Boyce, A., De Vos, W., Sintubin, M., Debacker, T.N., Burke, E.A.J.,

Viaene, W., 2002. Fluid flow, alteration and polysulphide mineralisation associated with a low-angle reverse shear zone in the Lower Palaeozoic of the Anglo-Brabant fold belt, Belgium. Tectonophysics 348, 73–92. https://doi.org/10.1016/S0040-1951(01)00250-5

Piessens, K., Muchez, P., Viaene, W., Boyce, A., De Vos, W., Sintubin, M. and Debacker, T., 2000. Alteration and fluid characteristics of a mineralised shear zone in the Lower Palaeozoic of the Anglo-Brabant belt, Belgium. *Journal of Geochemical Exploration*, *69*, pp.317-321

Regenspurg, S., Dilling, J., Mielcarek, J., Korte, F., & Schkade, U.-K. (2014). Naturally occurring radionuclides and their geochemical interactions at a geothermal site in the North German Basin. Environmental Earth Sciences, 72(10), 4131–4140. https://doi.org/10.1007/s12665-014-3306-6

Salminen, R. (Ed.), Batista, M. J., Bidovec, M., Demetriades, A., De Vivo, B., De Vos, W., Duris, M., Gilucis, A., Gregorauskiene, V., Halamic, J., Heitzmann, P., Lima, A., Jordan, G., Klaver, G., Klein, P., Lis, J., Locutura, J., Marsina, K., Mazreku, A., ... Tarvainen, T. (2005). Geochemical Atlas of Europe. Part 1: Background Information, Methodology and maps. Geological Survey of Finland. http://weppi.gtk.fi/publ/foregsatlas/articles.php

Sanjuan, B., Gourcerol, B., Millot, R., Rettenmaier, D., Jeandel, E.,Rombaut, A., 2022. Lithium-rich geothermal brines in Europe: An up-date about geochemical characteristics and implications for potential Li resources. Geothermics 101, pp. 102385.

Sanjuan, B., Millot, R., Innocent, Ch., Dezayes, Ch., Scheiber, J., Brach, M., 2016. Major geochemical characteristics of geothermal brines from the Upper Rhine Graben granitic basement with constraints on temperature and circulation. Chemical Geology 428, pp. 27-47.

Sanjuan, B., Pinault, J.-L., Rose, P., Gerard, A., Brach, M., et al. Geochemical fluid characteristics and main achievements about tracer tests at Soultz-sous-Forêts (France). EHDRA Scientific Conference, 2006, Soultz-sous-Forêts, France, 13p. hal-00773150.

Sarath, K.V., Shaji, E. and Nandakumar, V., 2023. Characterization of trace and heavy metal concentration in groundwater: A case study from a tropical river basin of southern India. *Chemosphere*, *338*, p.139498.

Seo, H., Lee, J.H., Park, S., Oh, J., Choi, J., Lee, J.T. and Yun, S.T., 2023. Lithium Distribution in Thermal Groundwater: A Study on Li Geochemistry in South Korean Deep Groundwater Environment. *Economic and Environmental Geology*, *56*(6), pp.729-744

Sharma, N., Westerhoff, P., Zeng, C., 2022. Lithium occurrence in drinking water sources of the United States. Chemosphere 305, 135458. https://doi.org/10.1016/j.chemosphere.2022.135458

Spötl, C., Longstaffe, F. J., Ramseyer, K., & Rüdinger, B. (1999). Authigenic albite in carbonate rocks – a tracer for deep-burial brine migration? Sedimentology, 46(4), 649–666. https://doi.org/10.1046/j.1365-3091.1999.00237.x

Starkey, H.C., 1982. *The role of clays in fixing lithium* (No. 1278). US Government Printing Office

Sterpin, M., 1996. Onderzoek naar metallische mineralisaties in de Paleozoïsche sokkel van Vlaanderen. Project VLA/94-3.5, Universiteit Gent, Laboratorium voor Toegepaste Geologie en Hydrogeologie.

Stuyfzand, P. J. (1986). A new hydrochemical classification of water types. *Proceedings of the 9th Salt Water Intrusion Meeting (SWIM)*, Delft, Netherlands, 641-651.

Stuyfzand, P. J. (1989). A new hydrochemical classification of water types. Regional Characterization of Water Quality (Proceedings of the Baltimore Symposium, May 1989). IAHS Publ.no.182, pp.89-98.

Taner, M.F., Ercit, T.S. and Gault, R.A., 1998. Vanadium-bearing magnetite from the Matagami and Chibougamau mining districts, Abitibi, Quebec, Canada. *Exploration and Mining Geology*, *7*(4), pp.299-311

Thompson, J.F.H., Sillitoe, R.H., Baker, T., Lang, J.R., Mortensen, J.K., 1999. Intrusion-related gold deposits associated with tungsten-tin provinces. Miner. Depos. 34, 323–334.

Trompetter, W.J., Reyes, A.G., Vickridge, I.C., Markwitz, A., 1999. Lithium and boron distributions in

geological samples. Nucl. Instruments Methods Phys. Res. Sect. B Beam Interact. with Mater. Atoms 158, 568–574. https://doi.org/10.1016/S0168-583X(99)00333-X

Udagedara, D.T., Pitawala, H.M.T.G.A. and Dharmagunawardhane, H.A., 2014. Use of heavy metals and trace elements in groundwater as a tool for mineral exploration: A case study from Udawalawe, Sri Lanka. *Asian Journal of Water, Environment and Pollution*, *11*(4), pp.59-67

Van Camp, M., Walraevens, K., 2009. Recovery scenarios for deep over-exploited aquifers with limited recharge: methodology and application to an aquifer in Belgium. Environ. Geol. 56, 1505–1516. https://doi.org/10.1007/s00254-008-1248-6

Van Der Voet, E., Van Der Voet, E., Laenen, B., Rombaut, B., Kourta, M., & Swennen, R. (2020). Fracture characteristics of Lower Carboniferous carbonates in northern Belgium based on FMI log analyses. Geologie En Mijnbouw/Netherlands Journal of Geosciences. https://doi.org/10.1017/njg.2020.6

Van Keer, I., Ondrak, R., Muchez, Ph., Bayer, U., Dusar, M. and Viaene, W., 1998a. Burial history and thermal evolution of Westphalian coal-bearing strata in the Campine Basin (NE Belgium). Geologie en Mijnbouw 76, 301-310.

Vandenberghe, N., Dusar, M., Boonen, P., Sun Fan, L., Voets, R., Bouckaert, J., 2000. The Merksplas-Beerse geothermal well (17W265) and the Dinantian reservoir. Geologica Belgica 3/3-4, pp. 349-367.

Vasile ,M., Bruggeman, M., Van Meensel, S., Bos, S., Laenen, B., 2017. Characterisation of the natural radioactivity of the first deep geothermal doublet in Flanders, Belgium. Applied Radiation and Isotopes, Volume 126, pp. 300-303, https://doi.org/10.1016/j.apradiso.2016.12.030.

Verma, S. P., & Santoyo, E. (1997). New improved equations for NaK, NaLi and SiO2 geothermometers by outlier detection and rejection. Journal of Volcanology and Geothermal Research, 79(1–2), 9–23. https://doi.org/10.1016/S0377-0273(97)00024-3

Walraevens, K. (1987). Hydrogeologie en hydrochemie van het Ledo-Paniseliaan in Oost- en West-Vlaanderen. Ghent University, Ghent, Belgium

Walraevens, K., & Van Camp, M. (2004). Advances in understanding natural groundwater quality controls in coastal aquifers. In Proceedings of the 18th Salt Water Intrusion Meeting (Vol. 31, pp. 449-463).

Walraevens, K., Lebbe, L., De Ceukelaire, M., Van Houtte, E., De Breuck, W. (1994). Influence on groundwater quality of the Paleozoic Brabant Massif in Belgium due to overexploitation. Groundwater Quality Management, IAHS Publ., 220, 461-470.

Walraevens, K., Van Camp, M., De Ceukelaire, M., Van Burm, P., Lebbe, W., De Breuck, W., Gerard, P., Verplaetse, H., 1989. Hydrochemisch onderzoek van de gedeeltelijk afgesloten watervoerende lagen van de sokkel, het Krijt en het Landenian onder West-, Oost- en Frans-Vlaanderen. Natuurwetenschappelijk Tijdschr. 71, 53–73.

Walreavens, K. (1997). Notes of the course unit Groundwater chemistry, Ghent University, Belgium

Wang, D., Zheng, Y., Mathur, R., Qiu, K., Wu, H., Ren, H., Wang, E., Li, Y., Yi, J., 2021. Zinc and cadmium isotopic constraints on ore formation and mineral exploration in epithermal system: A reconnaissance study at the Keyue and Zhaxikang Sb–Pb–Zn–Ag deposits in southern Tibet. Ore Geol. Rev. 139, 104594. https://doi.org/10.1016/j.oregeorev.2021.104594

Wenselaers, P., Dusar, M. & Van Tongeren, P.C.H., 1996. Steenkoollaag methaangaswinning in het Kempisch kolenbekken 'Het proefproject te Peer'. Ministerie van de Vlaamse Gemeenschap, afdeling Natuurlijke Rijkdommen en Energie (Brussel), 67p.

Wu, H., Zhou, J., Hu, W., Sun, F., Kang, X., Zhang, Y., He, W., & Feng, C. (2022). Origin of authigenic albite in a lacustrine mixed-deposition sequence (Lucaogou Formation, Junggar Basin) and its diagenesis implications. Energy Exploration & Exploitation, 40(1), 132–154. https://doi.org/10.1177/01445987211042702

Yang, J., Liu, H., Tang, Z., Peeters, L. and Ye, M. (2022), Visualization of Aqueous Geochemical Data

Using Python and WQChartPy. Groundwater. https://doi.org/10.1111/gwat.13185
Yuan, X., Hu, Y., Zhao, Y., Li, Q., Iiu, C., 2021. Contribution of Hydrothermal Processes to the Enrichment of Lithium in Brines: Evidence from Water-Rock Interacting Experiments. Aquatic Geochemistry 27, pp. 221-239. https://doi.org/10.1007/s10498-021-09395-1
Zhang, Y., Tan, H., Cong, P., Rao, W., Ta, W., Lu, S., Shi, D., 2022. Boron and lithium isotopic constraints on their origin, evolution, and enrichment processes in a river–groundwater–salt lake system in the Qaidam Basin, northeastern Tibetan Plateau. Ore Geol. Rev. 149, 105110. https://doi.org/10.1016/j.oregeorev.2022.105110
Zukin, J.G., Hammond, D.E., Teh-Lung, K., Elders, W.A. (1987). Uranium-thorium series radionuclides in brines and reservoir rocks from two deep geothermal boreholes in the Salton Sea Geothermal Field, southeastern California. Geochimica et Cosmochimica Acta 51: 2719-2731, https://doi.org/10.1016/0016-7037(87)90152-9

APPENDICES

APPENDIX 1: DATA CAMPINE BASIN

Digital appendix

- Datatable Campine Basin
- Corrections logfile containing the data corrections as listed in Table 6

APPENDIX 2: GIS-FILES CAMPINE BASIN

Digital appendix

- QGIS-project containing the document wells in the Campine Basin
- QGIS (qml) layer style file containing the color coding for the wells in the Campine Basin as presented in this report

APPENDIX 3: ELEMENT CONCENTRATIONS SEAWATER

Element	Concentration		Source
	Mg/l	remark	
Al3+	0.0001	coastal: 0.6 to 131.96 µg/l ocean: 0.02 - 2.03 µg/l	Botté et al., 2022
As3-	0.0015	1 - 2 µg/l	Kalia, 2023
B3+	4.6		Fontes & Matray, 1993a
Ba2+	0.02		Salminen et al., 2005
Br-	68		Fontes & Matray, 1993a
Cd2+	0.00009	0.067 - .113 µg/l	Neff, 2002
Cl-	19780		Fontes & Matray, 1993a
Cr3+	0.000292	~ 80 to 550 ng/kg	Paulukat et al., 2016
Cu2+	0.0003	0.05 to 0.35 µg/l	Neff, 2002
F-	1.3		Salminen et al., 2005
I-	0.06		Salminen et al., 2005
K+	408		Fontes & Matray, 1993a
Li+	0.18		Fontes & Matray, 1993a
Mo4+	0.01		Molybdenum in freshwater and marine water
Ni2+	0.002		Nickel in freshwater and marine water
Pb2+	0.002		Lead in freshwater and marine water
Rb+	0.7		Fontes & Matray, 1993a
Sb3-	0.00024	0.24 µg/l	Caritat, 1998
Sn2+	0.01		Salminen et al., 2005
Sr2+	8.18		Fontes & Matray, 1993a
V5+	0.005		Vanadium in freshwater and marine water
Zn2+	0.005	0.5 - 5 ppb	Neff, 2002

APPENDIX 4: DATA BRABANT MASSIF

Digital appendix

- Datatable Campine Basin

APPENDIX 5: GIS-FILES BRABANT MASSIF

Digital appendix

- GDB containing the information in the Brabant Massif as presented in this report
- MPK file (ArcGIS) containing the information in the Brabant Massif as presented in this report

APPENDIX 6: CORRELATION MATRIX BRABANT MASSIF

Overall correlation matrix between hydrochemical species, including analysed major and trace elements for the samples of the Brabant Massif.

Elements	Na	K	Ca	Mg	Fe	NH4	Cl	SO4	HCO3	CO3	PO4	F	Br	I	NO3	NO2
Na	**1**	0.053	-0.059	0.003	-0.006	-0.088	0.215	0.106	0.046	0.001	-0.044	0.085	0.038	0.086	0.005	-0.114
K	0.053	**1**	0.221	0.521	0.041	-0.109	0.427	0.14	0.066	-0.005	-0.068	-0.13	0.013	0.221	0.038	-0.143
Ca	-0.059	0.221	**1**	**0.806**	0.264	-0.046	0.089	-0.157	0.057	-0.134	-0.075	-0.541	-0.062	-0.084	0.016	-0.057
Mg	0.003	0.521	**0.806**	**1**	0.244	-0.055	0.362	-0.07	0.092	-0.117	-0.16	-0.49	0.028	-0.044	0.046	-0.075
Fe	-0.006	0.041	0.264	0.244	**1**	-0.013	0.106	-0.043	0.1	0.001	-0.06	-0.142	0.002	-0.479	-0.038	-0.017
NH4	-0.088	-0.109	-0.046	-0.055	-0.013	**1**	-0.017	-0.085	-0.182	-0.087	0.406	-0.088	0.008	-0.159	-0.047	**1**
Cl	0.215	0.427	0.089	0.362	0.106	-0.017	**1**	0.386	0.125	0.042	-0.07	0.372	0.077	0.066	-0.004	-0.037
SO4	0.106	0.14	-0.157	-0.07	-0.043	-0.085	0.386	**1**	0.33	0.104	0.095	0.377	-0.025	0.119	0.011	-0.104
HCO3	0.046	0.066	0.057	0.092	0.1	-0.182	0.125	0.33	**1**	0.112	-0.052	0.223	-0.107	0.049	0.027	-0.239
CO3	0.001	-0.005	-0.134	-0.117	0.001	-0.087	0.042	0.104	0.112	**1**	0.085	0.044	0.014	-0.227	0.015	-0.108
PO4	-0.044	-0.068	-0.075	-0.16	-0.06	0.406	-0.07	0.095	-0.052	0.085	**1**	-0.067	0.313	-0.048	-0.051	**0.759**
F	0.085	-0.13	-0.541	-0.49	-0.142	-0.088	0.372	0.377	0.223	0.044	-0.067	**1**	0.129	-0.356	-0.021	-0.105
Br	0.038	0.013	-0.062	0.028	0.002	0.008	0.077	-0.025	-0.107	0.014	0.313	0.129	**1**	0.085	-0.163	-0.253
I	0.086	0.221	-0.084	-0.044	-0.479	-0.159	0.066	0.119	0.049	-0.227	-0.048	-0.356	0.085	**1**	0.49	0.473
NO3	0.005	0.038	0.016	0.046	-0.038	-0.047	-0.004	0.011	0.027	0.015	-0.051	-0.021	-0.163	0.49	**1**	0.091
NO2	-0.114	-0.143	-0.057	-0.075	-0.017	**1**	-0.037	-0.104	-0.239	-0.108	**0.759**	-0.105	-0.253	0.473	0.091	**1**
Sr_ppb	0.174	0.307	0.423	0.532	0.17	-0.099	0.315	0.069	0.241	0.112	-0.084	-0.148	-0.041	-0.026	0.036	-0.151
B_mgl	-0.06	-0.062	-0.046	-0.054	-0.011	**1**	0.012	-0.04	-0.195	-0.077	**0.854**	-0.089	0.195	-0.046	-0.034	**1**
SiO4	0.3	-0.188	-0.351	-0.351	-0.154	-0.096	0.048	**0.713**	0.156	-0.096	-0.195	0.399	0.43	0.104	-0.072	-0.101
Be_ppb	-0.045	-0.064	-0.106	-0.088	0.124		-0.158	0.363	0.145	-0.115	0.094	0.082	-0.118	-0.107	-0.168	0.497
Pb_ppb	0.284	0.126	-0.035	0.059	0.068	-0.081	0.294	0.129	0.229	0.12	0.107	0.108	-0.065	-0.471	0.34	-0.1
Zn_ppb	-0.1	0.039	0.347	0.232	0.063	-0.079	-0.031	-0.059	0.121	-0.147	-0.217	-0.181	0.347	0.051	0.093	-0.092

Elements	Na	K	Ca	Mg	Fe	NH4	Cl	SO4	HCO3	CO3	PO4	F	Br	I	NO3	NO2
Cu_ppb	0.023	0.018	-0.149	-0.134	-0.057	**0.632**	-0.004	0.114	-0.087	-0.13	0.574	0.011	0.046	0.071	0.281	**0.646**
Cd_ppb	-0.031	0.011	-0.07	-0.061	-0.009	-0.014	-0.004	-0.009	0.018	0.048	-0.031	0.154	**0.751**		-0.002	0.343
Mo_ppb	0.436	-0.053	-0.273	-0.218	-0.088	-0.106	0.301	0.432	0.183	0.081	-0.091	0.336			-0.018	-0.114
Co_ppb	0.194	0.137	-0.002	0.022	0.1	0.284	0.125	0.432	0.154	-0.016	0.476	-0.005			0.02	0.305
Ni_ppb	-0.093	0.136	0.231	0.25	0.081	0.031	-0.034	0.017	0.057	-0.099	-0.082	-0.206	**0.749**	-0.073	0.032	0.016
As_ppb	0.147	-0.062	-0.191	-0.167	-0.025	-0.046	0.063	0.294	-0.058	-0.109	-0.193	0.099	0.586	-0.071	-0.052	-0.046
Hg_ppb	**0.645**	0.414	0.372	0.451	0.264	0.109	0.595	0.17	0.448	0.424	-0.102	0.471	**-0.751**		-0.153	
Cr_ppb	-0.199	0.107	0.161	0.074	-0.022	-0.149	-0.114	-0.249	-0.027	-0.114	-0.018	-0.051	**-0.766**		-0.044	-0.241
Se_ppb	0.176	-0.094	-0.215	-0.216	-0.149	-0.111	0.103	0.13	0.004	-0.072	-0.235	0.267			-0.096	-0.118
Bi_ppb	0.333	0.006	-0.205	-0.165	-0.027	-0.07	0.281	0.244	0.063	0.055	0.265	0.177			-0.031	-0.084
Sn_ppb	0.244	0.45	0.213	0.349	0.055	-0.064	0.396	-0.012	-0.007	0.143	-0.017	-0.077	0.123	0.078	0.379	-0.078
Te_ppb	0.377	-0.039	0.193	0.232	0.297		0.397	-0.105	0.16	0.25		0.268			-0.049	
Sb_ppb	-0.074	-0.07	-0.05	-0.058	0.005	**0.999**	0.015	-0.048	-0.235	-0.088	0.591	-0.12	-0.403	-0.095	-0.047	**1**
Nb_ppb	-0.092	-0.124	-0.054	-0.065	-0.004	**0.999**	0.065	-0.084	-0.305	-0.195	**0.801**	-0.121			-0.026	**1**
Ba_ppb	-0.226	0.118	0.446	0.336	0.291	-0.282	-0.076	-0.228	0.146	0.192	-0.339	-0.282			-0.026	-0.32
W_ppb	0.134	-0.315	-0.374	-0.419	-0.102	-0.085	0.021	0.052	-0.168	0.035	0.183	0.373	-0.224		-0.113	-0.091
Pt_ppb	0.033	-0.019	-0.1	-0.11	-0.076	**0.858**	0.153	-0.126	-0.145	0.058	**0.862**	0.081			-0.066	**0.896**
Au_ppb	0.13	0.053	-0.105	-0.125	-0.066	0.587	0.118	0.082	-0.005	-0.15	0.572	0.066			-0.032	**0.743**
Ag_ppb	0.011	0.053	-0.068	-0.119	-0.047	0.036	-0.026	0.034	-0.033	-0.217	-0.042	0.039			-0.056	-0.009
Ta_ppb	0.303	0.109	0.215	0.113	0.28		0.114	0.279	0.362	0.024		0.354			-0.029	
Tl_ppb	-0.161	-0.088	-0.091	-0.081	-0.024		-0.114	-0.125	-0.064	-0.076		0.001			-0.097	
Li_mgl	**0.802**	0.376	-0.388	-0.187	-0.37	0.165	**0.756**	0.593	**0.648**	-0.188	-0.11	**0.829**	-0.262		-0.219	**-0.697**

Variables	Sr_ppb	B_mgl	SiO4	Be_ppb	Pb_ppb	Zn_ppb	Cu_ppb	Cd_ppb	Mo_ppb	Co_ppb	Ni_ppb	As_ppb	Hg_ppb
Na	0.174	-0.06	0.3	-0.045	0.284	-0.1	0.023	-0.031	0.436	0.194	-0.093	0.147	**0.645**
K	0.307	-0.062	-0.188	-0.064	0.126	0.039	0.018	0.011	-0.053	0.137	0.136	-0.062	0.414
Ca	0.423	-0.046	-0.351	-0.106	-0.035	0.347	-0.149	-0.07	-0.273	-0.002	0.231	-0.191	0.372
Mg	0.532	-0.054	-0.351	-0.088	0.059	0.232	-0.134	-0.061	-0.218	0.022	0.25	-0.167	0.451
Fe	0.17	-0.011	-0.154	0.124	0.068	0.063	-0.057	-0.009	-0.088	0.1	0.081	-0.025	0.264
NH4	-0.099	**1**	-0.096		-0.081	-0.079	**0.632**	-0.014	-0.106	0.284	0.031	-0.046	0.109
Cl	0.315	0.012	0.048	-0.158	0.294	-0.031	-0.004	-0.004	0.301	0.125	-0.034	0.063	0.595
SO4	0.069	-0.04	**0.713**	0.363	0.129	-0.059	0.114	-0.009	0.432	0.432	0.017	0.294	0.17
HCO3	0.241	-0.195	0.156	0.145	0.229	0.121	-0.087	0.018	0.183	0.154	0.057	-0.058	0.448
CO3	0.112	-0.077	-0.096	-0.115	0.12	-0.147	-0.13	0.048	0.081	-0.016	-0.099	-0.109	0.424
PO4	-0.084	**0.854**	-0.195	0.094	0.107	-0.217	0.574	-0.031	-0.091	0.476	-0.082	-0.193	-0.102
F	-0.148	-0.089	0.399	0.082	0.108	-0.181	0.011	0.154	0.336	-0.005	-0.206	0.099	0.471

Variables	Sr_ppb	B_mgl	SiO4	Be_ppb	Pb_ppb	Zn_ppb	Cu_ppb	Cd_ppb	Mo_ppb	Co_ppb	Ni_ppb	As_ppb	Hg_ppb
Br	-0.041	0.195	0.43	-0.118	-0.065	0.347	0.046	**0.751**			**0.749**	0.586	**-0.751**
I	-0.026	-0.046	0.104	-0.107	-0.471	0.051	0.071				-0.073	-0.071	
NO3	0.036	-0.034	-0.072	-0.168	0.34	0.093	0.281	-0.002	-0.018	0.02	0.032	-0.052	-0.153
NO2	-0.151	**1**	-0.101	0.497	-0.1	-0.092	**0.646**	0.343	-0.114	0.305	0.016	-0.046	
Sr_ppb	**1**	-0.047	-0.187	-0.159	0.139	0.068	-0.129	-0.046	-0.141	0.061	0.117	-0.097	0.431
B_mgl	-0.047	**1**	-0.069	-0.119	-0.032	-0.032	0.339	-0.002	-0.073	0.078	0.024	-0.037	**0.61**
SiO4	-0.187	-0.069	**1**	-0.048	-0.248	-0.096	-0.081	0.021	**0.627**	0.126	0.005	0.543	-0.587
Be_ppb	-0.159	-0.119	-0.048	**1**	-0.01	-0.046	0.345				0.308	**0.889**	
Pb_ppb	0.139	-0.032	-0.248	-0.01	**1**	0.001	0.212	0.111	-0.099	0.306	0.055	-0.155	**0.641**
Zn_ppb	0.068	-0.032	-0.096	-0.046	0.001	**1**	-0.038	0	-0.106	0.207	0.229	0.034	-0.202
Cu_ppb	-0.129	0.339	-0.081	0.345	0.212	-0.038	**1**	-0.034	-0.255	0.266	-0.012	-0.307	0.213
Cd_ppb	-0.046	-0.002	0.021		0.111	0	-0.034	**1**	-0.098	-0.052	0.089	-0.031	-0.226
Mo_ppb	-0.141	-0.073	**0.627**		-0.099	-0.106	-0.255	-0.098	**1**	-0.152	-0.013	0.472	0.17
Co_ppb	0.061	0.078	0.126		0.306	0.207	0.266	-0.052	-0.152	**1**	0.249	0.195	0.245
Ni_ppb	0.117	0.024	0.005	0.308	0.055	0.229	-0.012	0.089	-0.013	0.249	**1**	0.142	-0.222
As_ppb	-0.097	-0.037	0.543	**0.889**	-0.155	0.034	-0.307	-0.031	0.472	0.195	0.142	**1**	-0.466
Hg_ppb	0.431	**0.61**	-0.587		**0.641**	-0.202	0.213	-0.226	0.17	0.245	-0.222	-0.466	**1**
Cr_ppb	0.143	-0.072	-0.205		-0.164	0.162	-0.315	-0.083	0.209	-0.175	0.046	0.068	-0.116
Se_ppb	-0.112	-0.077	0.571		-0.279	-0.128	-0.448	-0.088	**0.647**	-0.3	0.015	0.589	**-0.76**
Bi_ppb	0.021	0.027	-0.297		0.282	-0.047	0.43	-0.039	-0.253	0.401	-0.147	-0.304	**0.948**
Sn_ppb	0.269	-0.051	-0.37	-0.09	0.375	0.093	0.132	-0.06	-0.164	0.107	-0.032	-0.276	0.54
Te_ppb	0.28	-0.135			0.179	-0.206	-0.444	-0.089	0.08	-0.249	-0.244	-0.011	
Sb_ppb	-0.043	**0.951**	-0.05	-0.062	-0.013	-0.008	0.3	-0.01	-0.054	0.123	0.053	0.416	-0.001
Nb_ppb	-0.062	**0.997**	-0.083		-0.012	-0.032	0.479	-0.006	-0.082	0.123	0.031	0.129	-0.143
Ba_ppb	0.271	-0.046	-0.228		-0.029	0.33	-0.097	-0.007	-0.19	0.042	0.065	-0.195	0.02
W_ppb	-0.337	-0.068	0.038		-0.112	-0.163	-0.138	0.027	0.102	-0.141	-0.125	0.204	0.109
Pt_ppb	-0.083	0.449	-0.126		-0.057	-0.052	0.2	0.034	0.084	-0.006	-0.053	-0.077	0.158
Au_ppb	-0.08	0.046	0.082		-0.043	-0.023	0.026	-0.029	0.06	-0.017	-0.071	0.064	-0.396
Ag_ppb	-0.025	0.002	0.034		0.292	0.004	0.118	-0.06	0.165	0.004	0.046	-0.048	-0.047
Ta_ppb	-0.002	0.449	0.279		0.001	-0.007	-0.086	0.023	0.308	-0.025	-0.095	-0.042	**0.781**
Tl_ppb	-0.084	-0.13	-0.125		-0.043	-0.058	-0.075	-0.034	-0.083	-0.034	-0.061	-0.11	-0.075
Li_mg/l													

Variables	Cr_ppb	Se_ppb	Bi_ppb	Sn_ppb	Te_ppb	Sb_ppb	Nb_ppb	Ba_ppb	W_ppb	Pt_ppb	Au_ppb	Ag_ppb	Ta_ppb	Tl_ppb	Li_mg/l
Na	-0.199	0.176	0.333	0.244	0.377	-0.074	-0.092	-0.226	0.134	0.033	0.13	0.011	0.303	-0.161	**0.802**
K	0.107	-0.094	0.006	0.45	-0.039	-0.07	-0.124	0.118	-0.315	-0.019	0.053	0.053	0.109	-0.088	0.376
Ca	0.161	-0.215	-0.205	0.213	0.193	-0.05	-0.054	0.446	-0.374	-0.1	-0.105	-0.068	0.215	-0.091	-0.388
Mg	0.074	-0.216	-0.165	0.349	0.232	-0.058	-0.065	0.336	-0.419	-0.11	-0.125	-0.119	0.113	-0.081	-0.187
Fe	-0.022	-0.149	-0.027	0.055	0.297	0.005	-0.004	0.291	-0.102	-0.076	-0.066	-0.047	0.28	-0.024	-0.37
NH4	-0.149	-0.111	-0.07	-0.064		**0.999**	**0.999**	-0.282	-0.085	**0.858**	0.587	0.036			0.165
Cl	-0.114	0.103	0.281	0.396	0.397	0.015	0.065	-0.076	0.021	0.153	0.118	-0.026	0.114	-0.114	**0.756**
SO4	-0.249	0.13	0.244	-0.012	-0.105	-0.048	-0.084	-0.228	0.052	-0.126	0.082	0.034	0.279	-0.125	0.593
HCO3	-0.027	0.004	0.063	-0.007	0.16	-0.235	-0.305	0.146	-0.168	-0.145	-0.005	-0.033	0.362	-0.064	**0.648**
CO3	-0.114	-0.072	0.055	0.143	0.25	-0.088	-0.195	0.192	0.035	0.058	-0.15	-0.217	0.024	-0.076	-0.188
PO4	-0.018	-0.235	0.265	-0.017		0.591	**0.801**	-0.339	0.183	**0.862**	0.572	-0.042			-0.11
F	-0.051	0.267	0.177	-0.077	0.268	-0.12	-0.121	-0.282	0.373	0.081	0.066	0.039	0.354	0.001	**0.829**
Br	**-0.766**			0.123		-0.403			-0.224						-0.262
I				0.078		-0.095									
NO3	-0.044	-0.096	-0.031	0.379	-0.049	-0.047	-0.026	-0.026	-0.113	-0.066	-0.032	-0.056	-0.029	-0.097	-0.219
NO2	-0.241	-0.118	-0.084	-0.078		**1**	**1**	-0.32	-0.091	**0.896**	**0.743**	-0.009			**-0.697**
Sr_ppb	0.143	-0.112	0.021	0.269	0.28	-0.043	-0.062	0.271	-0.337	-0.083	-0.08	-0.025	-0.002	-0.084	
B_mgl	-0.072	-0.077	0.027	-0.051	-0.135	**0.951**	**0.997**	-0.046	-0.068	0.449	0.046	0.002	0.449	-0.13	
SiO4	-0.205	0.571	-0.297	-0.37		-0.05	-0.083	-0.228	0.038	-0.126	0.082	0.034	0.279	-0.125	
Be_ppb				-0.09		-0.062									
Pb_ppb	-0.164	-0.279	0.282	0.375	0.179	-0.013	-0.012	-0.029	-0.112	-0.057	-0.043	0.292	0.001	-0.043	
Zn_ppb	0.162	-0.128	-0.047	0.093	-0.206	-0.008	-0.032	0.33	-0.163	-0.052	-0.023	0.004	-0.007	-0.058	
Cu_ppb	-0.315	-0.448	0.43	0.132	-0.444	0.3	0.479	-0.097	-0.138	0.2	0.026	0.118	-0.086	-0.075	
Cd_ppb	-0.083	-0.088	-0.039	-0.06	-0.089	-0.01	-0.006	-0.007	0.027	0.034	-0.029	-0.06	0.023	-0.034	
Mo_ppb	0.209	**0.647**	-0.253	-0.164	0.08	-0.054	-0.082	-0.19	0.102	0.084	0.06	0.165	0.308	-0.083	
Co_ppb	-0.175	-0.3	0.401	0.107	-0.249	0.123	0.123	0.042	-0.141	-0.006	-0.017	0.004	-0.025	-0.034	
Ni_ppb	0.046	0.015	-0.147	-0.032	-0.244	0.053	0.031	0.065	-0.125	-0.053	-0.071	0.046	-0.095	-0.061	
As_ppb	0.068	0.589	-0.304	-0.276	-0.011	0.416	0.129	-0.195	0.204	-0.077	0.064	-0.048	-0.042	-0.11	
Hg_ppb	-0.116	**-0.76**	**0.948**	0.54		-0.001	-0.143	0.02	0.109	0.158	-0.396	-0.047	**0.781**	-0.075	
Cr_ppb	**1**	0.423	-0.313	0.527	0.013	-0.061	-0.084	0.162	0.02	0.34	0.364	0.462	-0.328	0.109	
Se_ppb	0.423	**1**	-0.493	-0.259	0.55	-0.061	-0.11	-0.229	0.231	0.257	0.442	0.183	-0.048	-0.086	
Bi_ppb	-0.313	-0.493	**1**	0.371	0.319	-0.027	0.099	-0.043	0.115	-0.051	0.017	**0.714**	0.098	0.032	
Sn_ppb	0.527	-0.259	0.371	**1**		-0.051	-0.062	0.247	-0.136	0.193	0.129	0.225	-0.096	-0.107	
Te_ppb	0.013	0.55	0.319		**1**	0.165									
Sb_ppb	-0.061	-0.061	-0.027	-0.051	0.165	**1**	**0.989**	-0.048	-0.056	0.432	0.044	0.248	0.067	-0.069	0.359
Nb_ppb	-0.084	-0.11	0.099	-0.062		**0.989**	**1**	-0.042	-0.073	0.45	0.055	0.398	-0.111	0	
Ba_ppb	0.162	-0.229	-0.043	0.247		-0.048	-0.042	**1**	-0.112	-0.047	-0.077	0.051	-0.095	-0.125	
W_ppb	0.02	0.231	0.115	-0.136		-0.056	-0.073	-0.112	**1**	-0.087	0.009	-0.04	0.047	0.166	-0.245
Pt_ppb	0.34	0.257	-0.051	0.193		0.432	0.45	-0.047	-0.087	**1**	0.218	0.147	0.172	-0.069	
Au_ppb	0.364	0.442	0.017	0.129		0.044	0.055	-0.077	0.009	0.218	**1**	0.149	-0.319	0.205	
Ag_ppb	0.462	0.183	**0.714**	0.225		0.248	0.398	0.051	-0.04	0.147	0.149	**1**	0.041	-0.042	
Ta_ppb	-0.328	-0.048	0.098	-0.096		0.067	-0.111	-0.095	0.047	0.172	-0.319	0.041	**1**	-0.093	
Tl_ppb	0.109	-0.086	0.032	-0.107		-0.069	0	-0.125	0.166	-0.069	0.205	-0.042	-0.093	**1**	
Li_mgl						0.359			-0.245						**1**